

**Silver Nanoparticle biosynthesis and Bacterial  
Cellulose production by novel microorganisms:  
Characterization, bioactivity, and application  
towards bioremediation**

*A thesis submitted*

in Partial Fulfillment of the Requirements  
for the Degree of

Doctor of Philosophy

by

**Jhilam Majumder**

**INDEX NO. 08/18/Life Sc./25**



*to the*

**DEPARTMENT OF LIFE SCIENCE AND BIOTECHNOLOGY  
JADAVPUR UNIVERSITY**

July, 2023



DEPARTMENT OF LIFE SCIENCE AND BIOTECHNOLOGY

**Certificate from the supervisor**

This is to certify that the thesis entitled “**Silver Nanoparticle biosynthesis and Bacterial Cellulose production by novel microorganisms: Characterization, bioactivity, and application towards bioremediation**” submitted by Jhilam Majumder who got her name registered on 30.01.2018 with registration number [Index No.: 08/18/Life SC/25] for the award of **Ph.D. (Science)** degree of Jadavpur University, is absolutely based upon her own work under the supervision of **Prof. Ratan Gachhui** and that neither this thesis nor any part of it has been submitted for either any degree / diploma or any other academic award anywhere before.

*Ratan Gachhui.*

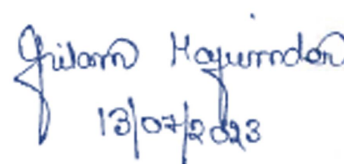
Prof. Ratan Gachhui  
Department of Life Science & Biotechnology  
**Jadavpur University**

**Ratan Gachhui, Ph. D.**  
Professor  
**Life Sc. & Biotechnology Dept.**  
Jadavpur University  
Kolkata - 700 032

Date: 13.07.2023

## DECLARATION

This is to certify that the thesis titled **Silver Nanoparticle biosynthesis and Bacterial Cellulose production by novel microorganisms: Characterization, bioactivity, and application towards bioremediation** has been authored by me. It presents the research conducted by me under the supervision of **Prof. Ratan Gachhui**. To the best of my knowledge, it is an original work, both in terms of research content and narrative, and has not been submitted elsewhere, in part or in full, for a degree. Further, due credit has been attributed to the relevant state-of-the-art and collaborations (if any) with appropriate citations and acknowledgements, in line with established norms and practices.



Jhilam Majumder  
13/07/2023

---

**Jhilam Majumder**

Department Of Life Science And Biotechnology

Jadavpur University

Dedicated to my family



# Acknowledgements

Acknowledging the persons whose contributions have helped you to shape your dream is difficult to express in words. However, I take this opportunity to thank them from the bottom of my heart. My family, Maa and Baba, *Mrs. Tripti Majumder*, and *Mr. Samiran Majumder* without their never-ending support and guidance would have pursued my dreams of enrolling in Ph.D. My grandparents, Dadu, and Didi, *Mr. Jnan Shankar Ghosh* and *Mrs. Gouri Ghosh* had also been my great support. My husband, *Prof. Pranamesh Chakraborty*, has been my pillar of strength and biggest motivator throughout my Ph.D. life, without his constant support my journey would not be successful.

I would like to express my sincere gratitude to my advisor *Prof. Ratan Gachhui* who showed me the way to think like a true researcher. Working ‘with’ him rather than ‘under’ them during my thesis helped me to grow up as a thinker. Their approach to solving any problem is something I would like to follow in my future life. Whatever I could achieve in the future, I owe a lot to them. I would also like to express my gratitude to other Professors *Parimal Karmakar*, *Paltu Kumar Dhal*, *Arunima Sengupta*, *Biswadip Das*, *Sougata Roy Chowdhury*, *Arghya Adhikary* without their help my journey of Ph.D. wouldn’t have been completed.

I would also like to thank my committee member *Prof. Joydeep Mukherjee* for their continuous guidance throughout this research. In this context, I acknowledge the efforts of all the teachers of my entire life who have shown me the path to follow.

The quality of any work depends on its place of origin. I am fortunate enough to share my work with some of my best friends, *Rubia Parvin* and *Rinky Bhadra*, she

has been there for every need and support and were the best colleague I have ever made. The discussions, debate, and fun that I had with them is something that has made my dissertation work more enjoyable.

## ABSTRACT

### **Silver Nanoparticle biosynthesis and Bacterial Cellulose production by novel microorganisms: Characterization, bioactivity, and application towards bioremediation**

Microorganisms obtained from kombucha tea (a worldwide consumable fermented beverage) include the following microbial strains namely *Glucanoacetobacter kombuchae* (RG3<sup>T</sup>), *Papiliotrema laurentii* (Y24<sup>T</sup>), and *Pichia manschurica* (CD1<sup>T</sup>) have been used to biosynthesize Silver Nanoparticle (Ag-NPs/NPs). The produced nanoparticles from each strain were assessed for both physical characterizations by various instrumental methods like TEM, SEM, DLS, Zeta Potential, FESEM, XRD, Ft-IR, etc. *Glucanoacetobacter kombuchae* (RG3<sup>T</sup>) (RG3-NPs) have been accessed for various bio-activities like broad-spectrum antibacterial effects towards a variety of Gram-positive and Gram-negative bacteria. Also, antioxidant, and cytotoxic properties against cell lines like MCF-7, HEPG-2, and Triple negative human breast cancer (TNBC) showed the nanoparticle superior efficiency. Therefore, it can be concluded that RG3-NPs points itself to be a significant bio-material with antibacterial, cytotoxic, and antioxidant properties.

Other strains like *Papiliotrema laurentii* (Y24<sup>T</sup>) and *Pichia manschurica* (CD1<sup>T</sup>) along with the characterization has also been accessed for the efficient degradation of 4-Nitrophenol (Y24-NPs), Azo dyes like Congo red and Malachite green (CD1-NPs). Further, NPs have been used to detect the presence of Fe(III)(Y24-NPs) and Hg(II)(CD1-NPs) in an aqueous solution with a detection limit of 1.8 M in the linear range of 5–150 M for Fe(III) and for Hg(II) it was 2.1.04 nM in the linear range of 10-80 nM. Both the NPs were tested for reusability and it was found that Y24-NPs were 94% reusable while CD1-NPs is 96%. The study, therefore, shows that both Y24-NPs and CD1-NPs hold great potential for environmental remediation with significant catalytic activity and reusability. Further, *Glucanoacetobacter kombuchae* (RG3) has been able to successfully produce Bacterial Cellulose (BC). The pro-

duced cellulose has been characterized by SEM, FESEM, XRD, FT-IR, and other properties like water holding and retention capacity, swelling rate, porosity, and tensile strength. Along with the characterization the produced Bacterial cellulose was further tested for other activities like industrial dye removal and antibacterial and cytotoxic effects. The produced Bacterial Cellulose, therefore, shows good efficiency that is to be applied in the field of filtration and bioremediation. Bacterial Cellulose and Silver Nanoparticles by the strain RG3T have been merged to produce a bio-composite. Characterization assessments were done by SEM, FESEM, XRD, FT-IR, DLS, and UV-Vis Spectroscopy. Bioactivity by antibacterial and cytotoxic potential has been measured successfully. Therefore, the bio-composite shows itself to be an antibacterial, cytotoxic, catalytic agent for filtration and bioremediation.

# Contents

<b>Acknowledgements</b>	<b>vii</b>
<b>List of Figures</b>	<b>xv</b>
<b>List of Tables</b>	<b>xxi</b>
<b>1 Introduction</b>	<b>1</b>
<b>2 <i>Glucanoacetobacter kombuchae</i> (RG3<sup>T</sup>), a novel bacteria for Ag-NPs biosynthesis: Characterization and comprehensive evaluation of bioactivity</b>	<b>5</b>
2.1 Introduction . . . . .	5
2.2 Materials and Methods . . . . .	8
2.2.1 Chemicals & reagents . . . . .	8
2.2.2 Preparation of bacterial cell exudate . . . . .	8
2.2.3 Bio-green Synthesis of Silver nanoparticle using bacterial cell exudate and it's optimization . . . . .	9
2.2.4 Characterization of RG3-NPs . . . . .	9
2.2.5 Antioxidant Assay . . . . .	11
2.2.6 ABTS Radical Scavenging Assay . . . . .	12
2.2.7 Antibacterial Assay . . . . .	12
2.2.8 Cell Culture . . . . .	13
2.3 Results and Discussions . . . . .	14
2.3.1 Dynamic Light scattering (DLS) & Zeta Potential . . . . .	14

2.3.2	Scanning Electron Microscopy (SEM) . . . . .	14
2.3.3	Transmission Electron Microscopy (TEM) . . . . .	15
2.3.4	FTIR Analysis . . . . .	15
2.3.5	UV-Vis Spectroscopy . . . . .	16
2.3.6	XRD . . . . .	17
2.3.7	Antioxidant Activity . . . . .	18
2.3.8	Antibacterial Activity . . . . .	19
2.3.9	Cytotoxic Activity . . . . .	21
2.4	Conclusions . . . . .	22
<b>3</b>	<b>Efficient degradation of 4-nitrophenol and colorimetric detection of Fe (III) by biogenic silver nanoparticles of <i>Papiliotrema laurentii</i></b>	<b>25</b>
3.1	Introduction . . . . .	25
3.2	Materials and Methods . . . . .	28
3.2.1	Chemicals & reagents . . . . .	28
3.2.2	Preparation of Y24 cell resuspension exudate . . . . .	29
3.2.3	Bio-green Synthesis of Silver nanoparticles from yeast cell resuspension exudate . . . . .	29
3.2.4	Characterization of Y24-NPs . . . . .	30
3.2.5	Catalytic Activity . . . . .	30
3.2.6	Colorimetric detection of Fe(III) . . . . .	31
3.3	Results and Discussions . . . . .	31
3.3.1	Optimization of Synthesis Conditions . . . . .	31
3.3.2	Characterization of bio-synthesized AgNPs . . . . .	33
3.3.3	Catalytic Activity . . . . .	37
3.4	Conclusions . . . . .	48
<b>4</b>	<b>Effective degradation of azo dyes and colorimetric detection of Hg<sup>2+</sup> by biogenic silver nanoparticles of <i>Pichia manshurica</i></b>	<b>51</b>
4.1	Introduction . . . . .	51

4.2	Materials and Methods . . . . .	54
4.2.1	Chemicals & reagents . . . . .	54
4.2.2	Preparation of CD1 cell resuspension exudate . . . . .	55
4.2.3	Bio-green synthesis of Silver nanoparticles from yeast cell re- suspension exudate . . . . .	55
4.2.4	Characterization of CD1-NPs . . . . .	56
4.2.5	Optimization of AgNPs Synthesis Conditions . . . . .	56
4.2.6	Catalytic activity of CD1-NPs . . . . .	57
4.3	Results and Discussions . . . . .	58
4.3.1	Optimization of AgNPs Synthesis Conditions . . . . .	58
4.3.2	Characterization of bio-synthesized AgNPs . . . . .	59
4.3.3	Catalytic Activity . . . . .	62
4.3.4	Colorimetric detection of $\text{Hg}^{2+}$ . . . . .	70
4.4	Conclusions . . . . .	76
<b>5</b>	<b>One step synthesis and fabrication of a novel AgNPs-BC composite</b>	
	<b>: Characterizations and bioactivity</b>	<b>77</b>
5.1	Introduction . . . . .	77
5.2	Materials and Methods . . . . .	80
5.2.1	Chemicals & reagents . . . . .	80
5.2.2	Microbial strain . . . . .	81
5.2.3	Preparation of Bacterial Cellulose (BC) and biocomposite (AgNPs-BC) formation and purification. . . . .	81
5.2.4	Charcterization of the pellicle . . . . .	82
5.2.5	Optimization of the synthesis conditions . . . . .	82
5.2.6	Ag ion release rate measurements . . . . .	82
5.2.7	Antibacterial property . . . . .	83
5.2.8	Cell Culture . . . . .	84
5.2.9	Cell Survivability Assay . . . . .	84
5.3	Result and discussion . . . . .	85

5.3.1	One step synthesis of the AgNPs-Bc bio-composite . . . . .	85
5.3.2	Optimization of the Synthesis Conditions . . . . .	85
5.3.3	FESEM . . . . .	86
5.3.4	SEM and EDAX analysis . . . . .	86
5.3.5	FTIR Analysis . . . . .	87
5.3.6	XRD . . . . .	88
5.3.7	Antibacterial Activity . . . . .	89
5.3.8	Cytotoxic Activity . . . . .	91
5.3.9	Silver ion release . . . . .	92
5.4	Conclusions . . . . .	93
<b>6</b>	<b>Conclusions</b>	<b>95</b>
6.1	Chapter 2 . . . . .	95
6.2	Chapter 3 . . . . .	96
6.3	Chapter 4 . . . . .	96
6.4	Chapter 5 . . . . .	97
	<b>List of Publications</b>	<b>97</b>
	<b>References</b>	<b>107</b>



# List of Figures

2.1	(a) Schematic procedure of RG3-AgNPs formation by green method; (b) Tenable mechanism of RG-NPs formation. . . . .	10
2.2	(a) Dynamic light scattering analysis; (b) Surface zeta potential of RG3-NPs . . . . .	14
2.3	Surface morphology by scanning electron microscopy of (a) RG3-NPs and (b) Control sample . . . . .	15
2.4	Transmission Electron Microscopy analysis of (a) RG3-NPs and (b) Control sample . . . . .	16
2.5	(a) FTIR spectrum analysis, (b) UV-Vis Spectroscopic study, and (c) XRD study of the synthesized RG3-NPs. . . . .	18
2.6	Antioxidant property analysis of RG3-NPs by (a) DPPH scavenging assay and (b) ABTS Radical Scavenging Activity assay . . . . .	19
2.7	Colony count of each bacterial strain after being exposed to different concentrations of RG3-NPs . . . . .	21
2.8	Bactericidal activities of RG3-NPs against sample Gram Positive strain <i>Bacillus cereus</i> at (a) 0 µg/ml (Control), (b) 5 µg/ml, (c) 25 µg/ml, and (d) 50 µg/ml . . . . .	22
2.9	Bactericidal activities of RG3-NPs against sample Gram Negative strain <i>Vibrio cholerea</i> at (a) 0 µg/ml (Control), (b) 5 µg/ml, (c) 25 µg/ml, and (d) 50 µg/ml . . . . .	22

2.10	Cytotoxic effect of RG3-NPs (a) HEPG-2 hepatocellular carcinoma cell lines, (b) MCF-7 breast carcinoma cell lines, (c) MDA-MB-468 corresponds to Triple Negative Breast Cancer (TNBC) cell lines. The results are mean $\pm$ SD from 3 independent experiments in each case. Values that share different letter have statistically significant difference between each other (Mann-Whitney U Test with $p \leq 0.05$ ) . . .	23
3.1	Optimization of Y24-NPs synthesis with reference to (a) Different conc. of $\text{AgNO}_3$ with 0.1 g of glucose and observed for 45 minutes, (b) Different conc. of glucose with a fixed concentration of 2mM $\text{AgNO}_3$ for 45 minutes, (c) Different temperature ranges starting from $20^\circ$ to $37^\circ$ , (d) Different reaction times varying from 5 to 60 minutes. . . .	32
3.2	Y24-NPs analysis by (a) ZETA Potential; (b) DLS study. . . . .	34
3.3	Microscopic Characterization of Y24-NPs by (a) FESEM imaging and (b) Control sample without $\text{AgNO}_3$ ; (c) SEM imaging (d) Control image without $\text{AgNO}_3$ . . . . .	35
3.4	TEM analysis of (a) Y24-NPs and (b) Control sample without $\text{AgNO}_3$ ; (c) FTIR study of Y24-NPs (d) XRD analysis of the biogenic nanoparticle. . . . .	36
3.5	Catalytic reduction of 4-NP by Y24-NPs and estimation of its effects by other parameters like, (a) When only $\text{NaBH}_4$ has been used without any catalysts and observed for 30 minutes, (b) Different conc. of catalysts ( $\text{AgNPs}$ ) ranging from 1 mM, 1.5 mM, 2 mM, and 2.5 mM respectively (c) Different conc. of 4-NP like 0.1 mM, 0.5 mM, 1 mM, 1.5 mM, and 2 mM respectively, (d) Different conc. of $\text{NaBH}_4$ ranging from 0.05 mM, 0.1 mM, 0.2 mM respectively. All the experimental set up were kept for 8 minutes. . . . .	38

3.6	(a) Effect of reaction time in the catalytic degradation of 4-NP by Y24-NPs. The experimental setup was observed from the time period between 0 to 8 minutes, (b) First order-kinetic plot of 4-NP degradation by the catalysts for 2, 3, 4, 5, 6, 7, and 8 minutes respectively.	41
3.7	Reusability analysis of Y24-NPs after five repetitive cycles by (a) UV-Vis Spectroscopic analysis at each cycle, (b) Efficiency percentage of five successive cycles of the catalyst for reduction of 4-NP using NaBH <sub>4</sub> , (c) TEM analysis of the catalysts, (d) XRD pattern study of the catalysts after five consecutive cycles.	43
3.8	Possible mechanism of 4-NP degradation by the biogenic Y24-NPs by catalytic activity.	44
3.9	(a) Selectivity and sensitivity study by UV-Vis spectroscopic analysis of Y24-NPs solution in the presence of various metal ions, (b) UV-Vis Spectroscopic study of the quantitative determination of Fe(III) of different conc. ranging from 5 to 3000 $\mu$ M with the bio-catalysts, (c) To test in real water samples, different of conc. Fe(III) to analyse its absorbance intensity by Uv-Vis Spectroscopy, (d) The plot of sensitivity versus relative Fe(III) conc.	45
3.10	The catalysts after five cycles of repeated reuse have been analyzed for (a) TEM imaging of Y24-NPs solution after incubation in 120 $\mu$ M Fe(III) ions, (b) Efficiency percentage of five successive cycles of the catalyst for detection of Fe(III), and (c) Zeta Potential estimation analyse the catalysts after the reuse.	46
3.11	Possible colorimetric sensing mechanism by the biogenic Y24-NPs	48
4.1	(a) TEM analysis, and (b) SEM analysis of CD1-NPs, (c) XRD study, and (d) FTIR analysis of the nanoparticles.	60

4.2	Optimization of the Congo red (CR) dye degradation activity by CD1-NPs with the following parameters, (a) Effect of the concentration of CD1-NPs, (b) Effect of the concentration of CR on dye degradation, (c) Effect on different pH on CR degradation, (d) Effect of different reaction time of Congo red dye with the catalysts. . . . .	63
4.3	(a) UV-Vis Spectral analysis of the catalysts up to five cycles, (b) First order-kinetic plot of Congo red, (c) TEM analysis of the catalysts after the fifth cycle for morphological analysis, and (d) XRD pattern analysis of the catalysts after fifth cycles (inlet showing the five recycling of CD1-NPs). . . . .	65
4.4	(a) Reaction time of degradation of both CR and MG by CD1-NPs starting from 5 minutes to 45 minutes, (b) First order-kinetic plot of the mixture dyes. . . . .	67
4.5	(a) UV-Vis spectral analysis of CD1-NPs solution in the presence of various metal ions, (b) Sensitivity of $\text{Hg}^{2+}$ at different concentration (c) Quantitative determination of $\text{Hg}^{2+}$ , (d) The plot of sensitivity versus relative $\text{Hg}^{2+}$ concentration. . . . .	72
4.6	(a) Zeta Potential analysis of CD1-NPs after the reuse, (b) TEM image of CD1-NPs solution after incubation in 80 nM $\text{Hg}^{2+}$ ions at different concentration. . . . .	73
5.1	(a) XRD study of the synthesized biocomposite with the bacterial cellulose, and (b) FTIR analysis of the biocomposite along with bacterial cellulose. . . . .	87
5.2	Edax study of (a) bacterial cellulose, and (b) AgNPs-Bc. . . . .	87
5.3	(a) XRD study of the synthesized biocomposite with the bacterial cellulose, and (b) FTIR analysis of the biocomposite along with bacterial cellulose. . . . .	88

5.4	Antibacterial activity assessment by Disc diffusion assay of the bacteria namely, (a) <i>E. coli</i> (Gram-negative bacteria) and (b) <i>S.aureus</i> (Gram-positive bacteria). . . . .	90
5.5	Colony count method analysis and Bactericidal activities of AgNPs-Bc against sample Gram Positive strain <i>Bacillus cereus</i> at (a) 0 µg/ml (Control), (b) 5 µg/ml, and Gram Negative strain <i>E. coli</i> , (c) 50 µg/ml, (d) 0 µg/ml (Control). . . . .	91
5.6	Cytotoxic activity by Mtt assay by the cell lines A549 and WI38. . .	92

# List of Tables

2.1	Table representing FTIR data of the synthesized RG3-NPs . . . . .	17
2.2	Mean and SEM values of IC50 obtained from antioxidant activity . .	19
2.3	Mean and SEM values of IC50 obtained from antibacterial activity .	21
2.4	Mean and SEM values of LD50 obtained from cytotoxic activity . . .	22
3.1	Tap water quantification of $\text{Fe}^{3+}$ at different concentrations using Y24-NPs. . . . .	47
4.1	Comparison table for degradation efficiency and duration of different azo dyes. . . . .	74
4.2	Comparison study of the detection of $\text{Hg}^{2+}$ ions. . . . .	75
4.3	Real water quantification of $\text{Hg}^{2+}$ at different concentrations using CD1-NPs. . . . .	75

# Chapter 1

## Introduction

Over the past years, nanotechnology has been emerging as the cutting-edge interdisciplinary technology along with the other branches of science and technology. These have gained significant importance because of its broad scope applications and promising outcomes that can be correlated to the unique properties of nanomaterials compared to other standard materials.

Preferably, cost effectiveness and non toxicity should be of primary focus for synthesising nanoparticles (NPs). When these two criteria are fulfilled, only then the focus needs to be shifted in obtaining the NPs with superior quality and utility. Innovations in the way of production and modifications of the NPs with different utilitarian groups of chemicals and also their conglomeration unlock a broad range of utmost utilization in the field of biotechnology. Metallic NPs are always in trends of nanotechnology owing to the fact of huge potentiality in the field of the areas of physical, chemical, medicine, pharmaceutical, and biotechnology. [83, 91].

Although there are a variety of metallic nanoparticles, among them silver NPs have gained significant importance due to their virtuous properties and their utility in the areas of photo-catalysts, photonics, micro-electronics, and lithography [110]. But the sole property of massive antimicrobial activity makes silver stands out alone in gratitude [4].

Silver nanoparticles (AgNPs) can be synthesised in various ways such as bottom up like pyrolysis, sol gel method, chemical method, physical method, physio-chemical

method, etc. [85]. These methods often result in generation of secondary pollutants that may further lead to toxicity towards the environment and also they require working under high temperature and pressure [96, 16]. In order to overcome these drawbacks, an economic, eco-friendly, feasible, and greener approach is the need of the hour. Therefore we propose a solution of eliminating the odds of all the physical and chemical approaches by introducing the bio-inspired method of NPs synthesis [4]. The greener method of synthesis is not only environmental cordial, but also can be waged to manufacture enormous volumes of NPs with nullifying contamination [82].

Apart from silver nanoparticles, bacterial cellulose being world's most abundant natural polymer is gaining much importance. It is renewable and biodegradable and so credits special consideration in the current global concern for the environment. Among the very few genera of cellulose-synthesize bacteria the best known are the various species of *Acetobacter*, *Agrobacteria*, *Rhizobia*, and the Gram-positive genus *Sarcina*. Of these, *Gluconacetobacter xylinum* of the *Acetobacteraceae* family produces a large amount of cellulose that is secreted as an extracellular pellicle.

Bacteria *Gluconacetobacter kombuchae*, strain RG3<sup>T</sup>, isolated from kombucha tea belongs to the family *Acetobacteraceae* is the first instance of any strain having both nitrogen- fixing and cellulose-producing activity [36]. Silver as nanoparticles shows excellent antimicrobial activity against bacteria, fungi, and virus and also the most preferred metal for its profound role in the field of high-sensitivity bimolecular detection, catalysis, biosensors, and medicine. Conventionally silver nanoparticles are synthesized by chemical method using chemicals as reducing agents like ion sputtering, chemical reduction, sol gel, etc., which may results for various biological risks due to their general toxicity [3] and thus engendering the serious concern to develop environment friendly processes. Considering the drawbacks of physio-chemical methods, cost-effective and energy efficient new alternative for AgNPs synthesis using microorganisms [112] and natural polymers as reducing and capping agents are emerging very fast. The association of nanotechnology and green chemistry will



unfold the range of biologically and cytological compatible metallic nanoparticles. Nowadays, Researchers are focusing heavily on prokaryotes as a means of synthesizing metallic nanoparticle like silver because of their abundance in the environment and their ability to adapt to extreme conditions. Bacterial (BC) possess good characteristics of high porosity and water permeability and thus is more favorable than another form of cellulose owing to the porous nature of the arrangement of the fibers variety of particles made from different materials such as natural and synthetic polymer, and biomaterial may acts as a template. As BC contains a significant amount of surface hydroxyl groups,  $\text{Ag}^+$  ions could be easily attached to BC.

The research study here focuses on the bacterial strain, namely, *Glucanoacetobacter kombuchae*, strain RG3<sup>T</sup>, which has been utilized for both silver nanoparticle (AgNPs) bio-synthesis and bacterial cellulose bio-production. Further, there is application on bioactivity and characterization. Two yeast strains namely, *Papiliotrema laurentii*, strain Y24 and *Pichia manschurica* strain CD1 were made to biosynthesis AgNPs and subjected to a test as catalytic reducers for 4-NP and Azo dyes in wastewater and also used as a highly sensitive probe for the colorimetric detection Fe (III) and Hg (II) in aqueous solution. Lastly, silver nanoparticles and bacterial cellulose produced by the strain RG3 have been bio-fabricated to apply as an antimicrobial, cytotoxic agent along with good reusability and stability. All these microbial strains were obtained from a popular fermented beverage, kombucha. All these are categorised into Chapters 2, 3, 4, and 5.

## Chapter 2

# *Glucanoacetobacter kombuchae* (RG3<sup>T</sup>), a novel bacteria for AgNPs biosynthesis: Characterization and comprehensive evaluation of bioactivity

### 2.1 Introduction

Silver nanoparticles (AgNPs) can be synthesised in various ways such as bottom up like pyrolysis, sol gel method, chemical method, physical method, physio-chemical method, etc. [85]. These methods often result in generation of secondary pollutants that may further lead to toxicity towards the environment and also they require working under high temperature and pressure [96, 16]. In order to overcome these drawbacks, an economic, eco-friendly, feasible, and greener approach is the need of the hour. Therefore we propose a solution of eliminating the odds of all the physical

and chemical approaches by introducing the bio-inspired method of NPs synthesis [4]. The greener method of synthesis is not only environmental cordial, but also can be waged to manufacture enormous volumes of NPs with nullifying contamination [82].

Over the past decades, there has been few studies pointing on the green synthesis method of NPs synthesis, including plant extracts, biodegradable polymers, and microbes. Particularly, microorganism based synthesis is the new trend because they are secured, sustainable, low cost and therefore environmental friendly too. In the last few years, bacteria have been widely explored to synthesize inorganic nanomaterials particularly gold and silver. It can be directly contributed to the property of versatility and survivability of the bacteria at higher concentrations of metallic ions [51].

Discovery of antibiotics has been a revolutionary milestone in the history of humans. Unfortunately, the utilization of the novel prodigy medication were followed by a quick increase in tolerant pathogen strain [97]. Frequent and improper use of antibiotics may be blamed for this. In order to find out an alternative for the same, nanotechnology can be applied to beat the drug resistance of many infectious bacteria. In fact, silver nanoparticle is one of the most suitable one to ht against the pathogenic strains. Moreover in India, main contaminants of polluted water are Enterobacteriaceae namely *Salmonella typhi*, *Escherichia coli*, *Shigella sonnei*, etc. Enterobacteriaceae contributes to water borne related disorders like diarrhoea, cholera, typhoid, and other infections. Since ancient times, silver has been the best choice among people for its robust antimicrobial effectiveness. Moreover, silver shows extensive span of efficiency towards various Gram-positive and Gram-negative bacteria, also chance of development of bacteria resistance is remarkably low too. [57].

Usefulness of AgNPs to the medical field is not only restricted to its antimicrobial effect but also gained much attention due to its cytotoxic effect. In some of the previous studies, opposed to cell line of human cervical cancer, it has been showed

that the efficiency of AgNPs towards apoptosis, pointing its role as anti cancer drug therapy [40, 44]. It has been estimated that AgNPs synthesised through biological method are safe to human cell upto 50 ug/ml of concentration. Therefore, the cytotoxic effect is an another important factor that needs attention. [1].

*Gluconacetobacter kombuchae*, strain RG3<sup>T</sup> has been isolated from a popular fermented tea, known as kombucha [36]. The GenBank accession numbers for the strain RG3<sup>T</sup> are respectively AY688433 and DQ141200. This potential Gram negative, rod shaped bacteria belongs to the Acetobacter family. This bacteria is also responsible for nitrogen fixation and cellulose formation as pointed by [36] . Here in this study, we have used this bacteria for the NPs synthesis by bio-green method. The present study aims to develop a feasible green alternative towards the synthesis of AgNPs and to enlighten its broad spectrum antimicrobial effect in some of the common Gram positive/negative bacteria including *Salmonella typhi*, *Shigella sonnei*, *Vibrio cholera*, *Bacillus cereus*, *E. coli*, and *Staphylococcus aureus*. Once its antibacterial property is successfully fulfilled, our attention is then shifted to explore its cytotoxic activity. The cytotoxicity has been measured against HEPG-2 hepatocellular carcinoma cell lines, MCF-7 breast carcinoma cell lines, and MDA-MB-468 corresponding to the Triple Negative Breast Cancer (TNBC) cell lines. HEPG-2 is a human hepatoma origin, non-tumorigenic with elevated proliferating rate and most frequently applied in drug catabolism and hepato-toxicity studies. MCF-7 is characterized with presence of estrogen, progesterone, and glucocorticoid receptors. Further, MDA-MB-48 holds for about 10-15 percentage of the breast cancer lines. This triple-negative breast cancer cited to the non availability of estrogen or progesterone receptors and is also responsible to produce insufficient protein commonly known as HER2. Studies have been conducted on RG3<sup>T</sup> NPs to check the cytotoxic activities of these cell lines.

Oxidants are produced as a result of normal metabolism in the body and also in the environment. These molecules are very reactive and can rapidly react with other cellular activities of the body leading to noxious effects in body including cancer and

other diseases. In order to get rid of these oxidants and its stresses, scavenging activity is helpful. Thus, DPPH (2,2- diphenyl-2-picrylhydrazyl hydrate) and ABTS (2, 2'-azino-bis 3-ethylbenzthiazoline-6-sulfonic acid) free radical scavenging activity has been performed to check the effectiveness of the produced AgNPs against oxidants. Therefore, it may be concluded that the produced NPs has a long way to go and establish itself as an antioxidant, antibacteria and anticytotoxic bio-material. Also, a deep interest has been generated towards further exploring and analysing this NPs for more potential benefits that are applicable towards the society. In the remaining text, RG3<sup>T</sup>AgNPs and RG3<sup>T</sup>NPs is referred to as RG3-NPs. Simultaneously, pellet resuspension of RG3<sup>T</sup> in de-ioned water for the entire experiment has been termed as cell exudate of bacteria or bacterial cell exudate or simply cell exudate.

## 2.2 Materials and Methods

### 2.2.1 Chemicals & reagents

Silver nitrate (AgNO<sub>3</sub>), Agar agar Powder, D-(+)-Glucose anhydrous, D-Mannitol, 2,2-diphenyl-2-picrylhydrazyl hydrate (DPPH), 2,2'-Azino-bis-(3-ethylbenzothiazoline-6-sulfonic acid) diammonium salt (ABTS) were purchased from Hi-media (Mumbai, India) and de-ionized water was used throughout the entire experiment. Every reagents used here were of unadulterated analytical grade and therefore used without any further purification.

### 2.2.2 Preparation of bacterial cell exudate

*Glucanoacetobacter kombuchae*, strain RG3<sup>T</sup> (=LMG 23726T=MTCC 6913T), was isolated from Kombucha tea( Kombucha is a sweet, slightly alkaline fermented beverage, consumed world widely specially by the South Asian Countries. Mannitol broth (Yeast extract 0.75% , Peptone 0.45% , Manitol 2.5%, pH 5) of 100 ml was prepared to grow 50 µl of previous culture of the strain RG3<sup>T</sup>, and kept overnight

at 30°C under shaking condition at 120 rpm. Next, the culture was centrifuged at 5000 rpm for 5 minutes and the pellet was collected, washed with deionized water twice. Washed pellet was re-suspended with 100 ml de-ionized water and again kept overnight at 30°C under shaking condition at 120 rpm. It was then centrifuged at 5000 rpm for 5 minutes, then the pellet was discarded and the supernatant was collected. The later was stored at 4°C for further use.

### **2.2.3 Bio-green Synthesis of Silver nanoparticle using bacterial cell exudate and it's optimization**

For the formation of AgNPs, different parameters such as concentration of AgNO<sub>3</sub> and glucose, pH, and reaction time were varied. Each parameter was varied keeping the other parameters constant to optimize the synthesis. These parameters were varied in the order of AgNO<sub>3</sub> concentration, followed by pH, glucose concentration, and finally reaction time. Based on the Zeta Potential and UV-Vis spectroscopy values obtained by varying these parameters, it was noted that RG3-NPs formation were optimized at ambient temperature with a pH of 7-7.5, AgNO<sub>3</sub> concentration of 17mg/ml of and 10mg/ml of glucose. Details of these experiment and variation of different parameters has been also shown in Supplementary Data.

Simultaneously, a control setup was established with only bacterial cell exudate and AgNO<sub>3</sub> without glucose. The result obtained indicated that the bacterial cell exudate plus AgNO<sub>3</sub> and glucose together lead to the formation of a brownish yellow coloured solution, while the controlled set up without glucose and only with the cell exudate content remained colourless (Figure 2.1). This indicates the importance of both bacterial exudate and glucose in AgNPs formation.

### **2.2.4 Characterization of RG3-NPs**

Various instrumentation analysis were done to check the existence of the produced bio-green NPs and to determine it's characteristics. The confirmation of genesis and escalation of NPs were surveiled through UV-vis Spectrophotometer (HITACHI U

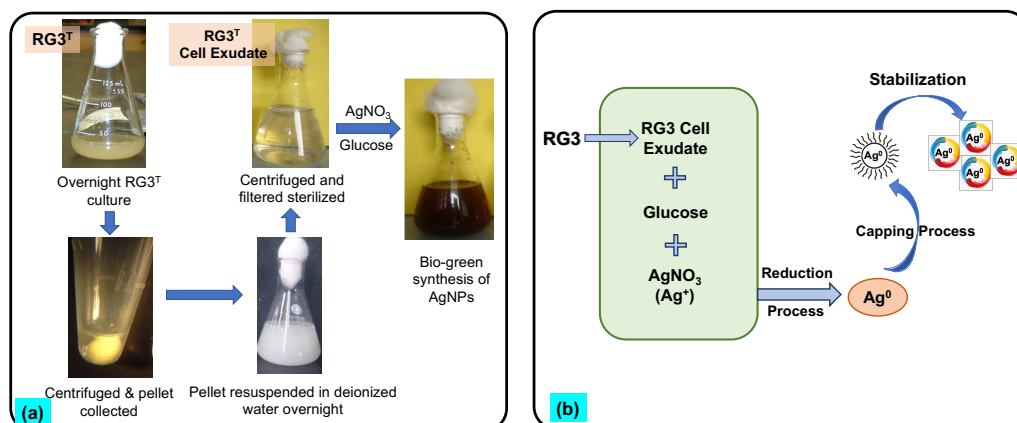


**Figure 2.1:** (a) Schematic procedure of RG3-AgNPs formation by green method; (b) Tenable mechanism of RG-NPs formation.

2900/ U 2910 UV VIS DOUBLE BEAM) settled to range including 200 to 800 nm. Crystalline nature attributed to metallic silver was examined through XRD (Rigaku, Miniflex). Morphological studies like shape and surface topographical analysis were carried out by SEM (Hitachi S-4500) and TEM (JEM-2100 Electron Microscope). The solution were made to centrifuged (5000 rpm, 5 minutes) and then the mixture was collected after discarding the supernatant for both XRD and SEM study. The poised AgNPs were vacuum dried & lyophilized for future use. (ELEYA speed Vac).

For TEM analysis, the sample were coated with carbon - copper grid thin film created by dropping minute quantity of the NPs. By using the blotting paper, any excess of the sample solution was soaked and then the film along the TEM grid were permitted to get dry for 5 minutes underneath a mercury lamp. The physique and form of the produced NPs was also noted. TEM study was conducted with a step up voltage of 200 kV to predict the accurate morphology and dimensions of the NPs . FTIR (Shimadzu FTIR spectrophotometer (FTIR 8400)) range were noted in the span of 4000–400  $\text{cm}^{-1}$ . To predict the contrasting functional groups directly or in-directly linked to NPs formation, different vibrational stretched were observed in spectrum study. With the help of the DLS (Dynamic Light Scattering) and analyzer of particle size [ZETA Seizers Nanoseries (Malvern Instruments Nano ZS)], precise size and distribution of the NPs were determined.

Antibacterial activities of the bio-green AgNPs were carried out on possible com-

mon varieties of human infective and non infective bacteria of Gram positive and Gram negative origin including *Salmonella typhi*, *Shigella sonnei*, *Vibrio cholerae*, *Bacillus cereus*, *E. coli*, and *Staphylococcus aureus* by colony count method. For cytotoxic studies, HEPG-2, MCF-7, and MDA-MB-48 cell lines were utilised. Further, for antioxidant activity, DPPH and ABTS assay were performed. Mannitol broth medium for growth, development, and maintenance of RG3<sup>T</sup> was used throughout the study.

## 2.2.5 Antioxidant Assay

### DPPH free radical scavenging assay

The antioxidant study of the bio-synthesized AgNPs was predicted utilizing the DPPH (2, 2-diphenyl-2-picrylhydrazyl hydrate) assesment [113]. Different concentrations (10, 20, 40, 60, 80, 100 µg/ml) of the biosynthesized AgNPs were prepared. 1 ml from the above concentrations were added to 3 ml of freshly made methanolic DPPH solution (0.1 mM) and thoroughly vortexed for an even mixture to form. Mixed solution were then made to incubate for a time of 30 minutes under dark condition at ambient temperature. The absorbance was observed at 517 nm operated via UV-Vis Spectrophotometer (HITACHI U 2900/ U 2910 UV VIS DOUBLE BEAM). After 30 minutes of incubation, another sample was prepared without the addition of bio-synthesized AgNPs and marked as sample. Throughout the entire assay, ascorbic acid was used as the standard. Percent inhibition of activity was counted using the following equation:  $[(A_o - A_s)/A_o] \times 100$ , where,  $A_o$  is absorbance of the control sample,  $A_s$  is absorbance of the biosynthesized AgNPs/Ascorbic acid. Finally the IC<sub>50</sub> value (the concentration of the biosynthesized AgNPs that is required to inhibit the 50% of the DPPH solution) of the AgNPs was determined. Throughout the entire experiments, mean values with standard error of mean (SEM) were determined based on the triplication of the assay.



### 2.2.6 ABTS Radical Scavenging Assay

Biosynthesized AgNPs has been tested again for free radical scavenging property using ABTS (2, 2'-azino-bis 3-ethylbenzthiazoline-6-sulfonic acid) assay according to a standard protocol [100]. Stock solution of ABTS was made by adding 7mM ABTS and 2.45 mM of potassium persulphate. The above mentioned mixture was set to be incubated for 12-16 hours in the dark following ambient temperature. Then ABTS stock solution was diluted to make the ABTS working solution to gain an absorbance of  $0.85 \pm 0.20$  at 734 nm. After that, the different concentrations (10, 20, 40, 60, 80, 100  $\mu\text{g/ml}$ ) of the biosynthesized AgNPs were prepared and 20  $\mu\text{L}$  of each of these concentrations were added 180  $\mu\text{L}$  of the working solution of ABTS followed by their incubation at room temperature for 30 minutes in dark. Absorbance of the mixture was measured at 734 nm operating an UV-Vis Spectrophotometer (HITACHI U 2900/ U 2910 UV VIS DOUBLE BEAM) after incubation for 30 minutes. The control sample was made with no addition of bio-synthesized AgNPs and Ascorbic acid was used as standard in this assay. The scavenging percent activity of the free radical was measured based the following equation, similar to DPPH activity:  $[(A_o - A_s)/A_o] \times 100$ , where,  $A_o$  is absorbance of the control sample,  $A_s$  is absorbance of the biosynthesized AgNPs/ Ascorbic acid. Finally the IC<sub>50</sub> value of the AgNPs was determined.

### 2.2.7 Antibacterial Assay

Two bacterial strains of Gram positive origin and three bacterial strains of Gram negative origin were sorted out for the antimicrobial study. The strains were cultured on Luria Bertani media for 24 hours at 37°C shaking incubator to obtain the fresh growth for the study. To each test tube containing 3 ml Luria Bertani broth, 50  $\mu\text{L}$  of the culture of each bacterial were inoculated. The AgNPs activity were assessed by *Staphylococcus aureus* (ATCC 25923), *Escherichia coli* (ATCC 25922), *Salmonella typhi* (MTCC 531), *Shigella sonnei* (MTCC 2957), *Vibrio cholerae* (N16961), *Bacillus cereus* (MTCC 430). Along with that, the following concentrations of the AgNPs

(17 mg/ml) solution at different concentrations (0.5, 1, 2, 5, 10, 15, 25, 50  $\mu$ l ) were added and kept to observe nightly at 37°C shaker incubator. On the adjoining day, the O.D value of each concentration was recorded, later spread on the Luria Bertani agar plate to assess the bacteriocidal or static activity by minimum bactericidal concentration (MBC) count and kept over at the same condition to observe the result.

### **2.2.8 Cell Culture**

The following cell lines of malignancy origin namely MCF-7, HEPG 2, and Triple-negative human breast cancer cell line MDA-MB-468 acquired from National Center for Cell Science (NCCS) Pune, India were sorted to perform the cytotoxic activity. The cells were maintained and cultured in specialized DMEM with 10% FBS (Fetal Bovine Serum), penicillin/streptomycin (100 units/ml) at 37°C and 5% CO<sub>2</sub>. Entire treatment was performed at 37°C and a minimum cell thickness is maintained to allow the rampant growth.

### **Cell Survivability Assay**

The cell survivability of RG3-NPs was studied considering the following cancer cell lines namely: MCF-7, HEPG 2, human triple negative breast cancer cell, MDA-MB-468 using MTT (4, 5-dimethylthiazol-2-yl)-2, 5-diphenyl tetrazolium Bromide). To summarize in brief, accessible to cells after being revealed to numerous ligand concentration were evaluated by MTT assay. The cells were sowed in 96-well plates at  $1 \times 10^4$  cells per well and made available to ligand at concentrations ranging from 0, 20, 40, 60, 80, and 100  $\mu$ M for 24 hrs. Followed by incubation and germination, the cells were cleaned with  $1 \times$  PBS two times followed by treating with solution of MTT (450  $\mu$ g/ml) continuously for a stretch of 3-4 hours at 37°C. The emerging formazan crystallines melted into solubilization buffer of MTT and transmittance were recorded at 570 nm by employing a spectrophotometer by comparing the value with control cells.

For statistical analyses to determine the differences between the treatment and control groups, Mann-Whitney U Test has been performed in post-hoc analyses ( $p \leq 0.05$ ).

## 2.3 Results and Discussions

### 2.3.1 Dynamic Light scattering (DLS) & Zeta Potential

The RG3-NPs displayed hydrodynamic property with a diameter of 197.8 nm (z-average size) and a polydispersity index (PDI) in zeta potential value of 0.251 as shown in Figure 2.2. The PDI values of the sample are much lower, indicating that they formed homogeneous solutions which are well conducive for biological applications. The RG3 nanoparticles exhibited a surface zeta potential of -31.8 mV. This high surface zeta potential indicates strong stability in aqueous solution. Hence, the stability is appreciable for biological solutions.

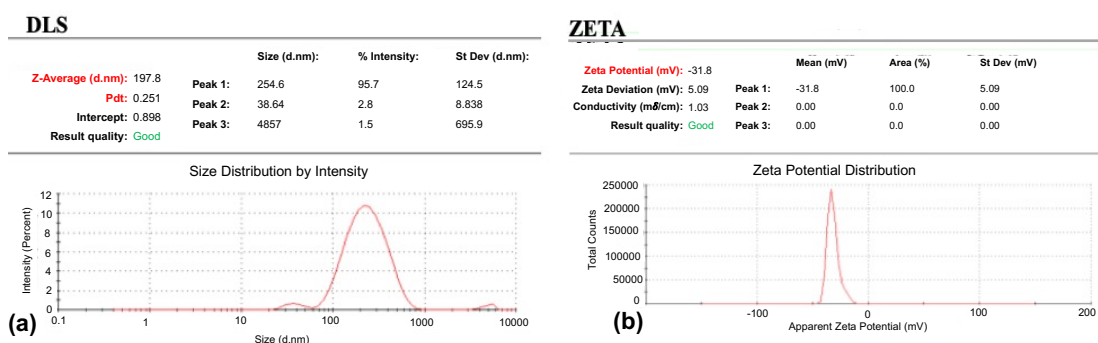


**Figure 2.2:** (a) Dynamic light scattering analysis; (b) Surface zeta potential of RG3-NPs

### 2.3.2 Scanning Electron Microscopy (SEM)

To investigate and analyse surface topography and also to determine average size of the AgNPs, SEM study were done which specifies different shape of the formed particles. The obtained green-combined AgNPs displayed the presence of polymorphism with respect to shapes like: flake type, spherical, and ellipsoidal. Also the images reveal few large particles that may be due to overlapping of one particle with another. The average dimensions of these green biosynthesized NPs were in

the scale of 35 nm – 65 nm respectively, as shown in Figure 5.1 where part (a) is for RG3-NPs and part (b) refers to the control sample with glucose.

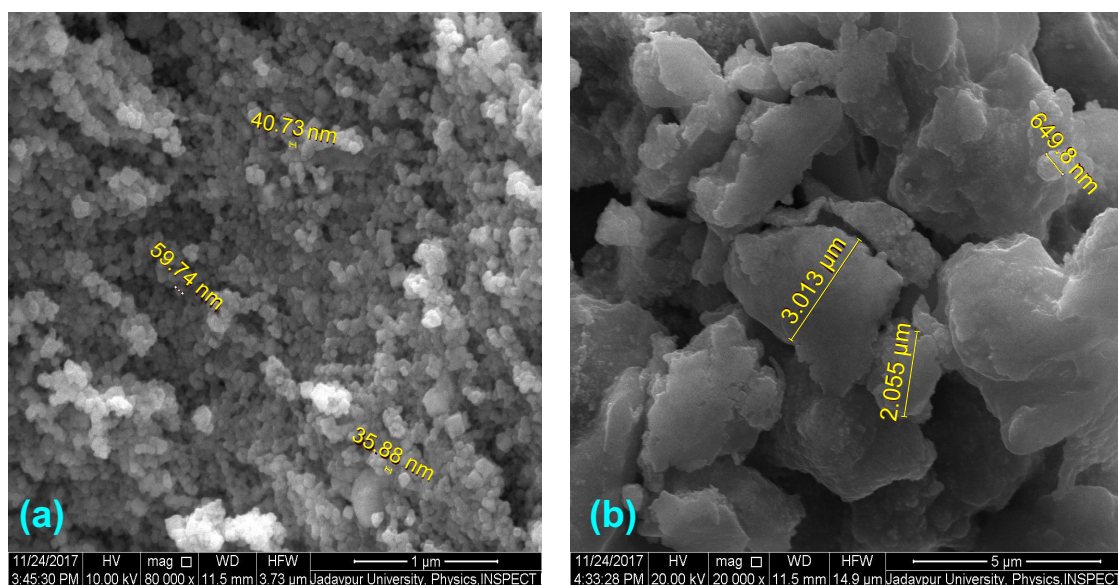


**Figure 2.3:** Surface morphology by scanning electron microscopy of (a) RG3-NPs and (b) Control sample

### 2.3.3 Transmission Electron Microscopy (TEM)

TEM inspection denotes nano-crystalline nature of the formed NPs and exhibits spherical morphology, which are often found to be agglomerated into small aggregates. The produced NPs were found to have an average size 20 nm, as shown in Figure 2.4. The TEM images also revealed a coated thin layer of glucose as the capping agent. Therefore, this can be used to explain the decent dispersion of NPs in the biologically reduced medium also in macroscopic scale.

### 2.3.4 FTIR Analysis

To investigate the possible mode of interaction of AgNPs with various functional groups, FTIR spectroscopy study were conducted. FTIR spectrum analysis indicates the existence of dissimilar functional classes at positional places, as shown in Figure 2.5a and Table 2.1. A stretch at  $1377\text{ cm}^{-1}$  pointed towards the symmetry stretched of a well known nitro compound which corresponds to the C-H bending of aldehyde groups, acquired from skeleton of glucose in aqueous medium [61]. The

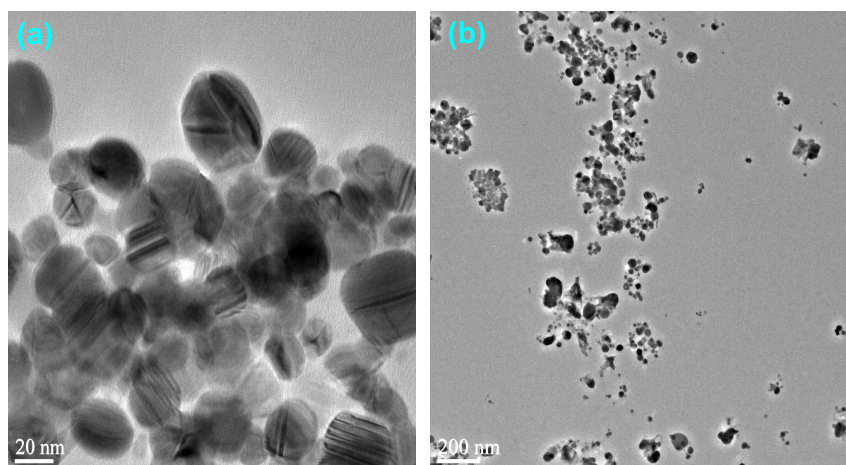


**Figure 2.4:** Transmission Electron Microscopy analysis of (a) RG3-NPs and (b) Control sample

indication of carbonyl group obtained at  $1635\text{ cm}^{-1}$  may be correlated to C–N and C–C stretching indicating protein existence and therefore directly indicates NPs formation [17]. Another well built symmetrical peak at  $2015\text{ cm}^{-1}$  were consonant to the O\C stretching mode [92]. Another powerful, fierce banding at  $2578\text{ cm}^{-1}$  can be allocated to both \NH2 in primary aromatic amines and \OH groups in alcohol [90]. The bands at  $3403\text{--}3799\text{ cm}^{-1}$  in the spectra are consistent with O–H stretching vibrations exhibiting alcohol and phenol.

From the above FTIR analysis, it can be well stated that the OH and C=O group present in glucose can be considered for the bio reduction of  $\text{Ag}^+$  ions foremost to Ag0 NPs formation. FTIR analysis further concludes the carbonyl group of amino acid remnants and peptides of the proteins shows greater affinity towards the metal ions. It thereby avoids agglomeration by establishing a safeguarding coat membrane and stabilizes them too. All peak changes here symbolize the contribution of functional groups to synthesize AgNPs.

### 2.3.5 UV-Vis Spectroscopy

For routine study of the optical properties particularly dependent on size effect and also for establishing metallic NPs, UV–Vis spectroscopy has been done [66]. The emergence and optimization of NPs were done by quantifying the absorbance in the span of 200–800 nm. Simultaneously, controlled set up was done by using only

**Table 2.1:** Table representing FTIR data of the synthesized RG3-NPs

Peak (cm <sup>-1</sup> )	Position	Mode of Vibration	Characteristics of Peak & Remarks	References
1377		Symmetry Stretching	Represents C-H bending mode of CH <sub>2</sub>	[61]
1635		Stretching	C=O correlated to C-N and C-C stretching indicates the presence of proteins (thus Nps)	[17]
2015		Symmetrical	O/C bands	[92]
2578		Symmetrical, bending	\NH <sub>2</sub> in primary aromatic amines and \OH groups in glucose	[90]
2731		Symmetrical, bending	-OH	
3403		Symmetrical & Assymetrical stretching	-OH	[24]
3799		Symmetrical, stretching	-OH	

glucose, AgNO<sub>3</sub>, and soup extract separately. At first for RG3<sup>T</sup>, the solution color changed from colourless to brownish yellow. Figure 2.5b shows the indication of the nanoparticle formation. Also the absorption peak for the RG3<sup>T</sup> was directed towards 440–400 nm and the location of the distinctive peak of absorption of biogenic AgNPs was found to be at 436, 422, 413, and 401 nm respectively. However, a prominent peak at 430 nm suggests the existence of AgNPs formation. The incident of absorption peak may be the anticipation of the Surface Plasmon Resonance (SPR) properties of metallic NPs that can be due to wavering of unbound electron on the top of the metallic NPs when they line up by resonance with respect to the wavelength exposed to radiation [131].

### 2.3.6 XRD

XRD is a direct approach to note the crystalline structure of the produced AgNPs. The result obtained, depicted in Figure 2.5c, clearly shows the significant peaks at ( $2\theta$ ) values of 38.39 and 44.87 which can be correlated to the (111) and (200) planes respectively [112, 99], where  $\theta$  is the half diffraction angle. By collation with JCPDS (file no: 89- 3722), the quintessential design of green-synthesized AgNPs can be established to have a leading structure [4]. The mean crystallite dimensions of the AgNPs evaluated using the diffractogram by calculating the Scherrer formula given by,  $D = K\lambda/(\beta\cos\theta)$ , where  $\lambda$  is the wavelength of the X-rays used for diffraction,  $K$  is a constant which is dependent on the crystal motif, and  $\beta$  is the full width at

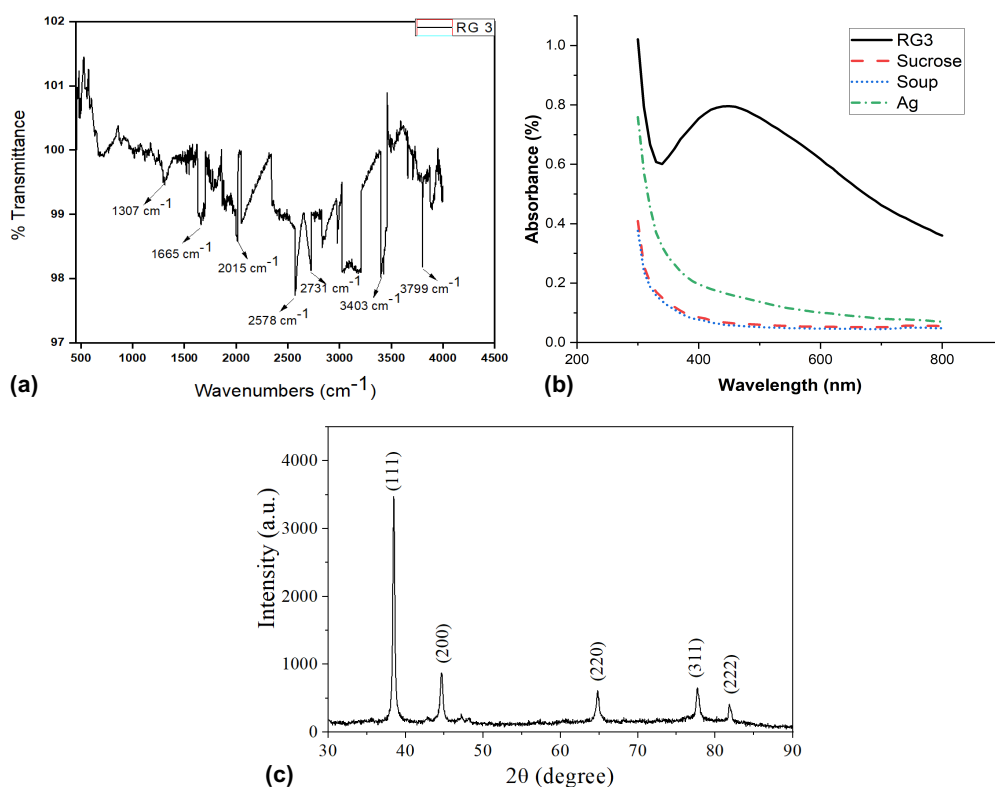


**Figure 2.5:** (a) FTIR spectrum analysis, (b) UV-Vis Spectroscopic study, and (c) XRD study of the synthesized RG3-NPs.

half maximum (FWHM) of a peak. The mean size and dimension of the particle obtained was 27 nm.

### 2.3.7 Antioxidant Activity

Biosynthesized AgNPs was tested for the unbound radical scavenging assay by using DPPH (2,2-diphenyl-2-picrylhydrazyl hydrate) and ABTS (2, 2'-azino-bis 3-ethylbenzthiazoline-6-sulfonic acid) assay according to the standard protocol [113, 100]. Different concentrations (10, 20, 40, 60, 80, and 100  $\mu\text{g}/\text{ml}$ ) was carried out for both the assay. The control sample was prepared without the addition of biosynthesized AgNPs. Ascorbic acid as the standard was used throughout the entire assay. The results procured are abridged in Table 2.2 and Figure 2.6.

It has been observed that the formed AgNPs possesses strong scavenging activity as compared to the controlled one. Also a shift in the scavenging activity was well noted with the increment of concentration in a quantity-dependent fashion. For the

DPPH assay, the set down scavenging activity was found to be lying between  $6.72 \pm 0.29$  at  $10 \mu\text{g/ml}$  to  $82.94 \pm 0.35$  at  $100 \mu\text{g/ml}$  with a mean  $\text{IC}_{50}$  value of  $53.76 \mu\text{g/ml}$  for the RG3-NPs. Simultaneously, scavenging activity were also observed when tested with ABTS assay. Here also a variety of concentrations ranging from 10 to  $100 \mu\text{g/ml}$  were used to observe the scavenging property. The lowest recorded scavenging property of RG3-NPs at  $10 \mu\text{g/ml}$  was found to be  $17.25 \pm 0.15$  to  $66.33 \pm 0.82$  at  $100 \mu\text{g/ml}$  with the average  $\text{IC}_{50}$  value of  $71.02 \mu\text{g/ml}$ . Using the Mann-Whitney U Test, the  $p$ -values for DPPH and ABTS assays were obtained to be 0.0142 and 0.0302 respectively ( $p \leq 0.05$ ). Thus, based on the results obtained by these two activities, we may say that our synthesized AgNPs from the bacteria RG3<sup>T</sup> is a potent antioxidant agent.

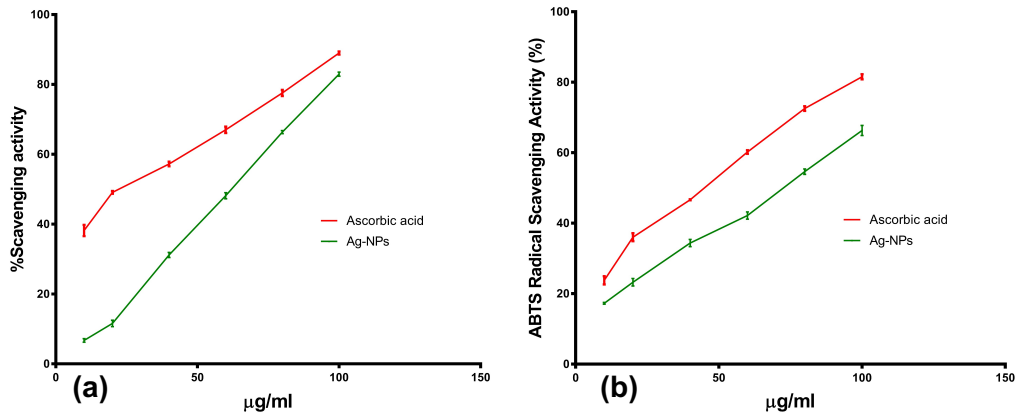


**Figure 2.6:** Antioxidant property analysis of RG3-NPs by (a) DPPH scavenging assay and (b) ABTS Radical Scavenging Activity assay

**Table 2.2:** Mean and SEM values of  $\text{IC}_{50}$  obtained from antioxidant activity

Method	Test Sample	$\text{IC}_{50}$ ( $\mu\text{g/ml}$ )	
		Mean	SEM
DPPH	Ascorbic Acid	27.09	0.83
	RG3-NPs	53.76	1.14
ABTS	Ascorbic Acid	46.16	0.33
	RG3-NPs	71.02	1.14

### 2.3.8 Antibacterial Activity

The synthesized RG3-NPs were tested for their antibacterial potency against few noted bacteria belonging to the Gram positive like *Staphylococcus aureus* ATCC



25923 and *Bacillus cereus* MTCC 430 & Gram negative origin strains such as *Escherichia coli* ATCC 25922, *Salmonella typhi* MTCC 98, *Shigella sonnei* MTCC and *Vibrio cholerae* N16961 using the colony count method, as shown in Figure 2.7. The antibacterial activity was done on the basis of concentration-dependent manner and it has been noted that with higher concentration, the efficiency of AgNPs increases. The concentration ranges from 0.5, 1, 2, 5, 10, 15, 25 and 50  $\mu\text{g/ml}$ . It can be predicted that for almost all the strains, 25–50  $\mu\text{g/ml}$  is the range where the maximal cell death occurs. The calculated IC 50 values of *S. sonnei*, *V. cholerae*, *B. cereus*, *S. typhi*, *E. coli*, *S. aureus* are 3.43, 2.12, 2.28, 3.67, 4.2 and 2.43  $\mu\text{g/ml}$  respectively as shown in Table 2.3. For all the strains, the efficiency of the synthesized AgNPs was noted in significant amounts. Our results clearly indicate greater efficiency of the produced NPs towards both the Gram Positive and Gram Negative strains.

For a long time silver has been best known for its contribution towards antibacterial effect [98]. Generally it is of the opinion that fitment of the AgNPs towards the cell membrane and its wall damages the intracellular bio-molecular structures occurred by itself AgNPs or its ions. Further they are also involved in oxidative stress that possibly associated in bacterial action of AgNPs. These mechanisms solely or conjointly intricate in action against bacteria. Moreover, silver being a Lewis acid is more prone to get attracted by a Lewis bases such as phosphorous and sulfur carrying bio-molecules which are the vital constituent of the cell membranes, DNA bases, and proteins [31, 11, 43]. Hence, it can be predicted that at first AgNPs pile up on the cell wall on then on the membrane producing predictable morphological changes, where decrement of the cytoplasm, membrane dis-integrity followed by eventual disruption of membrane by electron microscopy [91, 95, 45, 7, 52]. Also, the cations liberated from AgNPs may behave as a reservoir for  $\text{Ag}^+$  bactericidal agents [18].

The bio-green RG3-NPs displayed remarkable reaction towards all tested pathogenic bacteria subsequently followed by their anti-bacterial action indicated in Figure 8 and 9 for a sample Gram positive strain *Bacillus cereus* and Gram negative *Vibrio*

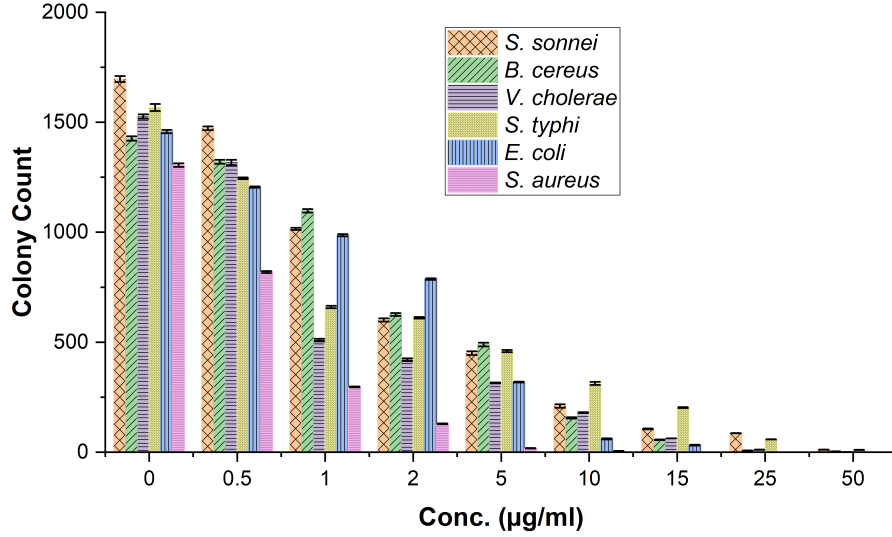


**Figure 2.7:** Colony count of each bacterial strain after being exposed to different concentrations of RG3-NPs

**Table 2.3:** Mean and SEM values of IC<sub>50</sub> obtained from antibacterial activity

S. No.	Bacteria	IC <sub>50</sub> (µg/ml)	
		Mean	SEM
1	<i>Escherichia coli</i>	4.20	0.75
2	<i>Salmonella typhi</i>	3.67	0.76
3	<i>Shigella sonnei</i>	3.43	0.65
4	<i>Bacillus cereus</i>	3.28	0.97
5	<i>Staphylococcus aureus</i>	2.43	0.97
6	<i>Vibrio cholerae</i>	2.12	0.81

*cholerae* respectively. It can be observed that as the concentration rises, the cell viability decreases. It is quite conventional that small sized NPs contains a higher surface zone and that additionally interacts to the bacterial cell in contrast to the large sized NPs [84]. Therefore, it can be concluded that RG3-NPs may be well utilized as an antibacterial agent.

### 2.3.9 Cytotoxic Activity

The anticancer properties of RG3-NPs were scrutinized on cancerous cell lines including HEPG-2, MCF-7, MDA-MB-468 using MTT assay. The cancer cells were subjected to different concentrations of these complexes for 24 hours. The LD<sub>50</sub> values of different cell line HEPG-2, MCF-7, and MDA-MB 468 was found to be 54.35, 55.78, and 52.76 µg/ml, as shown in Table 2.4. Cytotoxic levels for different concentrations were found to be significantly different from each other, based on

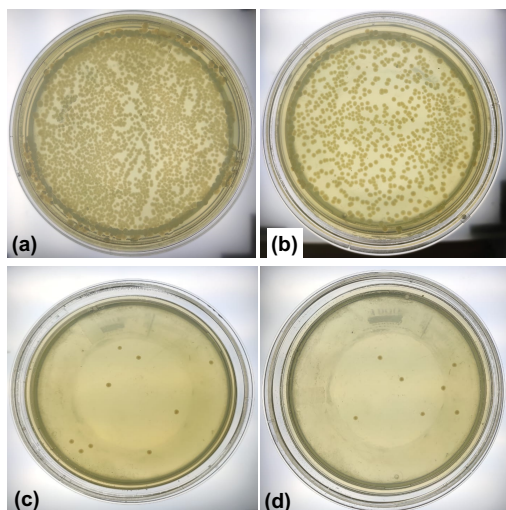


**Figure 2.8:** Bactericidal activities of RG3-NPs against sample Gram Positive strain *Bacillus cereus* at (a) 0 µg/ml (Control), (b) 5 µg/ml, (c) 25 µg/ml, and (d) 50 µg/ml

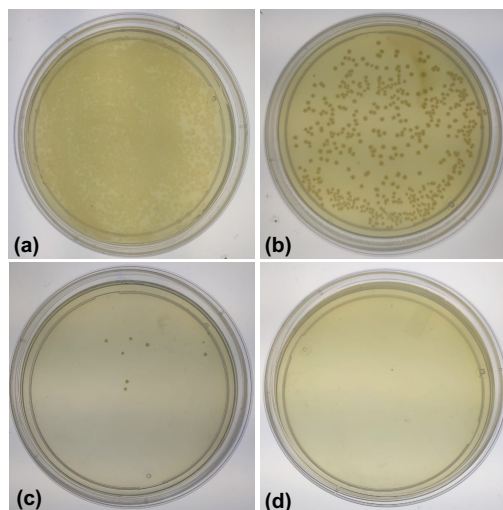


**Figure 2.9:** Bactericidal activities of RG3-NPs against sample Gram Negative strain *Vibrio cholerae* at (a) 0 µg/ml (Control), (b) 5 µg/ml, (c) 25 µg/ml, and (d) 50 µg/ml

Mann-Whitney U Test ( $p \leq 0.05$ ), as shown in Figure 5.6. The results prominently delineate that the cell practicability gets remarkably lowered in a dose-dependent approach and manifested outstandingly low LD50 value of 52.76 µg/ml for the MDA-MB 468 cell line. The specific attributes of LD50 values of the complexes are given in Table 2.4. In case of MDA-MD-468 cell line, where both estrogen and progesterone receptors are absent, the body cannot make sufficient amount of HER protein thereby promoting the growth of cancer cells in the body. The synthesized RG3-NPs showed good response by lowering those cancer cell lines potency.

**Table 2.4:** Mean and SEM values of LD50 obtained from cytotoxic activity

S. No.	Cell lines	LD50 (µg/ml)	
		Mean	SEM
1	HEPG-2	54.35	0.86
2	MCF-7	55.78	0.65
3	MDA-MB 468	52.76	0.74

## 2.4 Conclusions

In this study, a green route with innovation has been used to synthesize AgNPs by utilising a novel bacteria *Glucanoacetobacter kombuchae* (RG3<sup>T</sup>). The assessment of

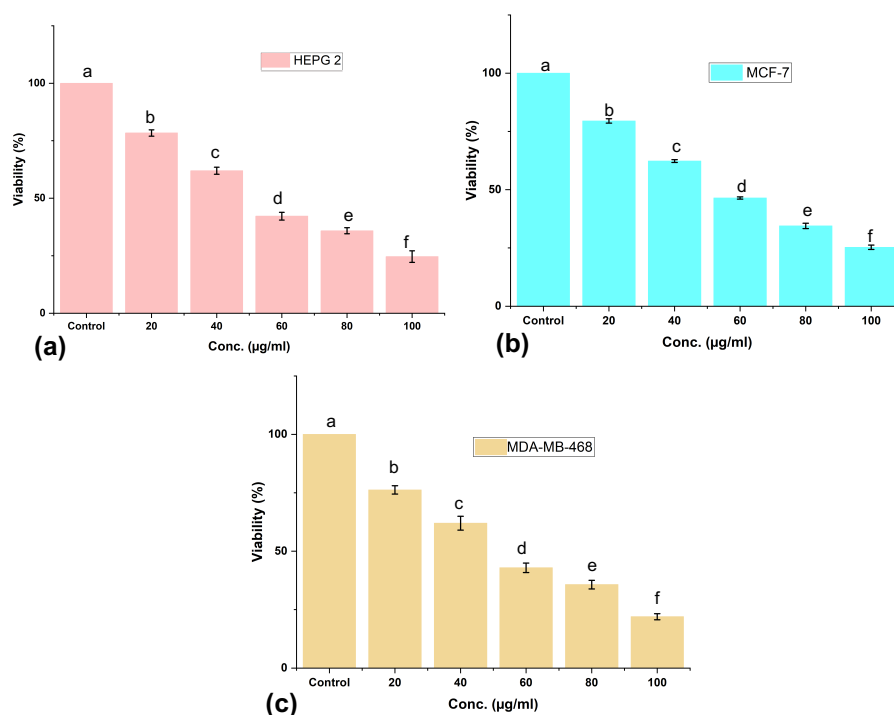


**Figure 2.10:** Cytotoxic effect of RG3-NPs (a) HEPG-2 hepatocellular carcinoma cell lines, (b) MCF-7 breast carcinoma cell lines, (c) MDA-MB-468 corresponds to Triple Negative Breast Cancer (TNBC) cell lines. The results are mean  $\pm$  SD from 3 independent experiments in each case. Values that share different letter have statistically significant difference between each other (Mann-Whitney U Test with  $p \leq 0.05$ )

RG3-NPs was done by obtaining physical characteristics like UV-Vis Spectroscopy, DLS, ZETA, SEM, TEM, XRD, and FTIR where it showed the stable nano size of 20 nm NPs with spherical shapes. The antimicrobial activity with few noted Gram positive strains like *B. cereus* and *S. aureus* and Gram negative strains like *V. cholerae*, *S. sonnei*, *S. typhi*, and *E. coli* were tested against NPs in different concentrations. The results clearly concluded that the synthesized NPs possess greater activity towards both the varieties. The antioxidant activity was tested by DPPH assay and ABTS assay. The scavenging activity was found to be lying between  $6.72 \pm 0.29$  at 10  $\mu\text{g/ml}$  to  $82.94 \pm 0.35$  at 100  $\mu\text{g/ml}$  with a mean IC<sub>50</sub> value of 53.76  $\mu\text{g/ml}$  for the RG3-NPs in DPPH activity. For ABTS assay, the lowest recorded scavenging property of RG3-NPs at 10  $\mu\text{g/ml}$  was found to be  $17.25 \pm 0.15$  to  $66.33 \pm 0.82$  at 100  $\mu\text{g/ml}$  with the average IC<sub>50</sub> value of 71.02  $\mu\text{g/ml}$ . The anti-carcereous effect of RG3-NPs shows promising results with LD<sub>50</sub> values of different cell line HEPG-2, MCF-7, and MDA-MB 468 was found to be 54.35, 55.78,

and 52.76  $\mu\text{g/ml}$ .

All the above features possessed by the bio-green synthesized AgNPs produced by the strain RG3<sup>T</sup> signifies itself to a potent antibacterial, antioxidant and cytotoxic agent. Further a deep interest is generated to analysing and explore for different applications which can be beneficial to the society. Also we are hopeful that this novel NPs can be utilized further in the various fields of science and technology.

## Chapter 3

# Efficient degradation of 4-nitrophenol and colorimetric detection of Fe (III) by biogenic silver nanoparticles of *Papiliotrema laurentii*

### 3.1 Introduction

Environmentally benign technologies in material science, particularly in nanotechnology studies, are gaining importance to meet the growing population's demand. Remarkably, the bio-green synthesis of nanoparticles has received significant attention and success in recent times. Although several nanoparticles serve well in nanotechnology and other fields, among them, silver nanoparticles are used largely due to their specific physical, chemical, and biological properties and application in the areas such as catalyst [22], photonics [79], micro-electronics [109], [134],[73],[72], antimicrobial activity [2], antioxidant and anticancerous activity [78] etc. The synthesis of metallic nanoparticles is an important factor in enhancing the potency

and practicability of the nanoparticles (NPs). Although there are a few notable methods for synthesis, among them, chemical, physical, and bio-inspired methods are commonly practiced. Out of these, bioinspired methods are gaining significant importance due to their non-toxic, non-hazardous, benign nature.

Owing to rapid industrialization and to full-fill the growing population demands, industrial effluents have become a serious threats to the environment. Industries such as textile discharge untreated effluents into the water bodies which normally constitute 80% of the total emissions produced by this industry [89]. There are high level of biochemical oxygen demand (BOD) and chemical oxygen demand (COD) in the residual waters of the textile industry. The color associated with textile dyes not only causes aesthetic damage to the water bodies but also prevents the penetration of light through water. This leads to a reduction in the rate of photosynthesis [46] and dissolved oxygen levels, affecting the entire aquatic biota [54]. The textile dyes act as toxic, mutagenic, and carcinogenic agents [10, 63, 126], that persist as environmental pollutants, and cross entire food chains favoring biomagnification. In this context, special mention should be made to organic textile dyes which, around 15–50%, do not bind to the fabric during the dyeing process and are released into wastewater which is commonly used in developing countries for the purpose of irrigation in agriculture [89]. 4-nitrophenol (4-NP) is one of the most notable phenolic dyes used in textile industries. However, 4-NP is a serious threat to the environment because of its carcinogenic, non-biodegradable properties. They are highly soluble and stable in aqueous solution [67]. Those dyes are often negative on soil microbial communities and on the germination and growth of plants [46].

The textile dyes are soluble organic compounds, especially those classified as reactive, direct, basic, and acids. Due to their high solubility in water, it is difficult to remove them by conventional methods such as adsorption involving carbon activation, flocculation, electro-coagulation, etc.[54]. Metal nanoparticles can be applied as catalysts for efficient degradation of organic dyes, particularly AgNPs [136]. On the other hand, the reduced form of 4-NP to 4-Aminophenols (4-AP) is less harmful

to the environment and this reduction can be done with a limited quantity of  $\text{NaBH}_4$  to achieve the best catalytic reaction [71]. Therefore, the process of bio-catalysis by AgNPs may be applied as an alternative green method to degrade 4-NP to 4-AP.

In recent years, AgNPs also play a vital role in the colorimetric detection of several harmful metals in both aquatic and biological environments [94], due to their strong SPR and optical properties depending on the size and shape. Various toxic metals ions like  $\text{Fe}^{2+}$ ,  $\text{Fe}^{3+}$  [102],  $\text{Hg}^{2+}$  [93],  $\text{Ni}^{2+}$  [101],  $\text{Cu}^{2+}$  [23],  $\text{Cr}^{2+}$  [59],  $\text{Pb}^{2+}$  [115],  $\text{Al}^{2+}$  [111],  $\text{Cd}^{2+}$  [33], etc. have already been successfully detected by AgNPs. Among these metal ions, iron metal contamination in water is the most common. Higher levels of iron in food and water may directly lead to hemoglobinopathy and can cause mild to severe damage in the vital organs of humans, like liver, pancreas, and heart, and in worst cases may lead to Alzheimer's and Parkinson's diseases [130]. AgNPs can be applied to address this problem by detecting and quantifying these metal ions, even at low concentrations. For colorimetric detection, the principal involved mainly is the change of colour or shift of the SPR band when the analyte binds to the catalysts [117]. The colorimetric sensing method by AgNPs provides a significant advantage over various other analytical sensitive instrumentations such as AAS, ICP-MS, XRF, etc., thereby making AgNPs more valuable and applicable in practical fields.

This study has been designed and applied to produce AgNPs using yeast cell resuspension or cell exudate from *Papiliotrema laurentii* strain Y24. Further, catalytic application for 4-NP degradation and colorimetric detection of Fe(III) ions from an aqueous medium has also been made. To the best of our knowledge, this is the first attempt to synthesize AgNPs using this yeast cell. *Papiliotrema laurentii* (formerly *Cryptococcus laurentii*) strain Y24 was isolated from Kombucha tea [26] in our laboratory [106] and deposited to Microbial Type Culture Collection of Chandigarh, India (MTCC 6930). Y24<sup>T</sup> belongs to the family of Rhynchogastremaceae. 4-NP has been selected in this study because of its role as a secondary pollutant from industries such as petroleum, textile, and manufacturing dye plants. Another



subject of study here is iron which is a common earth metal. Contamination of water by high iron content has been a serious threat worldwide, particularly in India. The nanoparticle synthesis process has been optimized and characterized with different instrumentation to obtain specific sizes, shapes, and characteristic features. Further, the performance of AgNPs with respect to their kinetic rate constants, stability, and reusability for the reduction of 4-NP in the presence of  $\text{NaBH}_4$  have also been investigated. Moreover, the applicability of AgNPs as a colorimetric sensor for Fe (III) determination has been demonstrated to obtain sensitivity and selectivity. Finally, real water testing was done successfully. In the remaining text, *Papiliotrema laurentii* has been mentioned as Y24<sup>T</sup> and Y24-AgNPs is referred to as Y24-NPs.

## 3.2 Materials and Methods

### 3.2.1 Chemicals & reagents

Chemicals namely, Silver Nitrate ( $\text{AgNO}_3$ , A.R. 99.9 %), Yeast Extract (Yeast Extract Powder. RM027), D-(+)-Glucose anhydrous, Peptone Type I, Bacteriological. RM667, Hydrochloric acid (HCl), Sodium Hydroxide (NaOH), p-Nitrophenol ( $\text{C}_6\text{H}_5\text{NO}_3$ ), Sodium Borohydride ( $\text{NaBH}_4$ ), other metal salts like Magnesium sulfate heptahydrate ( $\text{MgSO}_4 \cdot 7 \text{H}_2\text{O}$ ), Calcium sulfate ( $\text{CaSO}_4$ ), Copper (II) acetate monohydrate ( $\text{C}_4\text{H}_{10}\text{CuO}_5$ ), Nickel (II) chloride hexahydrate ( $\text{NiCl}_2 \cdot 6 \text{H}_2\text{O}$ ), ( $\text{K}_2\text{PtCl}_4$ ), Cobalt sulfate heptahydrate ( $\text{CoSO}_4 \cdot 7 \text{H}_2\text{O}$ ), Lead (II) nitrate, A.R. ( $\text{PbNO}_3$ ), Zinc Sulphate ( $\text{ZnSO}_4$ ), Iron (III) chloride anhydrous ( $\text{FeCl}_3$ ) were purchased from Himedia (Mumbai, India). Whatman filter paper No. 1 was purchased from Thomas Baker (Thomas Baker Chemicals, Pvt. Ltd. Mumbai, India). Deionized water was used throughout the entire experimentation procedure. All the above-mentioned reagents were of extra pure grade and therefore were used without any further purification.

### 3.2.2 Preparation of Y24 cell resuspension exudate

*Papiliotrema laurentii* (formerly *Cryptococcus laurentii*) strain Y24, deposited to Microbial Type Culture Collection of Chandigarh [106], India (MTCC 6930), was isolated from Kombucha tea [36]. Y24<sup>T</sup> was grown and maintained in modified YPD (Yeast, Peptone, Dextrose) media (Yeast extract 0.75%, Peptone 0.45%, Dextrose 2.5%, pH 5). 100 mL of YPD was made to grow with 50  $\mu$ L of the previous culture of Y24<sup>T</sup>, at 30°C under shaking condition at 120 rpm observed overnight. On the next day, the culture was centrifuged at 5000 rpm for 5 minutes and the pellet was collected and washed with deionized water twice to remove further impurities. This process was repeated twice. Then the washed cell pellet was resuspended with 100 mL deionized water and again kept overnight at 30°C under shaking conditions at 120 rpm. It was then centrifuged at 5000 rpm for 5 minutes and the pellet was discarded. The yeast cell resuspension exudate was collected in the form of a supernatant. The yeast cell resuspension exudate was stored at 4°C for further use [78].

### 3.2.3 Bio-green Synthesis of Silver nanoparticles from yeast cell resuspension exudate

The biogenic synthesis of AgNPs was done by adding AgNO<sub>3</sub> and the cell exudate of Y24 together in the concentration of 2 mM of AgNO<sub>3</sub> and 0.1 mM of dextrose and then observed for 45 minutes at room temperature. The glucose here in the bio-synthesis acts as a co-factor to enhance AgNPs formation along with Y24 cell exudate. The effects of temperature, reaction time, conc. of AgNO<sub>3</sub>, and conc. of glucose was further studied to optimize the formation of the nanoparticles. The formation of silver nanoparticles was noted by a change in the colour spectrum from colourless to brownish yellow as recognized by the naked eye. Further investigation was done by UV-Vis Spectroscopy, scanned in the range of 300-700 nm which showed a significant peak at around 430 nm, thereby confirming the nanoparticle formation. For further applications, nanoparticles were centrifuged at 10,000 rpm for 10 minutes

and washed twice with deionized water to remove unwanted impurities. The entire process of purification was repeated twice and vacuum dried (ELEVA speed Vac) and stored in dark for further use. The aqueous solution of Y24-NPs was used to carry out the catalytic reduction of 4-NP and colorimetric detection of Fe(III).

### 3.2.4 Characterization of Y24-NPs

The characteristics of the bio-synthesized nanoparticles were specified and validated using various instrumentation analyses. To detect the formation of the nanoparticle, UV-Vis Spectroscopy (HITACHI U 2900 / U 2910 UV VIS DOUBLE BEAM) was carried out in the range of 300 - 700 nm. Crystalline features of the green synthesized NPs were determined by XRD study (Rigaku, Miniflex). Surface structure analysis was performed by advanced microscopy instrumentations like SEM (Hitachi S-4500), TEM (JEM-2100 Electron Microscopy). To obtain information about the functional group that interacted to form the metallic NPs, FTIR (Shimadzu FTIR spectrophotometer (FTIR 8400) study was conducted in the ranges between 4000–400  $\text{cm}^{-1}$ . The precise size and charge distribution within the nanoparticles were examined with the help of DLS (Dynamic Light Scattering) and Zeta potential [ZETA Seizers Nanoseries (Malvern Instruments Nano ZS)]. To measure the concentrations of any elements, Atomic Absorption (AAS) study has been employed. (iCE 3500, Thermo Scientific, Germany)

### 3.2.5 Catalytic Activity

The catalysts (Y24-NPs) have been assessed against 4-NP degradation activity by optimizing different parameters. Firstly, to check the effect of different concentrations of  $\text{NaBH}_4$ , various concentrations of  $\text{NaBH}_4$  like 0.05 mM, 0.1 mM, 0.2 mM has been used along with 2 mM of AgNPs. Secondly, to assess the effect of 4-NP concentration on its reduction, different concentrations of 4-NP like 0.1 mM, 0.5 mM, 1 mM, 1.5 mM, and 2 mM was used along with AgNPs and  $\text{NaBH}_4$ . Thirdly, the effect on the catalyst's concentration has been studied using 1 mM, 1.5 mM,

2 mM, and 2.5 mM of AgNPs  $\text{NaBH}_4$ . Finally, the effect of reaction time is also observed from 0 to 8 minutes, Keeping the concentration of  $\text{NaBH}_4$  and AgNPs the same.

### 3.2.6 Colorimetric detection of Fe(III)

Initially, selectivity towards six different metal ions namely,  $\text{Fe}^{3+}$ ,  $\text{Zn}^{2+}$ ,  $\text{Ni}^{2+}$ ,  $\text{Mg}^{2+}$ ,  $\text{Ca}^{2+}$ , and  $\text{Cu}^{2+}$  with Y24-NPs was performed. UV-Vis Spectroscopy was done in the range of 300-600 nm to note the change if any. Further, to predict the sensitivity of the developed AgNPs-sensor, different concentrations of  $\text{Fe}^{3+}$  from the ranges between 5–3000  $\mu\text{M}$  were made to react with Y24-NPs solution and the SPR potency was determined. Quantitative determination of  $\text{Fe}^{3+}$  was done by increasing the concentration of  $\text{Fe}^{3+}$  from 0 to 3000 $\mu\text{M}$ . The resultants were scanned by UV-Vis Spectroscopy. To authenticate the feasibility of the detecting property of AgNPs, five tap water samples were mixed with different amounts of  $\text{Fe}^{3+}$  (5, 50, 120, and 210  $\mu\text{M}$ ) and studied. Further, Atomic Absorption Study (AAS) and the colorimetric sensor have been done to recheck and revalidate the quantity of  $\text{Fe}^{3+}$  ions.

## 3.3 Results and Discussions

### 3.3.1 Optimization of Synthesis Conditions

Different functional parameters including temperature, reaction time, metal ion concentrations, and glucose concentrations have been analysed to set up an optimal condition for nanoparticles formation. The concentrations of  $\text{AgNO}_3$  were fixed at 2 mM and the concentration of glucose was kept at 0.1 g with a total reaction time of 45 minutes. The temperature was kept constant at  $37^\circ\text{C}$  under dark conditions. These parameters were followed throughout all the experiments and for every experiment, control setups were also made and checked. The results obtained after each experiment were analysed and confirmed by UV-Vis Spectroscopy, DLS, and Zeta Potential respectively.

First, the reaction temperature was varied between 20°C to 45°C. At 45°C and 37°C, a prominent peak was noted at around 430 nm, as shown in Fig. 3.1(c). On the other hand, AgNPs formation at 20°C was very faint. It has been observed that the NPs tend to aggregate and agglomerate at that temperature, whereas it is more stable at 37°C. Therefore, the synthesis can be inferred to be green as it occurs at room temperature of 37°C, Fig. 3.1(c).

Second, the reaction time was varied between 5 minutes to 60 minutes, keeping other parameters intact. The synthesis was observed to be weak at 5 minutes; however, with the increase of reaction time from 10 minutes to 45 minutes, the rate of NPs production also increased, as shown in Fig 3.1(d). Beyond 45 minutes, there seems to be a rapid aggregation of NPs, making it more unstable. Therefore, the reaction time of 45 minutes has been considered in this study for Y24-NPs formation.

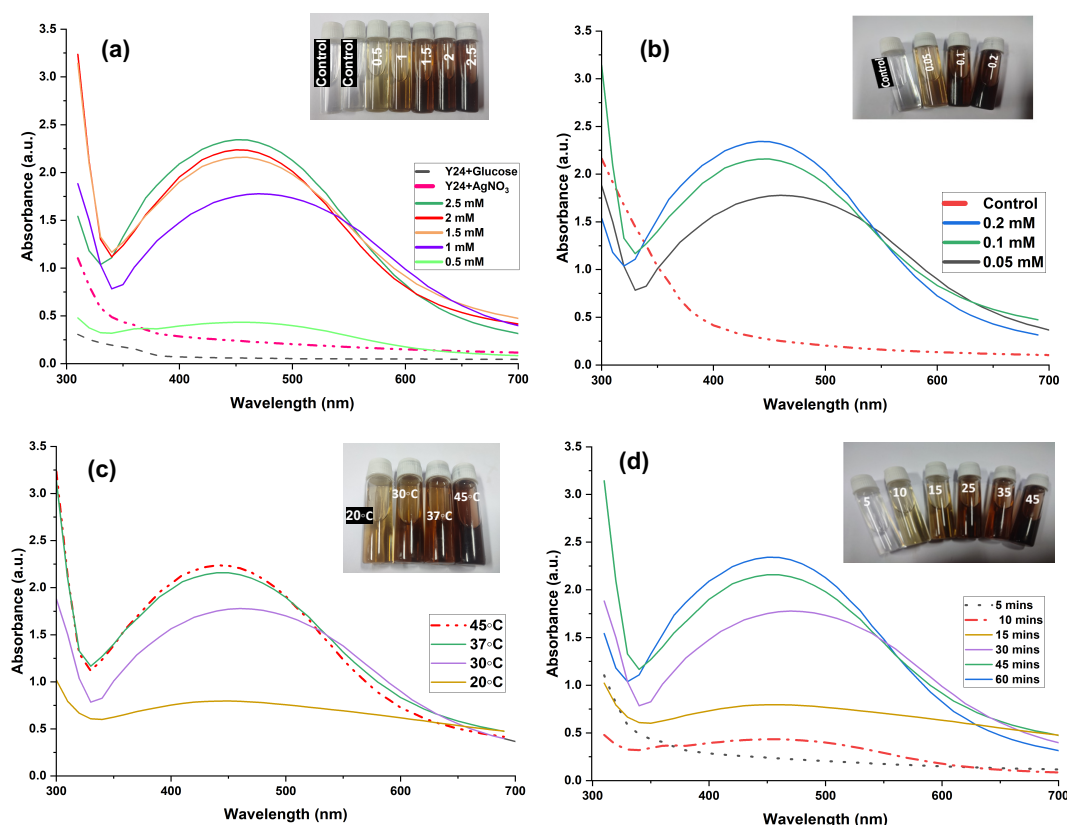


**Figure 3.1:** Optimization of Y24-NPs synthesis with reference to (a) Different conc. of  $\text{AgNO}_3$  with 0.1 g of glucose and observed for 45 minutes, (b) Different conc. of glucose with a fixed concentration of 2mM  $\text{AgNO}_3$  for 45 minutes, (c) Different temperature ranges starting from 20° to 37°, (d) Different reaction times varying from 5 to 60 minutes.

The metal ions and their concentrations are also crucial for the NPs formation.

The experiments were carried out by varying different concentrations of  $\text{AgNO}_3$  from 0.5 mM to 2.5 mM, keeping the other conditions constant. It was found that with the increase of  $\text{AgNO}_3$  concentration, the rate of reaction showed an increasing trend Fig. 3.1(a). However, at a concentration after 2 mM, aggregation of nanoparticles occurred, thereby suggesting 2 mM as the ideal  $\text{Ag}^+$  concentration for Y24-NPs formation.

After varying the reaction temperature, reaction time, and concentration of  $\text{Ag}^+$ , finally, glucose concentrations were also varied to optimize the biosynthesis of Ag-NPs. It has been observed that without glucose, only  $\text{AgNO}_3$  alone fails to contribute to nanoparticle formation, as shown in Fig. 3.1(b). However, when glucose was added along with  $\text{AgNO}_3$ , keeping the other parameters the same, nanoparticle formations occurred successfully. With the increase in glucose concentrations between 0.05 mM to 0.2 mM, the reaction rate increased. However, the synthesis seems to be stable at 0.1 mM of glucose.

### 3.3.2 Characterization of bio-synthesized AgNPs

#### Dynamic Light scattering (DLS) & Zeta Potential

The nanoparticle of strain Y24 reflected hydrodynamic features with a diameter of 385.3 nm (z-average size) (Fig. 3.2 b) and a polydispersity index (PDI) in zeta potential value of 0.547, as shown in Fig. 3.2(a). The PDI values of the sample were considerably low, showing that they produce homogeneous solutions which are favourable for biological applications. The nanoparticles manifested a surface zeta potential of -28.5 mV. This higher surface zeta potential stipulates strong steadiness in an aqueous solution. Therefore, the stability can be considered to be well-acknowledged for biological solutions. The neutral charge of Y24-AgNPs can possibly be due to the presence of negatively charged groups, such as  $-\text{OH}$  and  $-\text{COOH}$ , that encircles the nanoparticles. [75] [128].

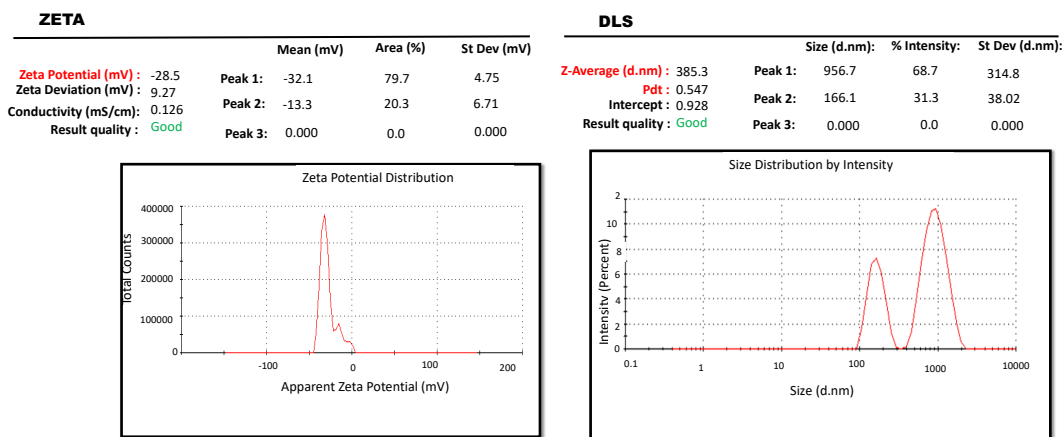


**Figure 3.2:** Y24-NPs analysis by (a) ZETA Potential; (b) DLS study.

## Scanning Electron Microscopy (SEM)

To analyze and investigate the exterior surface morphology and also to predict the average size of the AgNPs, SEM studies were performed to determine the variety of shapes of the produced nanoparticles. The obtained green-synthesized AgNPs reveals irregular to cubical shape. Some large particles were observed which may be the reason for the overlap of one particle with another. The average dimensions of these biosynthesized NPs were in the range of 20 nM – 35 nM respectively, as shown in Fig. 4.1. Here Fig. 4.1c shows Y24-NPs structural morphology and Fig. 4.1d shows the control sample of exudate with glucose only.

## Transmission Electron Microscopy (TEM)

TEM techniques are used to determine the particle shape with respect to size and morphology. An average size of 20 nM of nanoparticle was detected with glucose coated over the surface, as shown in Fig. 3.4a. Here, Fig. 3.4a denotes the TEM analysis of Y24-NPs, whereas Fig. 3.4b shows the control sample without AgNO<sub>3</sub>. Therefore, this indicates the fair dispersion of NPs in the biologically reduced medium, even on a macroscopic scale.

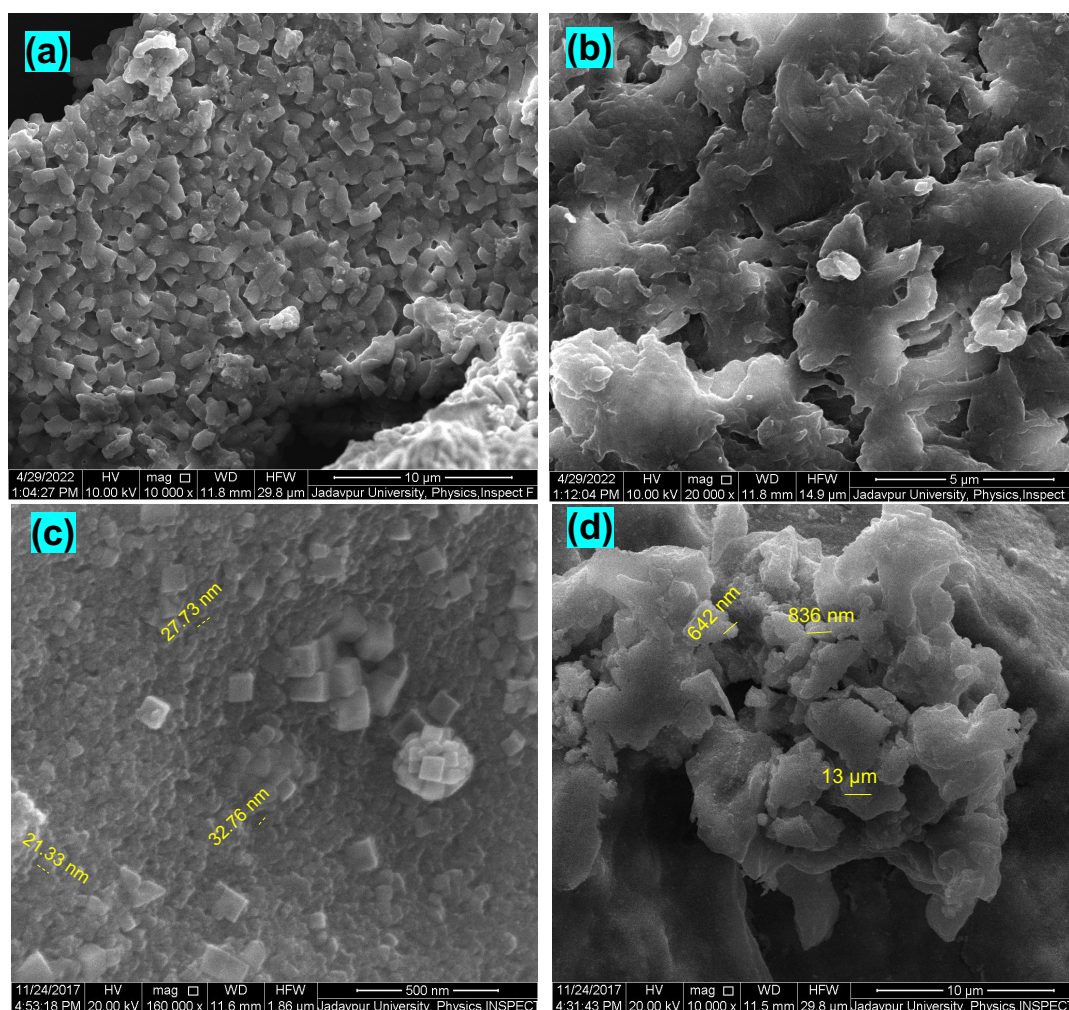


**Figure 3.3:** Microscopic Characterization of Y24-NPs by (a) FESEM imaging and (b) Control sample without AgNO<sub>3</sub>; (c) SEM imaging (d) Control image without AgNO<sub>3</sub>.

### FTIR Analysis

To comment on the possible manner of interaction of AgNPs with a variety of functional groups, FTIR spectroscopy studies were done. FTIR spectrum analysis signifies the presence of different functional groups at positional places, as shown in Fig.3.4c. The demarcation at  $1330\text{ cm}^{-1}$  directs concern about the symmetry stretch of a familiar nitro compound, which may be further linked to the C-H bending of aldehyde groups, possibly obtained from the skeleton of glucose in aqueous medium [61]. The demarcation of the carbonyl group that occurred at  $1637\text{ cm}^{-1}$  can be related to C-N and C-C bending, showing the existence of protein and thereby indicating NPs production. A well-built symmetrical peak at  $2849\text{ cm}^{-1}$  also relates to the aldehyde groups. Another powerful, fierce banding at  $2916\text{ cm}^{-1}$  can be



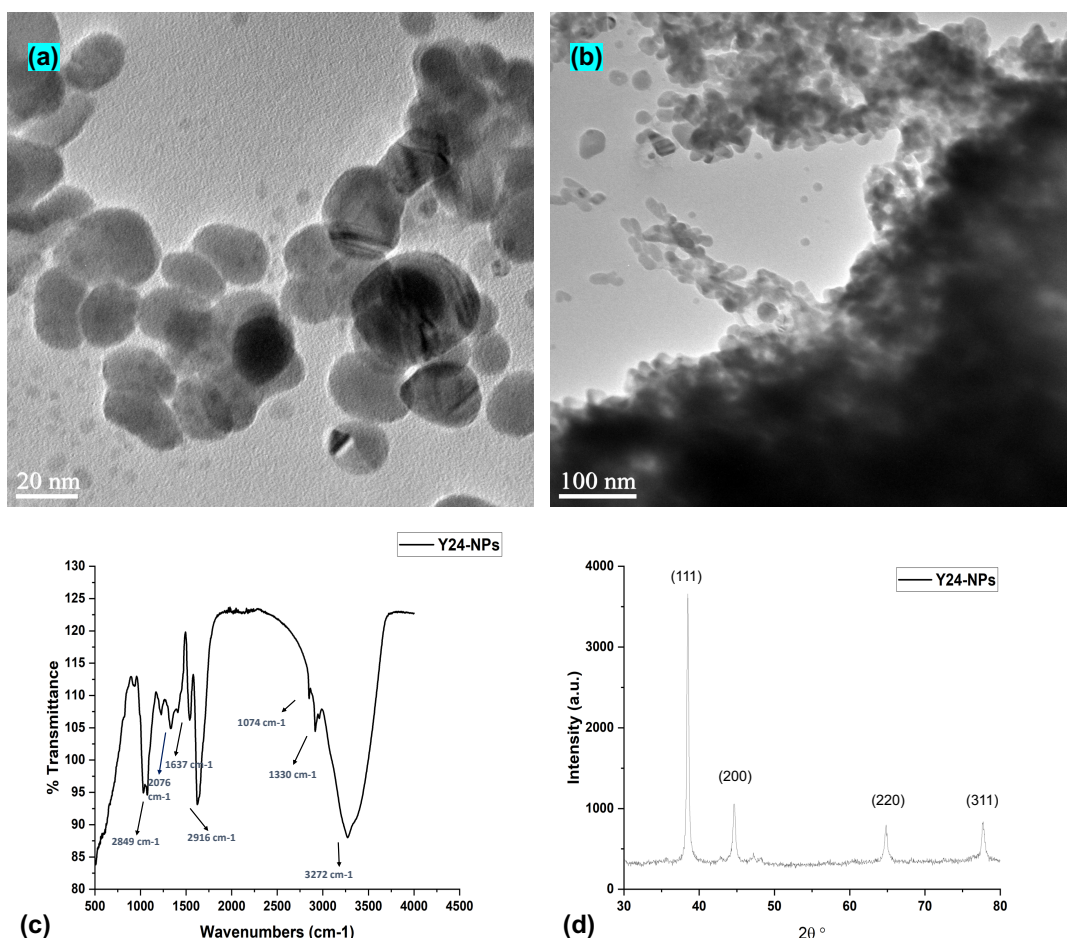


**Figure 3.4:** TEM analysis of (a) Y24-NPs and (b) Control sample without AgNO<sub>3</sub>; (c) FTIR study of Y24-NPs (d) XRD analysis of the biogenic nanoparticle.

assigned to dual  $\text{NH}_2$  in primary aromatic amines groups and  $\text{OH}$  groups in alcohol [108]. The bands at  $3272 \text{ cm}^{-1}$  in the spectral series are consonant to the O–H stretching vibrations predicting alcohol and phenol [108].

After the FTIR analysis, it may be well concluded that all the groups present are possibly responsible for the bioreduction of  $\text{Ag}^+$  ions to  $\text{Ag}^0$  in nanoparticle formation. Also, it may be concluded that the carbonyl group of amino acid residues and peptides of the proteins point towards the greater affinity with the metal ions. Therefore, these seem to prevent agglomeration by making a safeguard coat membrane and stabilizing them too. All peaks change here in Fig. 3.4c symbolize the presence of functional groups in synthesized AgNPs formation.

## XRD

To analyse and predict the crystalline morphology of the synthesized Y24-AgNPs, an XRD study has been carried out. In Fig. 3.4d, prominent peaks can be observed at  $(2\theta)$  values of 37.39, 43.88, 64.33, and 76.58 degrees which can be correlated to the (111), (200), (220), and (311) planes respectively [99], where  $\theta$  is the half diffraction angle. In correlation with JCPDS (file no: 89- 3722), the classical outline of bio green-synthesized AgNPs can be explained to contain a principal organization [2]. The mean average crystallite dimension of the AgNPs was determined using the diffractogram using the Scherrer formula:  $D = K\lambda/(\beta\cos\theta)$ , where  $\lambda$  is the wavelength of the X-rays used for diffraction,  $K$  is a constant which is dependent on the crystal motif, and  $\beta$  is the full width at half maximum (FWHM) of a peak. The mean size of the particle obtained was 20 nm.

### 3.3.3 Catalytic Activity

#### Conversion of 4-NP by Y24-AgNPs

The catalytic activity of the produced Y24-NPs from 4-Nitrophenol (4-NP) to 4-Aminophenol (4-AP) was explored in the presence of  $\text{NaBH}_4$ . This experiment is one of the significant mechanisms to evaluate the catalytic activities of metallic nanoparticles, particularly the ones generated from Pt, Ag, and Au [49]. Also, 4-NP has been selected as the subject model for the catalytic study because of its activity among other nitrophenols in different fields, such as dyes (particularly in the tannery for dark colouration), fabrication of fertilizers, explosives, rubber, pesticides, fungicides, etc. Being a common nitrophenol, this weak acid has got several toxic possibilities, for example, carcinogenic properties, non-biodegradability, and higher stability to persist in the environment. In addition to mild skin and eye irritability, this phenolic compound can seriously harm and cause injury to the central nervous system and other vital organs in the human body [126]. So, in order to nullify the toxicity of this phenolic compound, the transformation of 4-NP into 4-AP needs to be done. 4-AP is considered to be less harmful than 4-NP.

By considering the previously published works of conversion of 4-NP to 4-AP, we can divide the steps into three main stages, [10, 114]. The first stage involves the adsorption of the nitrophenols from the top of the AgNPs. The second step involves the transfer of electrons between nitrophenols and  $\text{NaBH}_4$  and its conversion to respective aminophenols. Finally, the aminophenols emerging from the top of AgNPs lead to the onset of the adsorption process, thereby making the surface of AgNPs ready for the new cycles [10, 114]. For these types of catalytic activities, it is important to note the following factors e.g., concentrations of the catalysts,  $\text{NaBH}_4$  (reducers), and the reaction times.

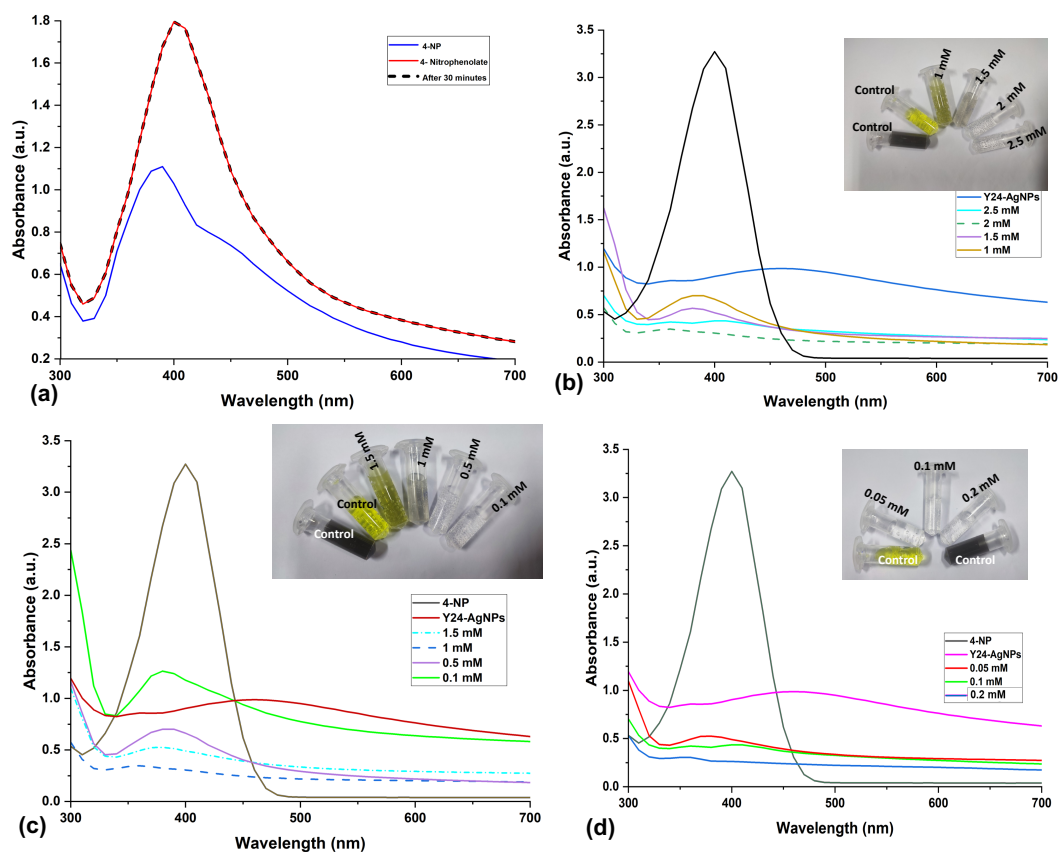


**Figure 3.5:** Catalytic reduction of 4-NP by Y24-NPs and estimation of its effects by other parameters like, (a) When only  $\text{NaBH}_4$  has been used without any catalysts and observed for 30 minutes, (b) Different conc. of catalysts (AgNPs) ranging from 1 mM, 1.5 mM, 2 mM, and 2.5 mM respectively (c) Different conc. of 4-NP like 0.1 mM, 0.5 mM, 1 mM, 1.5 mM, and 2 mM respectively, (d) Different conc. of  $\text{NaBH}_4$  ranging from 0.05 mM, 0.1 mM, 0.2 mM respectively. All the experimental set up were kept for 8 minutes.

#### *Effect of $\text{NaBH}_4$ concentration on 4-NP reduction:*

$\text{NaBH}_4$  is commonly used as a powerful reducing agent. It also plays a vital

role in the catalytic reduction of 4-NP. Initially, when  $\text{NaBH}_4$  is added to 4-NP, it induces a shift in the absorption peak from 380 nm to 420 nm, indicating the formation of 4-Nitrophenolate ions, as shown in Fig. 3.5a. This change also could be noted by the bare eye as the colour of the 4-NP solution changed from faint yellow to dark yellow colour on the inclusion of  $\text{NaBH}_4$ . The experimental setup was kept for observation and after 30 minutes, it was noted that there was no change in the absorption spectrum. Therefore,  $\text{NaBH}_4$  alone without the assistance of a catalyst is not sufficient enough to conduct the catalytic reduction of 4-NP. Also, the addition of the Y24-NPs alone to the 4-NP solution showed no change.

However, besides performing rapid reactions,  $\text{NaBH}_4$  may produce toxic effects at higher concentrations due to the presence of boron in it. Several studies have been performed with a higher concentration of  $\text{NaBH}_4$  than 4-NP to achieve a higher reaction rate and to get a perfect fit in the pseudo first-order reaction plot. According to the Environmental Protection Agency (EPA) and World Health Organization (WHO), the toxicity limit for boron is  $2.4 \mu\text{g mL}^{-1}$  [37, 70]. Although low concentration of  $\text{NaBH}_4$  results in a slower reaction rate, however, it can help to lower the toxicity produced by boron. Keeping this in mind, various concentrations of  $\text{NaBH}_4$  (0.05 mM, 0.1 mM, 0.2 mM) have been used in this study. For 0.1 mM and 0.2 mM, significant peaks were observed in the UV-Vis spectroscopy study, whereas a reduced peak was observed for 0.05 mM concentration, as shown in Fig. 3.5d. Therefore, considering the toxicity of boron at higher concentrations, the  $\text{NaBH}_4$  concentration has been fixed to 0.1 mM in this study. The other parameters, such as concentration of AgNPs and 4-NP have been kept constant at 2 mM and 1 mM, respectively, with a reaction time span of 8 minutes.

#### *Effect of AgNPs concentration on 4-NP reduction:*

The concentration of catalysts is an important factor to determine the rate of reaction. In this study, different concentrations of AgNPs have been used, including 1 mM, 1.5 mM, 2 mM, and 2.5 mM. At the end of the reaction, it was observed that the concentration of 2mM of AgNPs was best suited for the catalytic activity

because, for other concentrations, the reaction time was observed to be significantly longer, as shown in Fig. 3.5b.

*Effect of 4-NP concentration on 4-NP reduction:*

The effect of the reactant is also crucial for the catalytic reaction. In this study, this weak acid has been used as the benchmark to evaluate the catalytic activity of the metal nanoparticles. Different concentrations of 4-NP (0.1 mM, 0.5 mM, 1 mM, 1.5 mM, and 2 mM) have been used. At the end of the reaction, it has been observed that with a concentration of 1 mM of 4-NPs, the reaction occurred faster compared to the other concentrations. (Fig:3.5c).

*Effect of reaction time on 4-NP reduction:* In Fig. 3.6a, a graph of UV-Vis spectroscopy results has been plotted to show the progression of 4-NP in reaction with Y24-NPs from 0 minutes to 8 minutes. The result obtained indicates that a peak of 4-NP with Y24-NPs obtained at 400 nM remained unaltered even in presence of  $\text{NaBH}_4$ . Therefore,  $\text{NaBH}_4$  alone has no role in the reduction of 4-NP into 4-AP. After the addition of AgNPs, it has been observed that the peak gradually decreases with respect to the increase in the reaction time, thereby confirming successful degradation. The complete reduction was achieved quickly within 8 minutes.

The kinetics of this catalytic reaction can be obtained using the pseudo-first-order reaction:  $\ln(c/c_0) = -kt$ , where  $c_0$  is the original dye concentration (mg/L),  $c$  is the dye concentration (mg/L) with reference to time, and  $k$  is the rate constant (1/min). So, the reduction rate constant ( $k$ ) can be calculated from the plot of  $-\ln(A_t/A_0)$  versus reaction time  $t$ . From Fig. 3.6(b), the linear time-dependency of  $-\ln(A_t/A_0)$  can be clearly observed with a correlation coefficient  $R^2$  of 0.944, thereby authenticating the pseudo first-order kinetics reaction. The values from 2, 3, 4, 5, 6, 7, and 8 minutes were plotted to get the fit. The rate constant ( $k$ ) was found to be  $0.133 \text{ min}^{-1}$ , which shows that the rate of catalysis for Y24-NPs is significant.

*Possible mechanism of 4-NP reduction by AgNPs:*

One of the possible mechanisms of the biocatalysts (Y24-NPs) towards 4-NP reduction in the presence of  $\text{NaBH}_4$  is shown in Fig. 3.8. Since the nanoparticles

provide a large surface area, the reduction process can occur spontaneously there. Here, the catalyst Y24-NPs reacts instantly with the reducer ( $\text{NaBH}_4$ ). Simultaneously, the  $\text{BH}_4^-$  ions of  $\text{NaBH}_4$  get adsorbed onto the surface of the Y24-NPs and transfer hydrogen ions on the surface. Moreover,  $\text{BH}_4^-$  acts as an electron donor in the catalysis reaction. The substrate 4-NP similarly gets adsorbed onto the surface and is reduced by the  $\text{BH}_4^-$  to 4-AP. After the completion of the reduction process, the product (4-AP) leaves the surface of Ag and gets ready for the next catalytic cycle.

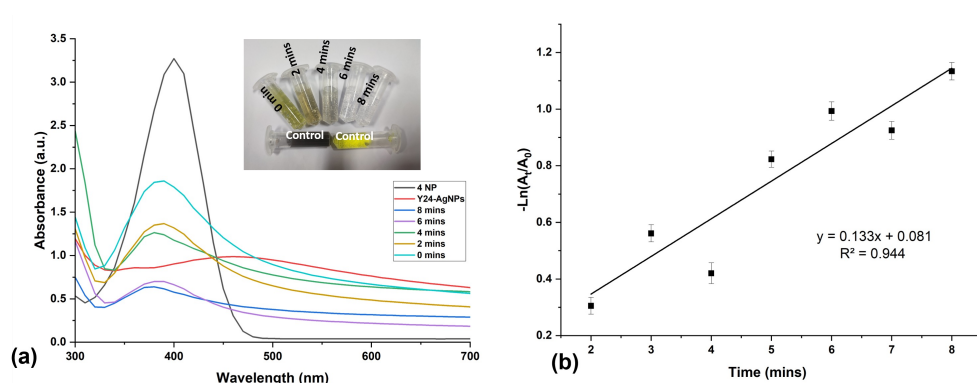


**Figure 3.6:** (a) Effect of reaction time in the catalytic degradation of 4-NP by Y24-NPs. The experimental setup was observed from the time period between 0 to 8 minutes, (b) First order-kinetic plot of 4-NP degradation by the catalysts for 2, 3, 4, 5, 6, 7, and 8 minutes respectively.

### Reusability of the catalysts:

For most metal-based catalysts, re-usability is an issue. To address this problem, catalyst evaluation was done by analyzing the structural stability and repeated re-usability of the bio-synthesized nanoparticle. In this study, five consecutive cycles have been carried out to assess the re-usability of the catalysts. Before each cycle, the catalysts were collected, washed thoroughly and dried for use in the next cycle. After five repeated cycles, UV-Vis Spectroscopy, (shown in Fig. 3.7a) was assessed in each cycle. It can be noted that there was a significant prominent peak at around 420 nm, which corresponds to the original UV-Vis Spectroscopy peak of Y24-NPs. The peak value for the other cycles remained at around 420 nm. Further, as we approached towards the final cycle, there was a slight deterioration in the absorption intensity,

although the peak remained more or less the same. This slight deterioration may be due to the aggregation of the dye molecules on the surface of the AgNPs. The conversion efficiency was noted above 94.46%. This higher efficiency of the catalysts strongly recommends its re-usability. The slight decrease in efficiency may be due to the process of collection and drying and degradation of the active site due to the adsorption of the by-products during the experimental procedure. The efficiency percentage ( $\alpha$ ) of the catalyst was calculated using the Equation given below

$$\alpha = \frac{C_0 - C_t}{C_0} \times 100$$

where  $C_0$  is the initial concentration and  $C_t$  is the concentration of 4-NP at the end stage.

As observed from Fig. 3.7, the efficiency was reduced by only 5.54% after 5 cycles. Initially, we conducted the catalyst efficiency tests for 7 cycles. The rate of reduction, however, didn't change significantly upto 5 cycles. This was also confirmed by UV-Vis spectroscopy, DLS, and ZETA Potential study. But a slight loss of catalyst was observed during the recovery process after each cycle. So, in order to minimize the loss of the catalyst, we kept the recycling procedure to 5 cycles only.

To confirm the efficiency of re-usability nature of the catalysts after 5 cycles, its structures have been assessed based on the TEM imaging, XRD pattern analysis, followed by Zeta Potential. The resulting catalysts after the TEM study (shown in Fig. 3.7c) showed average sizes in the range of 16-18 nM, which is almost similar to the original Y24-NPs TEM size (20 nM). XRD analysis (shown in Fig. 3.7d) was done to recheck the efficiency of the catalysts and it was found that the diffraction peaks occurred at  $2\theta$  values of 37.12, 43.28, 64.43, and 76.58 degrees for AgNPs. The unused Y24-NPs showed almost the same diffraction peaks at  $2\theta$  values of 37.12, 43.28, 64.43, and 76.58 degrees. Further, the catalyst's efficiency after Zeta Potential analysis showed a value of -19.4 mV, which is lower than the original value of Y24-NPs, which was -28.5 mV. This reduction in the Zeta Potential value could possibly be due to the increased adsorption of dye molecules from the surface of the

Ag<sup>+</sup> along with the simultaneous transfer of the hydrogen ions. Considering all the above facts from the structural analyses, it can be inferred that the catalysts can be highly stable with significant re-usability, which may be utilized in the practical field at a significantly lower cost.

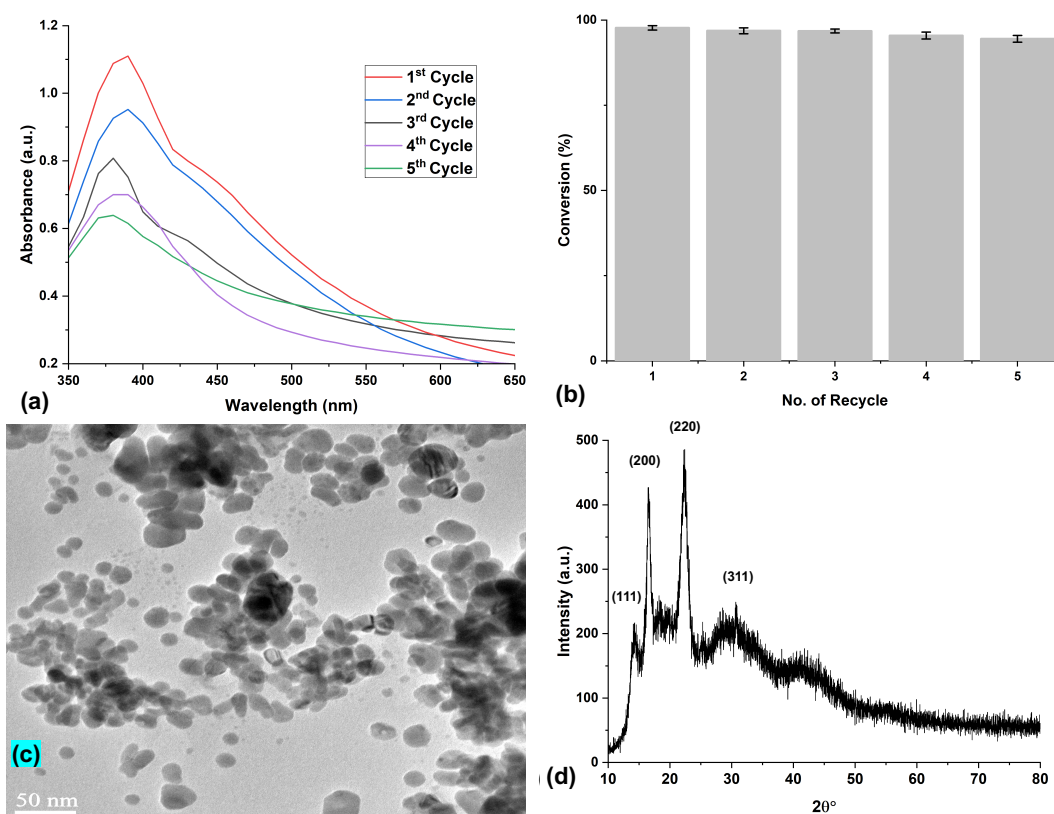


**Figure 3.7:** Reusability analysis of Y24-NPs after five repetitive cycles by (a) UV-Vis Spectroscopic analysis at each cycle, (b) Efficiency percentage of five successive cycles of the catalyst for reduction of 4-NP using NaBH<sub>4</sub>, (c) TEM analysis of the catalysts, (d) XRD pattern study of the catalysts after five consecutive cycles.

### Colorimetric detection of Fe(III)

Due to rapid industrialization, metal ion content in the ground and wastewater has become a serious threat to the ecology and environment. In order to address this problem, the detection and quantification of these metal ions at lower concentrations need to be focused on. Among the metal ions, iron metal contamination in water is the most common. Higher levels of iron in food and water may directly lead to haemoglobinopathy and can cause mild to severe damage in the vital organs of humans, like the liver, pancreas, and heart, and in worst cases may lead to



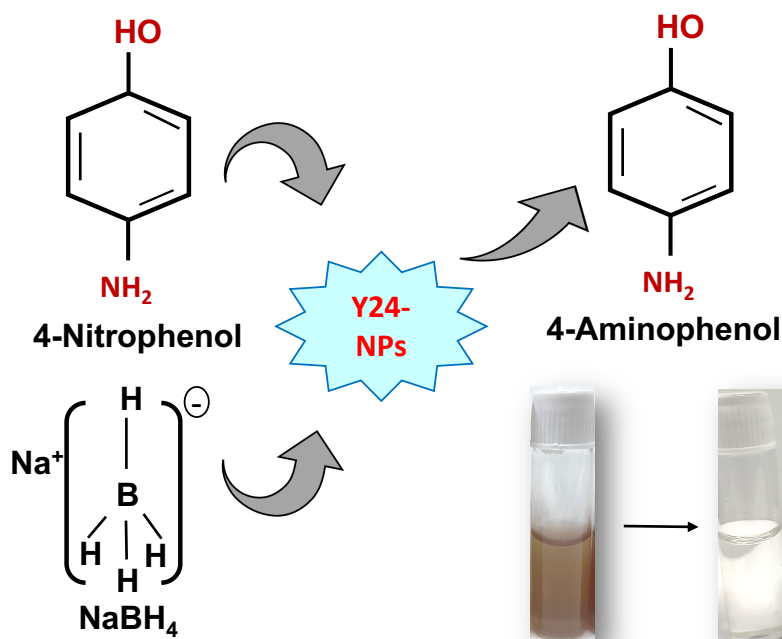


**Figure 3.8:** Possible mechanism of 4-NP degradation by the biogenic Y24-NPs by catalytic activity.

Alzheimer's and Parkinson's diseases [130], [135], [68]. Sometimes mild symptoms like nausea and vomiting are also very common. Therefore, in this study, among the other metals, iron has been specified for analysis. This study focuses on the use of bio-synthesized Y24-NPs as a probe for the detection of Fe<sup>3+</sup> ions.

#### *Selectivity and Sensitivity of Metal ions:*

Six different metal ions namely, Fe<sup>3+</sup>, Zn<sup>2+</sup>, Ni<sup>2+</sup>, Mg<sup>2+</sup>, Ca<sup>2+</sup>, and Cu<sup>2+</sup> have been tested with Y24-NPs for sensitivity and selectivity experiments. It was observed that with the addition of Ca<sup>2+</sup>, Ni<sup>2+</sup>, and Zn<sup>2+</sup>, there was a slight decrease in surface plasmon band, as observed by UV-Vis Spectroscopy in the range between 300-600 nm (Fig. 3.9a), while the colour remained unchanged. Meanwhile, there was a decline in the surface plasmon range along with the colour change from brownish yellow to colourless when Fe<sup>3+</sup> was introduced. Hence, the biosynthesized Y24-NPs show significant sensitivity to Fe<sup>3+</sup> metal ions and require further analysis for quantification and sensitivity assays.

In order to predict the sensitivity of the developed AgNPs-sensor, different concentrations of Fe<sup>3+</sup> from the ranges between 5–3000 µM were made to react with

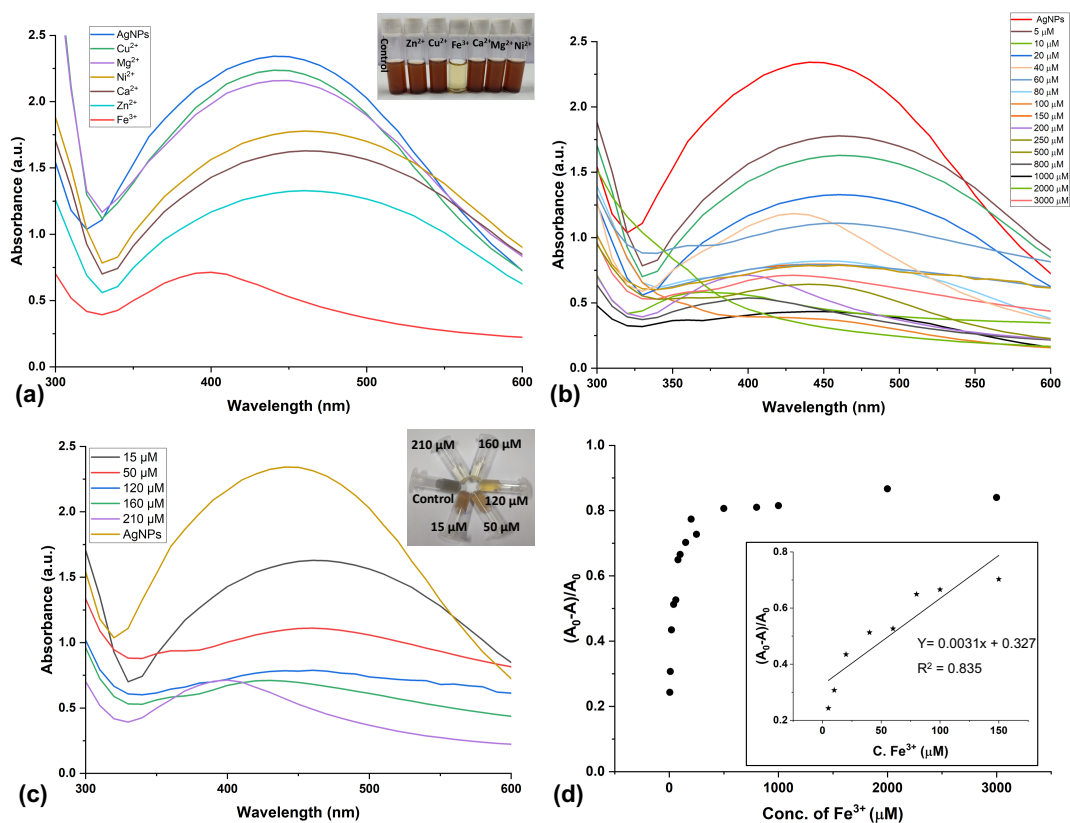


**Figure 3.9:** (a) Selectivity and sensitivity study by UV–Vis spectroscopic analysis of Y24-NPs solution in the presence of various metal ions, (b) UV-Vis Spectroscopic study of the quantitative determination of Fe(III) of different conc. ranging from 5 to 3000  $\mu\text{M}$  with the bio-catalysts, (c) To test in real water samples, different of conc. Fe(III) to analyse its absorbance intensity by Uv-Vis Spectroscopy, (d) The plot of sensitivity versus relative Fe(III) conc.

Y24-NPs solution and the SPR potency was determined. Fig. 3.9b shows a gradual decrease in the peak and low shift of direction of shorter wavelength when the concentration of  $\text{Fe}^{3+}$  increased from 5 to 800  $\mu\text{M}$ . This may be possibly due to the aggregation of nanoparticles and the chelation between the  $\text{Fe}^{3+}$  ions with AgNPs cluster.

#### *Quantitative determination of $\text{Fe}^{3+}$ ions*

$\text{Fe}^{3+}$  ion concentrations and the intensity of the surface plasmon range were measured to establish the quantification of  $\text{Fe}^{3+}$  ions. Fig. 3.9b shows that at concentrations of  $\text{Fe}^{3+}$  less than 1000  $\mu\text{M}$ , the cumulation of AgNPs occurred rapidly, as predicted by the diminishing of the band intensity. Fig. 3.9d describes the relative sensitivity plot of  $(A_0 - A)/A_0$  in comparison with  $\text{Fe}^{3+}$  concentrations between 0 to 3000  $\mu\text{M}$ , where  $A_0$  and  $A$  are the absorbance band for Y24-NPs surface plasmon

range band at zero and relative  $\text{Fe}^{3+}$  concentrations, respectively [42]. Throughout the entire tested  $\text{Fe}^{3+}$  concentration range, exponential relationship was observed. However, the linear relationship for the test was observed in the range of 5–150  $\mu\text{M}$ , which is interpreted by the regression equation  $(A_0 - A)/A_0 = 0.0031 [\text{Fe}^{3+}] + 0.327$  with a correlation coefficient of 0.835, as shown in Fig. 3.9d. The LOD value of the testing samples was predicted in accordance with the standard deviation method [104] and was obtained to be 1.8  $\mu\text{M}$ , which is below the maximum permissible level of  $\text{Fe}^{3+}$  (5.36  $\mu\text{M}$ ) in drinking water, as guided by the World Health Organization [60]. Thus Y24-NPs provide higher sensitivity towards the detection of the  $\text{Fe}^{3+}$  ions.

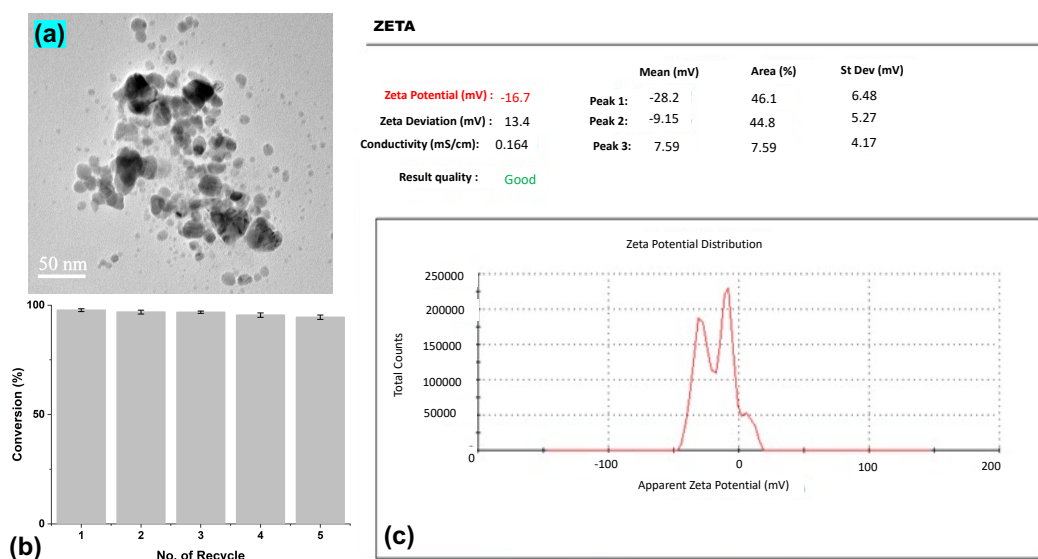


**Figure 3.10:** The catalysts after five cycles of repeated reuse have been analyzed for (a) TEM imaging of Y24-NPs solution after incubation in 120  $\mu\text{M}$   $\text{Fe}(\text{III})$  ions, (b) Efficiency percentage of five successive cycles of the catalyst for detection of  $\text{Fe}(\text{III})$ , and (c) Zeta Potential estimation analyse the catalysts after the reuse.

The entire process of colorimetric sensing was based on the principle of aggregation mechanism between AgNPs and  $\text{Fe}^{3+}$  ions. Aggregated nanoparticles generate signals of the shifted peak in the surface plasmon range as well as a change in the colour of the tested solution. These changes are observed with the help of UV-Vis Spectrometer and even noted by the naked eye too. Further, the aggregation mechanism between the NPs and the  $\text{Fe}^{3+}$  ions were analyzed by Zeta Potential and TEM study, shown in Fig. 3.10a. The Zeta Potential study of the Y24-NPs- $\text{Fe}^{3+}$  ions

showed a value of -16.7 mV which is lower than the Y24-NPs value (-28.5 mV), as shown in 3.10b. This decrease in value may be directly correlated to the aggregation between Y24-NPs and  $\text{Fe}^{3+}$  [117]. The Zeta Potential value is much lower than the absolute value in order to compensate for the negative charge of hydroxyl and carboxyl groups on the Y24-NPs surface by  $\text{Fe}^{3+}$  ions.[130]

#### *Test in real water samples*

To authenticate the feasibility of the discussed method, five tap water samples were mixed with different amounts of  $\text{Fe}^{3+}$  (5, 50, 120, and 210  $\mu\text{M}$ ) and studied, as shown in Fig. 3.9c. Further, Atomic Absorption Study (AAS) and the colorimetric sensor have been done to recheck and revalidate the quantity of  $\text{Fe}^{3+}$  ions and results are summarized in Table 4.3. The results clearly indicate that the nanoparticle-metal fabricated sensor provided high-accuracy measurements with the rate of recovery rate ranging from 98.7% to 100.3%. The result of AAS clearly indicated that concentrations in the tap water samples are proximate to AAS techniques. Therefore, the bio-synthesized Y24-AgNPs can be used as a highly precise colorimetric nanosensor for  $\text{Fe}^{3+}$  determination in water samples.

**Table 3.1:** Tap water quantification of  $\text{Fe}^{3+}$  at different concentrations using Y24-NPs.

Fe(III) Conc. ( $\mu\text{M}$ )	Determined Fe (III) Concentration ( $\mu\text{M}$ )		Recovery (%)
	AAS	Y24-NPs Assay	
15	$15.06 \pm 0.51$	$15.04 \pm 0.32$	100.3
50	$51.12 \pm 1.41$	$50.11 \pm 1.01$	100.2
120	$121.02 \pm 1.08$	$119.03 \pm 2.03$	99.2
160	$159.13 \pm 1.14$	$158.2 \pm 2.16$	98.9
210	$208.01 \pm 2.45$	$207.33 \pm 2.65$	98.7

#### **Sensing mechanism**

It was observed in the study that the increase in concentration of  $\text{Fe}_{3+}$  ions leads to decolorization of the AgNPs solution with SPR band quenching 3.9b. This could be correlated to the reduction in the quantity of AgNPs in the solution, which can be possibly due to the oxidation of  $\text{Ag}^0$  to  $\text{Ag}^+$  [123, 14]. Moreover, the visible

shift and widening of the SPR band on the inclusion of  $\text{Fe}^{3+}$  denotes the binding of  $\text{Fe}^{3+}$  ions to the AgNPs surface and stabilizes the nanoparticles, indicating the oxidation-reduction reaction between silver and iron ions [47]. [41] reported that AgNPs could be degraded by  $\text{Fe}^{3+}$  ions leading to a colorless solution of AgNPs and lowering the SPR band intensity. Some of the previous studies reported the catalysis of nanoparticles by the addition of a metal-oxidant such as  $\text{Fe}^{3+}$  and also simultaneously concluded a mechanism of the oxidation-reduction reaction between AgNPs and  $\text{Fe}^{3+}$  ions [64, 30, 48]. Therefore, on the basis of the previous reports and present studies, the detection mechanism of  $\text{Fe}^{3+}$  ions using Y24 stabilized AgNPs can be proposed as an oxidation-reduction reaction between AgNPs and  $\text{Fe}^{3+}$  ions, leading to the decomposition of AgNPs into  $\text{Ag}^+$  ions.

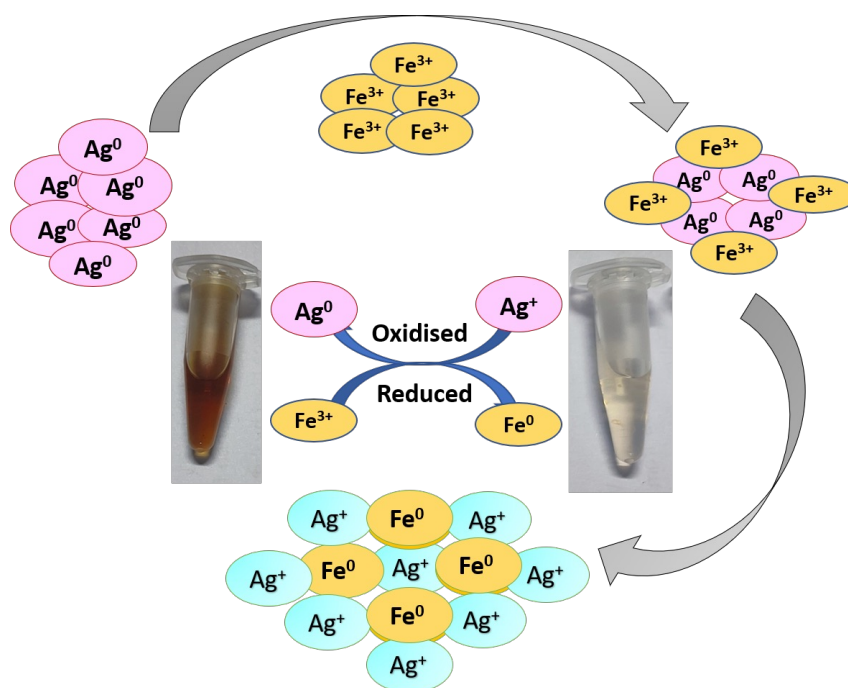


**Figure 3.11:** Possible colorimetric sensing mechanism by the biogenic Y24-NPs

### 3.4 Conclusions

The green synthesis of silver nanoparticles from a novel yeast strain, namely *Papiliotrema laurentii*(Y24<sup>T</sup>) has been performed. Different parameters have been varied to obtain optimal Y24-NPs. The morphological studies reveal its irregular to cubi-

cal shape with an average size of 20 nm. The analysis by XRD and FTIR reveals its monodispersity, different functional groups, and its interaction to stabilize the nanoparticles. The Zeta Potential study indicates a charge of -28.5 mV, which is considered as a good stabilized form of nanoparticles in an aqueous solution. In this study, two catalytic activities have been discussed using the catalyst Y24-NPs. For the catalytic degradation of 4-NP by Y24-NPs, the pseudo-first-order rate constant of 0.153 has been obtained and the reaction was completed within 8 minutes. Significant results have been obtained in the colorimetric detection of  $\text{Fe}^{3+}$  in a water sample with a LOD value of 1.8  $\mu\text{M}$ . Moreover, it was observed that even after five recycles, the catalyst Y24-NPs remains largely the same (reduced by 5.54% only after 5 recycles). These properties can be directly correlated to its recyclability and reusability. Therefore, the potent Y24-NPs prove themselves to be a significant catalytic agent with good reusability features, thereby being cost economic too.

## Chapter 4

# Effective degradation of azo dyes and colorimetric detection of $\text{Hg}^{2+}$ by biogenic silver nanoparticles of *Pichia manshurica*

### 4.1 Introduction

Environmentally cordial technologies are in great need in the field of material synthesis, and the biosynthesis of nanoparticles has received great attention too. The biogenic methods of synthesis that involves a variety of microorganisms like bacteria, fungi and actinomycetes, algae, and plant extracts are gaining importance as simple replacements to the chemical and physical methods. Studies showing synthesis from microbes such as yeasts are particularly important for the synthesis of inorganic nanoparticles (NPs) like Au and Ag. This can be directly attributed to the factor of versatility and survivability of the yeast species at higher concentrations of metallic ions [119]. Among the other nanoparticles, silver nanoparticles (AgNPs) are used largely due to its specified physical, chemical, and biological properties and application in the areas such as catalyst [38], photonics [79], micro-electronics [122],

and other activities like antimicrobial, antioxidant, anticancerous activities [78].

Due to rapid industrialization and to meet the growing population demands, industrial effluents have become a serious threat to the environment. The industries like textile, leather, paper, etc, release organic dyes in the form of their effluents [127]. Those dyes notably compromise the aesthetic quality of water bodies, thereby increasing the biological and chemical oxygen demand (BOD and COD), reducing the photosynthesis rate, and preventing plant growth and development [129]. Eventually, they enter the food chain, causing bioaccumulation that directly promotes toxicity, mutagenicity, and carcinogenicity. Among the notable organic dyes, commonly used in various fields are Congo red (CR) and Malachite green (MG) [32]. All these organic water-soluble dyes belong to the azo group. Azo dyes are the largest group of commercial dyes, including 70 % of the organic dyes generated in the world [38]. Congo red (CR) belongs to the benzidine-based anionic diazo dye and is responsible for causing allergic reactions by the metabolism of benzidine, which is a carcinogenic product [87]. Malachite green (MG) is a cationic water-soluble azo dye belonging to the triphenylmethane category. The toxicity of this dye depends on exposure time, temperature, and concentration. MG has been reported to cause carcinogenesis, mutagenesis, chromosomal fractures, teratogenicity, and respiratory toxicity [127]. They are also reported to cause serious harm to the central nervous system and other vital parts of the human body [27]. Both CR and MG has been selected as the subject model for the degradation study because of their wide utility among other azo dyes in different fields such as dying agent (particularly in textile, paper, and tannery industry), fabrication of fertilizers, rubber, pesticides, fungicides, staining of histological tissues, endospores, etc [9]. Therefore, the reduction of these dyes is important to address high environmental toxicity.

Azo dyes, being commercially important dyes, alone can contribute to almost 60% of water pollution. Degradation of these dyes is therefore much needed to restore the water quality and also to make it suitable for aquatic life. Bio-inspired green synthesized AgNPs provide one of the best solutions to the above-mentioned



problem. AgNPs, by their property, as potent absorbent [80], can be used as a catalyst [32] to degrade both CR and MG from the wastewater sources. In recent times, silver nanoparticles have been employed as catalysts in catalytic degradation of the harmful azo dyes [9]. Azo dyes successfully bind to the surface of the silver nanoparticles and due to reduction, they are reduced to produce the degraded product. The degraded products are chemically non-toxic and less harmful to the environment. Thereby AgNPs as nanocatalysts are more significant and applicable as biocatalysts in practical fields.

Heavy metals, mainly like  $\text{Pb}^{2+}$ ,  $\text{Cr}^{2+}$ ,  $\text{Ni}^{2+}$ ,  $\text{Cd}^{2+}$ ,  $\text{Mn}^{2+}$ ,  $\text{Hg}^{2+}$  are being released from the industry to the environment, which causes the hazardous effect to both humans and environment [32]. Among the other heavy metals, mercury is a persistent, bioaccumulative, toxic pollutant. Mercury may exist in three forms depending on the environmental condition, such as mercury salt, organic mercury, and inorganic mercury. Methyl mercury is the most toxic form of mercury and is responsible to cause tumors in the human body. Thereby, it enters the food chain by consumption of the methyl mercury accumulated fishes [8].

Several studies in recent times showed AgNPs to be a successful catalyst in the colorimetric detection of several harmful metals in both aquatic and biological environments [32, 103, 117]. A study conducted by [117], offers a solution to address  $\text{Hg}^{2+}$  contamination in an aqueous solution with the help of nanoparticle acting as a catalyst to colorimetrically detect and quantify the metal ions at low concentrations. The principle of colorimetric detection governs mainly the color change or shift of the SPR band when the analyte binds to the catalysts [93]. Moreover, colorimetric sensing deployed by AgNPs provides a significant advantage over various other analytically sensitive instrumentations such as AAS, ICP-MS, XRF, etc., [55, 119] thereby making silver nanoparticles more significant and applicable in practical fields.

The present study has been designed to biosynthesize AgNPs using yeast cell resuspension or cell exudate from *Pichia manshurica* strain CD1. CD1 belonging to

the phylum Ascomycota and subphylum Saccharomycotina. The GenBank accession number of the strain CD1 is KY799109. To the best of our knowledge, this is the first attempt to synthesize AgNPs using this yeast cell *Pichia manshurica*, strain CD1 have been extracted from Kombucha tea [25, 36]. The biogenic nanoparticle were applied as bio-catalysts to assess the catalytic property in azo dyes (Congo red and Malachite green) degradation and also to detect the presence of  $\text{Hg}^{2+}$  ion by colorimetric sensing. The azo dye degradation was done in much efficient time and the colorimetric detection were done at nano-molar level. Further quantification and real water sample testing were successfully performed. The nano-catalysts showed efficient reusability up to 5 cycles. The study therefore attempts to apply silver nanoparticles of *Pichia manshurica*, strain CD1 as a catalyst for bioremediation with practical utility. In the remaining text, *Pichia manshurica* has been mentioned as CD1<sup>T</sup> and CD1-AgNPs are referred to as CD1-NPs.

## 4.2 Materials and Methods

### 4.2.1 Chemicals & reagents

Chemicals required for the experimentation were as follows; Silver Nitrate ( $\text{AgNO}_3$ , A.R. 99.9 %), Yeast Extract (Yeast Extract Powder. RM027), D-(+)- Glucose anhydrous, Peptone Type I, Bacteriological. RM667, Hydrochloric acid (HCl), Sodium Hydroxide (NaOH), Sodium Borohydride ( $\text{NaBH}_4$ ), other metal salts like Magnesium sulfate heptahydrate ( $\text{MgSO}_4 \cdot 7 \text{H}_2\text{O}$ ), Calcium sulfate ( $\text{CaSO}_4$ ), Copper (II) acetate monohydrate ( $\text{C}_4\text{H}_{10}\text{CuO}_5$ ), Mercuric chloride ( $\text{HgCl}_2$ ), Manganese dioxide ( $\text{MnO}_2$ ), Zinc Sulphate ( $\text{ZnSO}_4$ ), were purchased from Hi-media (Mumbai, India). Whatman filter paper No. 1 was purchased from Thomas Baker (Thomas Baker Chemicals, Pvt. Ltd. Mumbai, India). De-ionized water has been used throughout the experimentation procedure. All the above-mentioned reagents were of extra pure grade and therefore were used without any further purification.

#### 4.2.2 Preparation of CD1 cell resuspension exudate

*Pichia manshurica* strain CD1 was isolated from Kombucha tea [25]. CD1 was grown and maintained in modified YPD (Yeast, Peptone, Dextrose) media (Yeast extract 0.75%, Peptone 0.45%, Dextrose 2.5%, pH 5). 100 ml of YPD broth were made to grow 50 µl of the previous culture of CD1, at 30°C under shaking condition at 120 rpm observed overnight. On the next day, the culture was centrifuged at 5000 rpm for 5 minutes and the pellet was collected and washed with de-ionized water twice to remove further impurities. This process was repeated twice. Then the washed cell pellet was resuspended with 100 ml de-ionized water and again kept overnight at 30°C under shaking conditions at 120 rpm. It was then centrifuged at 5000 rpm for 5 minutes and the pellet was discarded. The yeast cell resuspension exudate was collected in the form of a supernatant. The yeast cell resuspension exudate was stored at 4°C for further use.

#### 4.2.3 Bio-green synthesis of Silver nanoparticles from yeast cell resuspension exudate

The biogenic synthesis of AgNPs was done by the addition of AgNO<sub>3</sub> to the cell exudate of CD1 together in the concentration of 2 mM of AgNO<sub>3</sub> and 0.1 mM of dextrose and then observed for 45 minutes at room temperature. The dextrose here in this study acts as a co-factor to enhance AgNPs formation along with CD1 cell exudate. The effects of temperature, reaction time, concentration of AgNO<sub>3</sub>, and concentration of glucose was further studied to optimize the formation of the nanoparticles. The formation of silver nanoparticles was noted by a change in the color spectrum from colorless to brownish yellow as recognized by the naked eye. Further absorption measurements were done by UV-Vis Spectroscopy, by scanning in the range of 300-700 nm. For future applications, nanoparticles were centrifuged at 10,000 rpm for 10 minutes and washed twice with deionized water to remove any unwanted impurities. The entire process of purification was repeated twice and vacuum dried (ELEYA speed Vac) and stored in the dark for further use. The

aqueous solution of CD1-NPs was used to carry out the catalytic degradation and colorimetric detection.

#### **4.2.4 Characterization of CD1-NPs**

The characteristics of the bio-synthesized nanoparticles were specified and validated using various instrumentation analyses. To detect the formation of the nanoparticles, UV-Vis Spectroscopy (HITACHI U 2900 / U 2910 UV VIS DOUBLE BEAM) was carried out in the range of 300 - 700 nm. Crystalline features of the green synthesized NPs were determined by XRD study (Rigaku, Miniflex). Surface structure analysis was performed by advanced microscopy instrumentations like SEM (Hitachi S-4500), TEM (JEM-2100 Electron Microscopy). To obtain information about the functional group that interacted to form the metallic NPs, FTIR (Shimadzu FTIR spectrophotometer (FTIR 8400) study was conducted in the ranges between 4000–400  $\text{cm}^{-1}$ . The precise size and charge distribution within the nanoparticles were examined with the help of DLS (Dynamic Light Scattering) and Zeta potential [ZETA Seizers Nano series (Malvern Instruments Nano ZS)]. To measure the concentrations of any elements, Atomic Absorption (AAS) study has been employed (iCE 3500, Thermo Scientific, Germany).

#### **4.2.5 Optimization of AgNPs Synthesis Conditions**

Different parameters like the effect of temperature, reaction time, metal ion concentrations, and glucose concentrations have been varied to set up an optimal condition for nanoparticle formation. The optimized conditions for AgNPs were fixed as follows, 2 mM  $\text{AgNO}_3$ , 0.1 mM of glucose at 37°C temperature for 45 minutes under dark conditions. The above parameters were followed throughout all the experiments and for every experiment, control sets up were also made and checked. The results obtained after each experiment were analyzed and confirmed by UV-Vis Spectroscopy, DLS, and Zeta Potential respectively.

#### 4.2.6 Catalytic activity of CD1-NPs

##### *Degradation of Congo red (CR) and Malachite green (MG)*

CD1-NPs were tested for azo dyes degradation mainly by Congo red (CR) and Malachite green (MG) to test for the catalytic activity. The following parameters were considered while setting up the experiment, like firstly the effect of AgNPs concentration on CR and MG dyes reduction has been performed by varying different concentrations of AgNPs like 0.5 mM, 1 mM, and 1.5 mM along with a controlled sample containing only AgNPs solution and 0.1 mM of NaBH<sub>4</sub> were used. Secondly, the effect of the concentration of the reactant were studied since this is another important factor for the experiment. Here for both the dyes, the concentrations were used such as 0.5 mM, 1 mM, and 1.5 mM. Thirdly, pH has been varied in the range of pH 5, pH 7, and pH 9 to find the optimal results. Lastly, the reaction time of both dyes was observed. For CR dye a reaction time of 0 to 30 minutes and for MG dye a reaction time of 0 to 40 minutes has been observed.

In order to calculate the degradation efficiency of the catalysts in the degradation of both dyes, the following equation has been used :

$$\alpha = \frac{C_0 - C_t}{C_0} \times 100$$

where,

$\alpha$  = absorbance;  $C_0$  = initial concentration of the dye molecules;  $C_t$  = final concentration of the dye molecules at the end stage. [13]

##### *Catalytic degradation of the mixed dyes*

After individual dye activity was accessed, another set of experiments was carried out by mixing both the dyes (CR and MG) in the ratio of 1:1 concentration with 0.1 mM of NaBH<sub>4</sub> and 1.5 mM of the catalysts for the duration of 45 minutes.

#### **Colorimetric detection of Hg<sup>2+</sup> by CD1-NPs**

To predict the sensing ability of CD1-NPs, Colorimetric sensing was performed. To begin with the experiment, initially six different metal ions namely Fe<sup>3+</sup>, Zn<sup>2+</sup>,

$\text{Mn}^{2+}$ ,  $\text{Mg}^{2+}$ ,  $\text{Ca}^{2+}$ ,  $\text{Hg}^{2+}$ , and  $\text{Cu}^{2+}$  have been tested with CD1-NPs for the sensing assay. Further  $\text{Hg}^{2+}$  has been selected for both sensitivity and selectivity tests. For sensitivity tests  $\text{Hg}^{2+}$  concentrations were varied from 1 nM to 1 mM. For sensitivity measurement, 1 nM to 80 nM concentrations of  $\text{Hg}^{2+}$  were varied and experiments were performed. Further to test in real water samples, different concentrations of  $\text{Hg}^{2+}$  like, 25, 50, 75, and 100 nM were used.

## 4.3 Results and Discussions

### 4.3.1 Optimization of AgNPs Synthesis Conditions

In order to optimize the biogenic AgNPs, initially, at first, the temperatures were varied ranging from 20°C to 45°C. At 45°C and 37°C, a prominent peak was noted at around 430 nm. AgNPs formation at 20°C was indistinct. It has been observed that the NPs tend to aggregate and agglomerate at that temperature, whereas the NPs were found to be more stable at 37°C. Simultaneously, another intense peak was noted at 30°C, but the peak at 37°C was found to be more stable. Therefore, the synthesis can be inferred to be green as it occurs at a room temperature of 37°C.

Secondly, the various reaction times and their effects on nanoparticle formation in the time span between 5 minutes to 30 minutes were conducted, considering the other parameters fixed. At 5 minutes, the synthesis was poor but however, with the increasing reaction time from 10 minutes to 25 minutes, the rate of production of NPs also increased, as shown in Figure 3.1b. Beyond 30 minutes, there seems to be a rapid aggregation of NPs, making it more unstable. Therefore, the reaction time of 30 minutes has been considered for CD1-NPs formation.

For the successful formation of nanoparticles, metal ions, and their concentrations are important. The experiments were conducted by a different variety of concentrations of  $\text{AgNO}_3$  ranging from 1 mM to 2.5 mM, keeping the other parameters constant. It was found that with increasing concentration, the rate of reaction was rapid. However, at a concentration after 2 mM, aggregation of nanoparticles occurs.

The stable also seems to be low by increasing the concentrations beyond 2 mM, thereby suggesting 2 mM as the ideal Ag<sup>+</sup> concentration for CD1-NPs formation.

After varying with temperature, reaction time, and concentration of Ag<sup>+</sup>, finally, glucose concentrations were also varied to optimize. It has been observed that without glucose, only AgNO<sub>3</sub> alone fails to contribute to nanoparticle production. However, when glucose was added along with AgNO<sub>3</sub> keeping the other parameters like the temperature set at 37°C, the concentration of AgNO<sub>3</sub> of 2 mM with a pH of 7, distinct nanoparticle formation occurred. Although with the rise in glucose concentrations between 0.05 mM to 0.2 mM, reactions were rapid, it seems to be stable at 0.1 mM of glucose. Therefore, after the experiments it were concluded that the CD1-NPs formation best occurred at a Temperature of 37°C, with a pH of 7 following 2 mM of AgNO<sub>3</sub> along with 0.1 mM of glucose.

### **4.3.2 Characterization of bio-synthesized AgNPs**

#### **Dynamic Light scattering (DLS) & Zeta Potential**

The nanoparticles produced by the yeast strain CD1 exhibited hydrodynamic features pointing to a diameter of about 199.5 nm (z-average size). The polydispersity index (PDI) value was found to be 0.279. The relatively much lower PDI value in the tested sample indicates the homogeneous nature that is well suited to apply in biological fields.

The nanoparticles showed a surface zeta potential of -27.4 mV. This value can be directly correlated to the wilful steadiness of the biogenic nanoparticles in an aqueous solution. Hence the stability may be well acknowledged for the biological solutions.

#### **Scanning Electron Microscopy (SEM)**

SEM studies were performed to analyze and investigate the outer surface morphology. SEM determines the shapes and predicts the average size of the produced NPs. The biogenic CD1-NPs revealed spherical morphology. The presence of some large

particles was observed which may be co-related to the overlapping of a particle with another particle. 20 nM – 40 nM are the average dimensions of the biogenic NPs, as shown in (Figure4.1b).

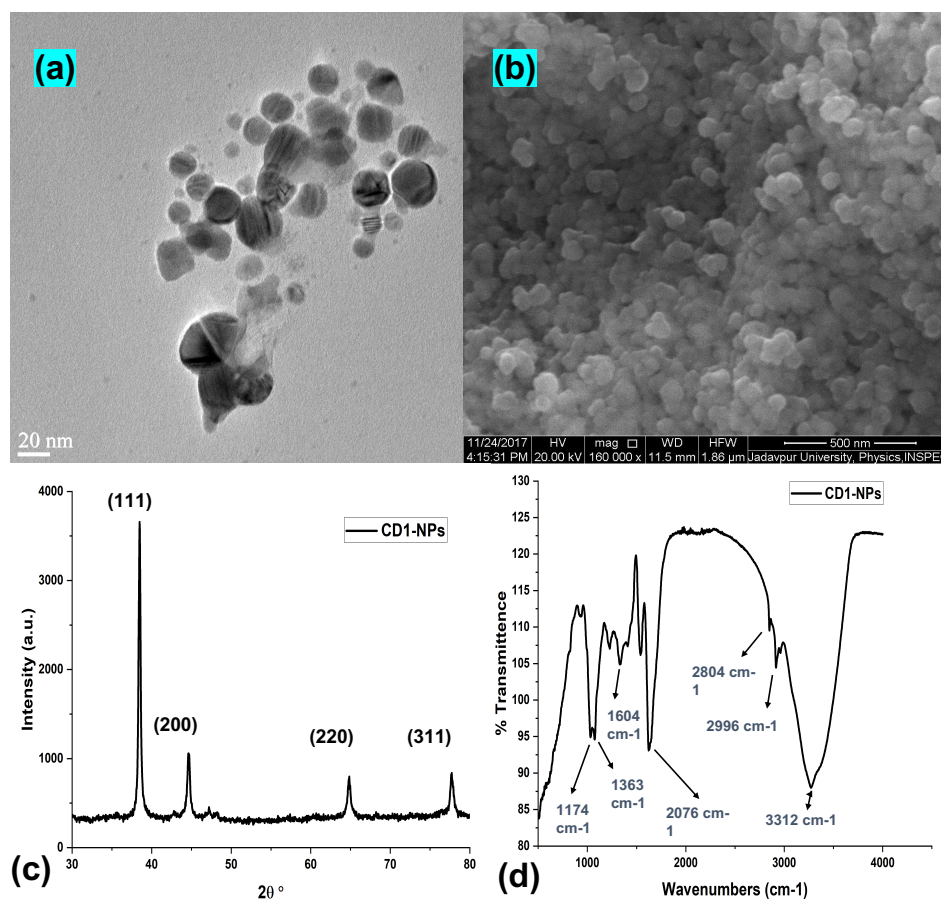


**Figure 4.1:** (a) TEM analysis, and (b) SEM analysis of CD1-NPs, (c) XRD study, and (d) FTIR analysis of the nanoparticles.

### Transmission Electron Microscopy (TEM)

TEM studies determine the particle shape with respect to size and morphology. An average size of 22 nM, Figure 4.1a, was detected with a coating of glucose on the top of the surface. Therefore, this study denotes the stable dissipation of NPs in the biologically reduced medium.

### FTIR Analysis

To analyse and predict the realizable pattern of interactivity of AgNPs with many different functional groups, FTIR spectroscopy studies were performed. FTIR anal-



ysis points to the presence of different functional groups at positional places, as shown in, Figure 4.1d. The sharp distinction at  $1363\text{ cm}^{-1}$  directs to the symmetrical stretch of a related nitro compound, which further may be linked to the C-H bending of aldehyde groups [61], that possibly obtained from the structure of glucose in an aqueous medium. The variety of the carbonyl group occurring at  $1604\text{ cm}^{-1}$  is to be related to C-N [17], and C-C bending, exhibiting the existence of protein and therefore may be correlated to the NPs production. A well-constructed symmetrical peak at  $2804\text{ cm}^{-1}$  also contributes to the aldehyde groups [90]. Another prominent, banding at  $2996\text{ cm}^{-1}$ , can be assigned to both the NH<sub>2</sub> in primary aromatic amine groups and OH groups in alcohol. The bands at  $3312\text{ cm}^{-1}$  are in accordance with the O-H stretching vibrations concluding alcohol and phenol groups [90].

FTIR analysis indicates that the interaction between all the above-mentioned groups is possibly responsible for the bio-reduction of Ag<sup>+</sup> ions to Ag<sup>0</sup> in nanoparticle formation. Further, it may be concluded that the carbonyl group of amino acid residues and peptides of the protein points to considerable affinity towards the metal ions. Therefore, these seem to prevent agglomeration by creating a coated membrane and balancing them too. Every peak changes here in Figure 4.1d, are to signify the presence of functional groups in synthesized AgNPs formation.

## XRD

XRD studies provide ideas about the crystalline morphology of the biogenic AgNPs. In Figure 4.1c, prominent peaks can be observed at  $(2\theta)$  values of 37.38 and 43.88 which can be related to the (111) and (200) planes respectively, where  $\theta$  is the half diffraction angle. In correlation with JCPDS (file no: 89- 3722), the classical outline of bio-genic CD1-NPs can be explained to contain a principal organization. The mean average crystallite dimensions of the AgNPs were determined by using the diffractogram using the Scherrer formula as,  $D = K\lambda/(\beta\cos\theta)$ , where  $\lambda$  is the wavelength of the X-rays used for diffraction, K is a constant which is dependent on the crystal motif, and  $\beta$  is the full width at half maximum (FWHM) of a peak.

The mean size and dimension of the particle obtained was 22 nm.

### 4.3.3 Catalytic Activity

#### Degradation of Congo Red and Malachite Green by CD1-AgNPs

Both Congo red (CR) and Malachite green (MG) has been selected as the subject model for the degradation study because of their wide utility among the other azo dyes in different fields also have been reported to cause various severe toxicity. Therefore, in order to mitigate their toxicity, effective, smart, and, environmentally cordial degradation by silver nanoparticles in the presence of  $\text{NaBH}_4$  have been performed. The catalytic degradation of these azo dyes by biogenic CD1-NPs has been determined initially spectrophotometrically under various experimental parameters. The azo bonds of both the dyes on degradation produce a variety of aromatic amine products. Practically, the reduction of these dye molecules in aqueous media is not possible without sodium borohydride ( $\text{NaBH}_4$ ).  $\text{NaBH}_4$  acts as a reducing agent since the reaction is thermodynamically accomplished but kinetically unrealizable. Therefore, the use of silver nanoparticles as a nanocatalyst provides support and a pathway through the transfer of electrons between the receptor (dyes) and the donor (borohydride) ion ( $\text{BH}_4^-$ ). Furthermore, AgNPs provide an appropriate surface media for attachment of both the dye agents and borohydride ion ( $\text{BH}_4^-$ ) for their degradation purpose. Hence, CD1-NPs favor the CR and MG dye degradation process in a much shorter period. The following experimental parameters were varied to obtain the accuracy of the dye degradation phenomenon.

*Effect of AgNPs concentration on CR and MG dyes reduction:* The concentration of catalysts is a crucial factor to determine the rate of reaction. Among the other varied concentrations of AgNPs, concentrations like 0.5 mM and 1 mM showed a prominent peak around 420 nm but the absorbance seems low. The control sample here was the AgNPs solution which showed a peak around 420 nm. In the case of concentration 1.5 mM, there seems a reduction in the absorbance intensity with significantly lesser time. Therefore, the concentration of 1.5 mM of AgNPs was best

suited for the catalytic activity. This can be seen in Figure 4.2b for CR dyes.

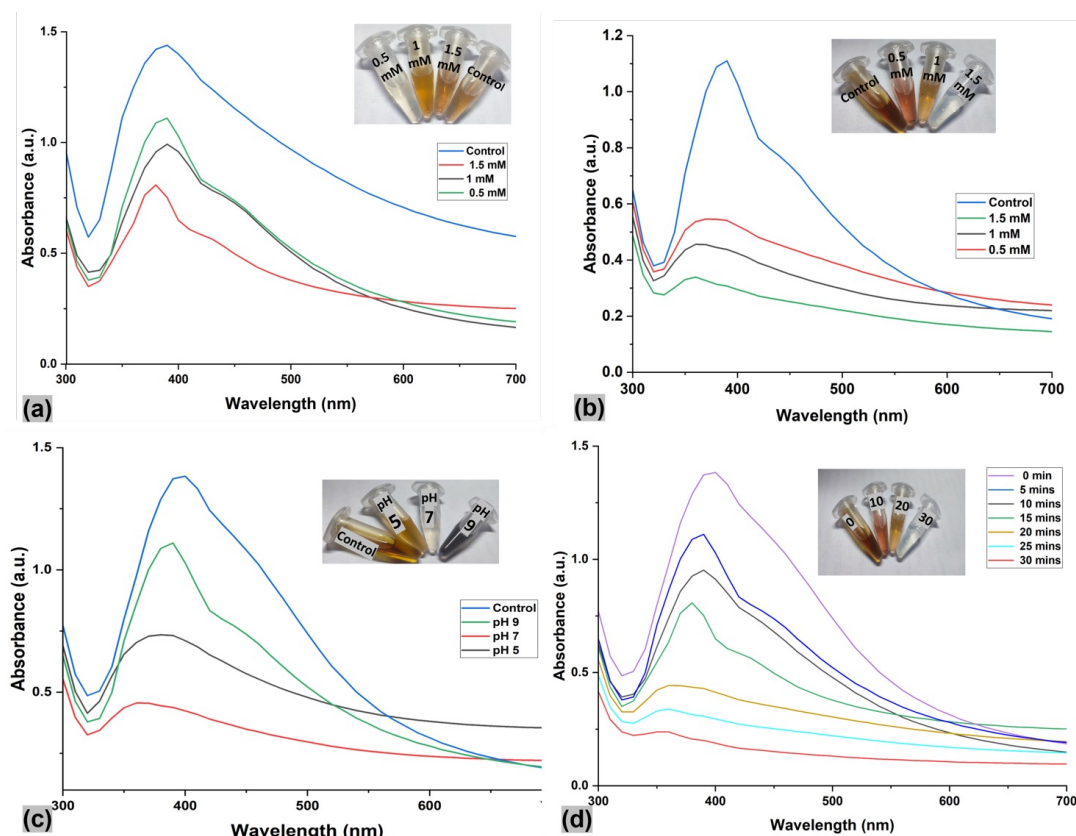


**Figure 4.2:** Optimization of the Congo red (CR) dye degradation activity by CD1-NPs with the following parameters, (a) Effect of the concentration of CD1-NPs, (b) Effect of the concentration of CR on dye degradation, (c) Effect on different pH on CR degradation, (d) Effect of different reaction time of Congo red dye with the catalysts.

#### *Effect of CR and MG concentration:*

The effect of the concentration of reactant is important to determine to quantify the catalytic reaction. In this study, these azo dyes (CR and MG) have been used as the benchmark to predict the catalytic activity of the metal nanoparticles (AgNPs). For the activity to check the effect of the concentrations of both CR and MG, different concentrations were used such as 0.5 mM, 1 mM, and 1.5 mM have been used. At the end of the reaction, it has been observed that with the concentration of 0.5 mM of both CR and MG, the reaction occurred faster, as shown in Figure 4.2b for CR. Here the concentrations of AgNPs and  $\text{NaBH}_4$  were kept at 1.5 mM and 0.1 mM respectively with a reaction time of 30 minutes for CR and 40 minutes for MG.

#### *Effect of pH on CR and MG reduction:*

Optimum pH is essential to quantify the rate of reaction. Here pH has been varied in the range of pH 5, pH 7, and pH 9. It was found that for both the dyes, pH 7 is the most ideal one, as shown in Figure 4.2c for CR dye. All the other parameters were kept constant.

*Effect of reaction time on CR and MG reduction:*

In Figure 4.2d, a graph of UV-Vis spectroscopy result has been plotted to show the progression of CR in reaction with CD1-NPs from 0 minutes to 30 minutes. It has been noted that for CR the degradation process completes in 30 minutes and for MG degradation occurs at 40 minutes. The result obtained indicates that a peak of CR with CD1-NPs obtained at 400 nM remained unaltered even in the presence of  $\text{NaBH}_4$ . Therefore,  $\text{NaBH}_4$  alone has no role in the degradation of dyes. After the addition of AgNPs, it has been observed that the peak gradually decreases with respect to the increase in reaction time, thereby confirming successful degradation. The complete reduction was achieved within 30 minutes for CR and 40 minutes for MG.

By using the pseudo-first-order reaction, the kinetics of the catalytic reaction may be obtained for both the dyes:  $\ln(c/c_0) = -kt$ , where  $c_0$  is the original dye concentration (mg/L),  $c$  is the dye concentration (mg/L) with reference to time, and  $k$  is the rate constant (1/min). So, the reduction rate constant ( $k$ ) can be calculated from the plot of  $-\ln(A_t/A_0)$  versus reaction time  $t$ . From Figure 4.3b, the linear time-dependency of  $-\ln(A_t/A_0)$  can be clearly observed with a correlation coefficient  $R^2$  of 0.985 (CR) and  $R^2$  of 0.989 (MG), thereby authenticating the pseudo-first-order kinetics reaction. The rate constant ( $k$ ) was found to be  $0.0612 \text{ min}^{-1}$  (CR) and for (MG) it was 0.0636, which shows that the rate of catalysis for CD1-NPs is significant. In order to calculate the degradation efficiency of the catalysts in the degradation of the both dyes, the following equation have been used

$$\alpha = \frac{C_0 - C_t}{C_0} \times 100$$

Previous studies conducted by [69] have shown the catalytic degradation of Mala-

chite green dye by gooseberry extract mediated AgNPs within 140 minutes with an efficiency of degradation is 69.23 %, whereas a similar study conducted by [121] by *Lagenaria siceraria* peel waste mediated silver nanoparticles synthesis reported the degradation of Congo red within 16 minutes with 92 % degradation efficiency. Simultaneously more degradation studies have been conducted by a number of researchers, as shown in Table 4.1. By comparing with the previously reported studies, the CD1-NPs showed the maximum degradation efficiency of Congo red (CR) was 98.86 % within 30 minutes and for Malachite green (MG) the degradation efficiency was 97.54 % in 40 minutes respectively.

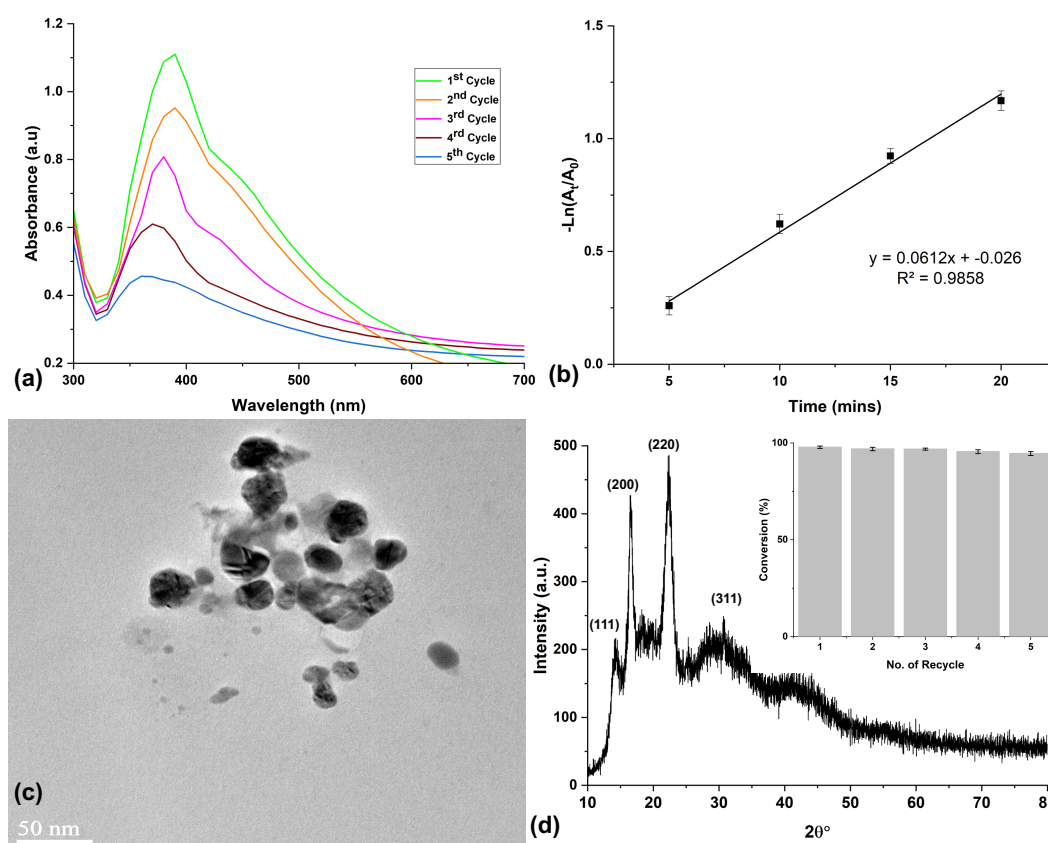


**Figure 4.3:** (a) UV-Vis Spectral analysis of the catalysts up to five cycles, (b) First order-kinetic plot of Congo red, (c) TEM analysis of the catalysts after the fifth cycle for morphological analysis, and (d) XRD pattern analysis of the catalysts after fifth cycles (inlet showing the five recycling of CD1-NPs).

To predict the durability of CD1-NPs as catalyst, evaluation was done by measuring their structure stability and reusability. In the study, five consecutive cycles have been carried out to determine the reusability of the catalysts. It was noted that after five repeated cycles, no remarkable changes in conversion were observed, the

efficiency for the catalysts towards dye degradation were about  $\geq 94\%$ , confirming the higher efficiency towards its re-usability, Figure 4.3, shows the recyclable ability of the catalysts. The slight decrease in efficiency may be due to the process of collection and drying and degradation of the active side due to absorption of the dye products during the experiments. Further, the catalyst structures have also been assessed based on the TEM study, XRD pattern analysis Figure.4.3d, and followed by Zeta Potential. The tested catalysts showed the same structure as compared to the original structure whereas the Zeta Potential showed  $-9.4$  mV, which is lower than CD1-NPs. The reduction in Zeta Potential value could be due to aggregation of CD1-NPs. Taking into considering of all the factors, it may be concluded that the catalysts due to its high reusability and stability may be utilized in the practical field at a significantly lower cost.

### **Catalytic degradation of the mixture of both Congo red (CR) and Malachite green (MG) by CD1-NPs**

After the successful degradation of both CR and MG by CD1-NPs with the efficiency rate of  $98.86\%$  and  $97.54\%$  for both the dyes, another set of experiments was performed by mixing both dyes in the ratio of 1:1 to test for catalytic activity and also to obtain the degradation efficiency of the catalysts. The experiment was set up using the dyes in the ratio of 1:1 with  $0.1$  mM of  $\text{NaBH}_4$ , and  $1.5$  mM of the catalysts for 45 minutes. The initial timings (0 minutes) till complete degradation (when the colour changes were visible from dark to almost transparent) were recorded by UV-Vis Spectroscopy. The results were obtained after every 5 minutes starting from 0 minutes and continuing till 45 minutes. The complete degradation occurred at 45 minutes, as shown in Figure 4.4a.

By using the pseudo-first-order reaction, the kinetics of the catalytic reaction may be obtained for both the dyes:  $\ln(c/c_0) = -kt$ , where  $c_0$  is the original dye concentration (mg/L),  $c$  is the dye concentration (mg/L) with reference to time, and  $k$  is the rate constant ( $1/\text{min}$ ). So, the reduction rate constant ( $k$ ) can be cal-

culated from the plot of  $-\ln(A_t/A_0)$  versus reaction time  $t$ . From Figure 4.4b, the linear time-dependency of  $-\ln(A_t/A_0)$  can be clearly observed with a correlation coefficient  $R^2$  of 0.8298 thereby authenticating the pseudo-first-order kinetics reaction. The rate constant ( $k$ ) was found to be  $0.0112 \text{ min}^{-1}$ , which shows that the rate of catalysis for CD1-NPs is significant. Further the degradation efficiency was calculated with the help of the equation,

$$\alpha = \frac{C_0 - C_t}{C_0} \times 100$$

where,  $C_0$  = initial OD value;  $C_t$  = final OD value.

In our study, for the mixed dye the initial OD value was 1.8 while the final OD value was 0.15. Therefore, the degradation efficiency of both the dye was found to be 91.68 % within 45 minutes.

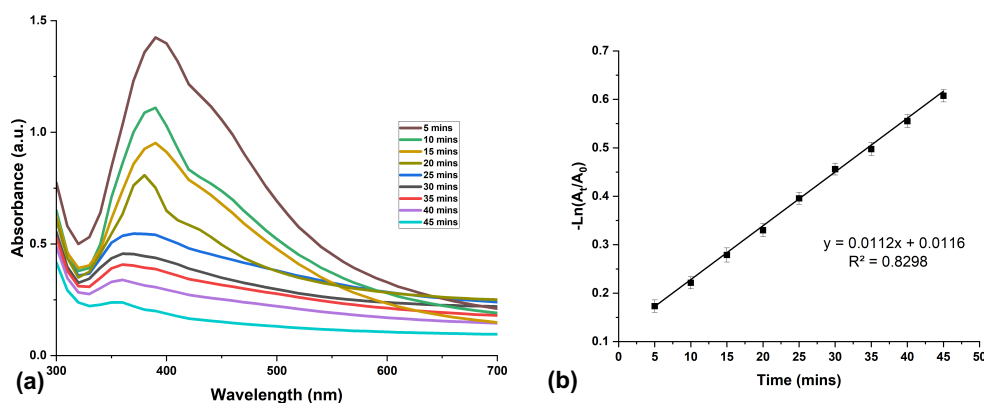


**Figure 4.4:** (a) Reaction time of degradation of both CR and MG by CD1-NPs starting from 5 minutes to 45 minutes, (b) First order-kinetic plot of the mixture dyes.

### Possible mechanism of azo dye degradation

Metal nanoparticles act as an efficient catalytic agent for degrading dyes by favoring the smooth electron transfer between the donor and the acceptor. The dye degradation process starts when both acceptor and donor materials get absorbed on the nanomaterial surface through an electron transfer reaction. In order to make the degradation process both thermodynamically realizable and kinetically feasible  $\text{NaBH}_4$  was used as a reducing agent along with AgNPs. Therefore, the use of

silver nanoparticles as nanocatalysts provides an effective pathway for the transfer of electrons between the receptor (CR and MG) and the donor (borohydride ion (BH<sub>4</sub><sup>-</sup>)). Additionally, silver nanoparticles facilitate a suitable surface on which to attach CR and MG molecules and borohydride ions (BH<sub>4</sub><sup>-</sup>) for their interaction with each other to form the degradation products. These nanocatalysts render the CR dye degradation process kinetically feasible, and the reduction is completed in a much shorter time.

### **Reusability of the catalysts:**

The ability to reuse is a concern for most metal-based catalysts. To overcome the problem, catalyst efficiency evaluation was done by analyzing the structural stability and repeated re-usability of the catalysts, CD1-NPs. In this study, up to five consecutive cycles were carried out to assess the re-usability of the catalysts. Before each cycle, the catalysts were collected, washed thoroughly, and dried for use in the next cycle. UV–Vis Spectroscopy, (shown in Fig. 4.3a, was assessed in each cycle. It can be noted that there was a significant prominent peak at around 420 nM, which may be correlated to the original UV-Vis Spectroscopy peak of CD1-NPs. The peak value for the other cycles remained at around 420 nM. Further, as we approached towards the final cycle, there was a slight deterioration in the absorption intensity, although the peak remained more or less the same. This slight deterioration may be due to the aggregation of the dye molecules on the surface of the AgNPs. The conversion efficiency was noted above 94.56%. This higher efficiency of the catalysts strongly suggests its re-usability. The slight decrease in efficiency may be due to the process of collection and drying and degradation of the active site due to the adsorption of the by-products during the experimental procedure. The efficiency percentage ( $\alpha$ ) of the catalyst was calculated using the Equation given below

$$\alpha = \frac{C_0 - C_t}{C_0} \times 100$$



where,  $C_0$  is the initial concentration of the dye and  $C_t$  is the concentration of the dye molecules at the end stage.

In our study,  $C_0$  for CR dye was 1 mg/L while  $C_t$  after 5 recycles was found to be on an average of 0.9456 mg/L. Therefore, the catalyst's efficiency for CR after five consecutive cycles of use was found to be 94.56%. As observed from Fig. 4.3, the efficiency was reduced by only 5.44% after 5 cycles of repeated use. Initially, we conducted the catalyst efficiency tests for 7 cycles. The rate of catalyst efficiency, however, didn't change significantly beyond 5 cycles. This was also confirmed by UV-Vis spectroscopy, DLS, and ZETA Potential study. But a slight loss of catalyst was observed during the recovery process after each cycle. So, in order to minimize the loss of the catalyst, we kept the recycling procedure up to 5 cycles only.

To confirm the efficiency of the re-usability nature of the catalysts after cycles, its structures have been assessed based on the TEM imaging, XRD pattern analysis, followed by Zeta Potential. The resulting catalysts after the TEM study (shown in Fig. 4.3c) showed average sizes in the range of 17-19 nM, which is almost similar to the original CD1-NPs TEM size (22 nM). XRD analysis (shown in Fig. 4.3d) was done to recheck the efficiency of the catalysts and it was found that the diffraction peaks occurred at  $2\theta$  values of 36.12, 43.28, 65.43, and 77.58 degrees for AgNPs. The unused CD1-NPs showed almost the same diffraction peaks at  $2\theta$  values of 36.12, 43.28, 65.43, and 77.58 degrees. Further, the catalyst's efficiency after Zeta Potential analysis showed a value of -20.14 mV, which is lower than the original value of CD1-NPs, which was -27.4 mV. This reduction in the Zeta Potential value could be possibly due to the increased adsorption of dye molecules from the surface of the Ag+ along with the simultaneous transfer of the hydrogen ions. Thereby, considering all the above facts from the structural analyses, it can be inferred that the catalysts are highly stable with significant re-usability, which may be utilized in the practical field at a significantly lower cost.

#### 4.3.4 Colorimetric detection of $\text{Hg}^{2+}$

Rapid industrialization is possibly the major cause of high metal ion content in the ground and wastewater. This has become a serious threat to the ecology and environment. A feasible solution to address this problem is the detection and quantification of those metal ions at lower concentrations. Among the metals, mercury is well notable because of its environmental hazard caused by both natural and man-made sources and thereby regarded as global public health issue. Mercury is poisonous in all forms including inorganic, organic, or elemental forms [117, 103]. Methyl mercury is a neurotoxicant as it can damage the developing brain by crossing the placenta and blood-brain barriers easily. The threat to the unborn is, therefore, of particular concern. It can also trigger depression and suicidal tendencies, paralysis, kidney failure, Alzheimer's disease, speech and vision impairment, allergies, hypothermia, and even impotence [117]. Even miniscale increase in methyl mercury exposure may adversely affect the cardiovascular system, as per the UNEP's Global Mercury Assessment report. Water is a major threat because of its possible neurological toxicity in fish, wildlife, and humans. In this study, biogenic CD1-NPs have been used as a probe for the detection of  $\text{Hg}^{2+}$  ions from aqueous solutions.

##### *Selectivity of Metal ions:*

Six different metal ions namely,  $\text{Fe}^{3+}$ ,  $\text{Zn}^{2+}$ ,  $\text{Mn}^{2+}$ ,  $\text{Mg}^{2+}$ ,  $\text{Ca}^{2+}$ ,  $\text{Hg}^{2+}$ , and  $\text{Cu}^{2+}$  have been tested with CD1-NPs for selectivity analysis. It was observed that with the addition of  $\text{Ca}^{2+}$ ,  $\text{Mg}^{2+}$ , and  $\text{Mn}^{2+}$ , there was a little decrease in surface plasmon band, as observed by UV-Vis Spectroscopy in the range between 300-700 nm, shown in Figure 4.5a, while the colour of the testing solutions remained the same. The further decrease was noted when  $\text{Pb}^{2+}$  and  $\text{Fe}^{3+}$  were added, but no colour change of the testing solution was observed. Meanwhile, there was a gradual decline in the surface plasmon range along with the colour change from brownish yellow and eventually colourless when  $\text{Hg}^{2+}$  was introduced. Hence, the biosynthesized CD1-NPs show significant sensitivity to  $\text{Hg}^{2+}$  metal ions and thereby require further analysis for its quantification and sensitivity assays.

### *Sensitivity of $Hg^{2+}$*

In order to predict the sensitivity of the developed nanosensor based on CD1-NPs, different concentrations of  $Hg^{2+}$  (1 nM-1 mM) were analyzed, and their absorption spectrum potency, zeta potential, and particle size were also simultaneously determined. The results indicated that the intensity of absorption spectra decreased with an increase in the concentration of  $Hg^{2+}$  from 1 nM to 1 mM. Similarly, the particle size measurement denoted for 1 nM  $Hg^{2+}$  was recorded around  $-18 \pm 2$  nM, and the zeta potential was found to be at  $-31.25 \pm 3$  mV. But with the increase of  $Hg^{2+}$  concentration, the particle size also increases, and the zeta potential values are found to decrease. At 1 mM  $Hg^{2+}$  ion concentration, the particle size was found to be  $558 \pm 13$  nM and the zeta potential value was measured at  $-10.09 \pm 1$  mV. Figure 4.6a, shows a gradual decrease in the peak and low shift of direction of shorter wavelength when the concentration of  $Hg^{2+}$  increased from 1 nM to 1 mM.

Further, to predict the sensitivity of the probe at nanomolar levels, different concentrations of  $Hg^{2+}$  (1 nM - 80 nM) were assessed and compared with the absorption spectrum, particle size, and zeta potential analysis. It was found that at 1 nM  $Hg^{2+}$  concentration the particle size and zeta potential values are 389.3 and -10.7 mV respectively when compared with the values at 80 nM  $Hg^{2+}$  particle size and the zeta potential are 583.6 and -28.7 mV. This may be due to the fact of aggregation of nanoparticles and the chelation between the  $Hg^{2+}$  ions with AgNPs mass.

### *Quantitative determination of $Hg^{2+}$ ions*

$Hg^{2+}$  ion concentrations and the intensity of the surface plasmon range were measured to establish the quantification of  $Hg^{2+}$  ions (Figure 4.5c) shows that at concentrations of  $Hg^{2+}$  less than 50 nM, aggregation of AgNPs occurred rapidly, as denoted by the decline of the band intensity. Figure 4.5d, describes the relative sensitivity plot of  $(A_0 - A)/A_0$  in comparison with  $Hg^{2+}$  concentrations between 1 to 80 nM, where  $A_0$  and  $A$  are the absorbances band for CD1-NPs surface plasmon range band at zero and relative  $Hg^{2+}$  concentrations, respectively (Gao et al., 2015). The entire tested  $Hg^{2+}$  concentration range, the exponential relationship was noted.

However, the linear relationship for the test was observed in the range of 10-80 nM, which can further be interpreted by the regression equation  $(A_0-A)/A_0 = 0.0066 [Hg^{2+}] + 0.1377$  with a correlation coefficient of 0.988, as shown in Figure 4.5(d). The LOD value of the testing samples was predicted in accordance with the standard deviation method [55] and was obtained to be 21.04 nM. Previous studies conducted by [28] on  $Hg^{2+}$  detection by *Vigna mungo* beans mediated AgNPs showed the detection limit of 130 nM in the linear range of 10-100  $\mu$ M. Another studies conducted by [93] by green tea extracts mediated AgNPs synthesis in the detection of  $Hg^{2+}$  following the linear range of 20 - 160  $\mu$ M with a detection limit of 20 -140  $\mu$ M. Similar other previous studies has been compared with the present study in a tabular form showing in Table 4.2. Therefore, CD1-NPs show higher sensitivity towards the colorimetric detection of the  $Hg^{2+}$ .

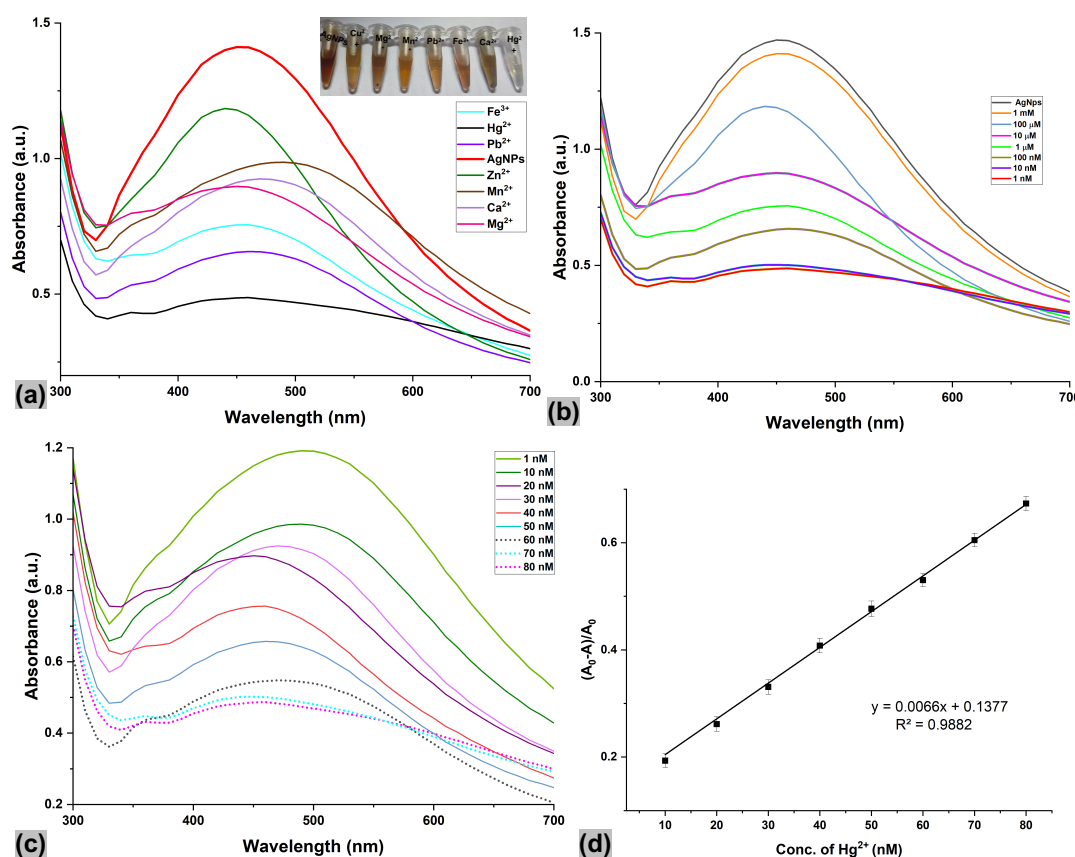


**Figure 4.5:** (a) UV-Vis spectral analysis of CD1-NPs solution in the presence of various metal ions, (b) Sensitivity of  $Hg^{2+}$  at different concentration (c) Quantitative determination of  $Hg^{2+}$ , (d) The plot of sensitivity versus relative  $Hg^{2+}$  concentration.

The whole phenomenon of colorimetric sensing was based on the principle of

aggregation mechanism in between AgNPs and  $\text{Hg}^{2+}$  ions. Nanoparticles on aggregations generate signals to shift peaks in the surface plasmon range and a change in the color of the tested solution. UV-Vis Spectrometer analysis helps to note the changing color of the tested solutions and can even be noted by the naked eye too. Further, the aggregation mechanism between the NPs and the  $\text{Hg}^{2+}$  ions analyzed by Zeta Potential and TEM study, shown in Figure 4.6a. The Zeta Potential study of the CD1-NPs- $\text{Hg}^{2+}$  ions showed a value of -10 mV which is lower than the CD1-NPs value (-27.4 mV). This lower value may be directly contributed to the fact of aggregation between CD1-NPs and  $\text{Hg}^{2+}$ . To justify the compensation for the negative charge of hydroxyl and carbonyl groups on the CD1-NPs surface by  $\text{Hg}^{2+}$  ions, the Zeta Potential value is much lower than the absolute value.

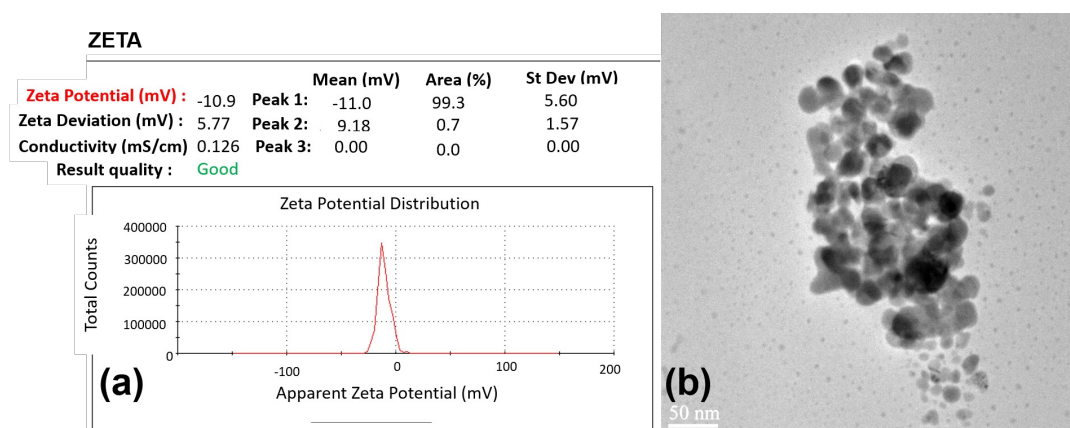


**Figure 4.6:** (a) Zeta Potential analysis of CD1-NPs after the reuse, (b) TEM image of CD1-NPs solution after incubation in 80 nM  $\text{Hg}^{2+}$  ions at different concentration.

### *Test in real water samples*

To authenticate the viability of the discussed method, five tap water samples collected from the local sources were mixed with different amounts of  $\text{Hg}^{2+}$  (25, 50, 75, and 100 nM) and analysed. Further, Atomic Absorption Study (AAS) in colorimetric sensing has been done to recheck and revalidate the quantity of  $\text{Hg}^{2+}$  ions. The results were summarized in Table 4.3. The results clearly indicate that the nanoparticulate-metal fabricated sensor provided high-accuracy measurements with the rate of recovery rate ranging from 98.5% to 100.2%. The result of AAS clearly indicated that concentrations in the tap water samples are proximate to AAS

**Table 4.1:** Comparison table for degradation efficiency and duration of different azo dyes.

Sensor	Dye	Efficiency (%)	Duration (mins)	Reference
AgNPs synthesised from Gooseberry Extract	MG	69.2	140	[69]
Bio-mediated AgNPs	CR, MO, MR	$\geq 90$	MO: 10; CR, MR: 20	[105]
Biosynthesised AgNPs using <i>Moringa oleifera</i> plant extract	MG	91.6	15	[29]
<i>Lagenaria siceraria</i> peel waste extract mediated AgNPs	CR	92.0	16	[121]
Bioactive molecules coated AgO-NPs synthesis from <i>Curcuma zanthorrhiza</i>	MG	94.7	240	[6]
<i>Pichia manshurica</i> (CD1) mediated biosynthesis of AgNPs	MG, CR	CR: 98.8; MG: 97.5	CR: 30; MG:40	Present study

techniques. Therefore, the bio-synthesized CD1-AgNPs can be used as a highly precise colorimetric nanosensor for  $\text{Hg}^{2+}$  determination in water samples.

### Sensing mechanism

It was observed in the study that the increase in the concentration of  $\text{Hg}^{2+}$  ions leads to decolorization of the AgNPs solution with SPR band quenching. This could be correlated to the reduction in the quantity of AgNPs in the solution, which can be possibly due to the oxidation of  $\text{Ag}^0$  to  $\text{Ag}^+$  [32]. Moreover, the visible shift and widening of the SPR band on the inclusion of  $\text{Hg}^{2+}$  denotes the binding of  $\text{Fe}^{3+}$  ions to the AgNPs surface and stabilizes the nanoparticles, indicating the oxidation-reduction reaction between silver and mercury ions [103, 127] reported that AgNPs could be degraded by  $\text{Hg}^{2+}$  ions leading to a colorless solution of AgNPs and lowering the SPR band intensity. Some of the previous studies reported

**Table 4.2:** Comparison study of the detection of  $\text{Hg}^{2+}$  ions.

Sensor	Linear range	Detection limit	Reference
Citrate and melamine (MA) mediated ligands for the surface modification of AgNPs	10 –100 $\mu\text{M}$	1.80 $\mu\text{M}$	[65]
Biosynthesis of AgNPs using <i>Epilobium parviflorum</i> Green Tea Extract	0.5–5.0 $\mu\text{M}$	58.11 nM	[39]
3 - (Trimethoxysilyl) propyl methacrylate stabilized AgNPs	1 nM–1 mM	20–100 nM	[19]
Chlorophyll functionalized green synthesized AgNPs	0.1 to 200 $\mu\text{M}$	100 $\mu\text{M}$	[133]
$\gamma$ -aminobutyric acid and citrate ion AgNPs (GABA-Cit@AgNPs)	5–35 $\mu\text{M}$	2.37 $\mu\text{M}$	[103]
<i>Vigna mungo</i> beans mediated Ag-NPs	0.1–1 $\mu\text{M}$	130 nM	[28]
Green tea extracts mediated Ag-NPs synthesis	20 to 160 $\mu\text{M}$	20–140 $\mu\text{M}$	[93]
<i>Pichia manshurica</i> (CD1) mediated biosynthesis of AgNPs	10-80 nM	21.04 nM	Present study

**Table 4.3:** Real water quantification of  $\text{Hg}^{2+}$  at different concentrations using CD1-NPs.

$\text{Hg}^{2+}$ Conc. ( $\mu\text{M}$ )	Determined $\text{Hg}^{2+}$ Concentration ( $\mu\text{M}$ )		Recovery (%)
	AAS	CD1-NPs Assay	
25	25.16 $\pm$ 0.52	25.14 $\pm$ 0.34	100.2
50	51.42 $\pm$ 1.41	50.11 $\pm$ 1.03	99.7
75	76.02 $\pm$ 1.06	74.65 $\pm$ 2.23	99.2
100	101.13 $\pm$ 1.12	98.2 $\pm$ 2.36	98.5

the catalysis of nanoparticles by the addition of a metal-oxidant such as  $\text{Hg}^{2+}$  and also simultaneously concluded a mechanism of the oxidation-reduction reaction between AgNPs and  $\text{Hg}^{2+}$  ions [127, 93]. Therefore, it may be summarized that the detection mechanism of  $\text{Hg}^{2+}$  ions using by biogenic CD1-NPs may be proposed as an oxidation-reduction reaction between AgNPs and  $\text{Hg}^{2+}$  ions, leading to the

decomposition of AgNPs into  $\text{Ag}^+$  ions.

## 4.4 Conclusions

Biogenic production of AgNPs was done using a novel yeast strain, *Pichia mansuetrix* (CD1<sup>T</sup>). The average diameter of the nanoparticle was found to be approximately 22 nM. The nanoparticle showed efficient catalytic efficiency against Congo red (98.86% within 30 minutes) and Malachite green (97.54% in 40 minutes). To achieve further efficiency, both the dyes were mixed in the same ratio and degradation was completed in 45 minutes with 91.86% efficiency. Successful colorimetric detection of  $\text{Hg}^{2+}$  was done with a detection value of 21.04 nM. The catalysts showed reusability up to 5 cycles with 94% efficiency.



## Chapter 5

# One step synthesis and fabrication of a novel AgNPs-BC composite : Characterizations and bioactivity

### 5.1 Introduction

Nowadays, nanomaterials have attracted increasing interest due to their multifunctional properties such as electrical conductivity, strength and hardness, chemical reactivity, and versatile biological activity. The chemical and physical features of nanomaterials are different from those of their bulk materials. Nanoparticles (NPs), especially metal oxide nanoparticles (MNPs) are widely used as a class of nanomaterials. The use of MNPs as antimicrobials, fillers, industrial catalysts, chemical-sensing devices, and semiconductors are among their broad applications. They are also useful in the development of cosmetics, microelectronics, medical applications, and water purification.

Cellulose is the most abundant biomass and renewable resource on earth, is biodegradable, biocompatible and non-toxic, and can be converted into cellulose derivatives and regenerated materials one of the most promising materials with broad applications. More recently, cellulose-based nanocomposites and their derivatives

have attracted great attention and showed more and more importance over the last two decades due to their high value-added applications in science and technology.

Silver from the ancient point of time is the best choice for a wound healing agent. It has the highest electrical and thermal conductivity of any metal. Silver occurs in pure form, as an alloy with other metals, or in minerals. Silver ions and compounds can kill bacteria, algae, and fungi; therefore, silver will help to purify, sanitize, and filter water [34]. Natural cellulose obtained from bacteria is the most abundant biopolymer on earth, has been used for thousands of years and their use continues today as one of the most exploited renewable raw materials. In recent years, a new cellulose material, bacterial cellulose, has attracted more and more attention in both scientific and industrial applications. The presence of a large number of hydroxyl and ether groups on the cellulose chain can effectively stabilize AgNPs via strong chemical interactions. Cellulose has the potential to be utilized as a purification or separation membrane if modified with metal oxides, since cellulose does not have inherent antibacterial property hence their conjugation with silver has been utilized for the antimicrobial applications [12]. By considering the inherent reduction ability to metal ions by hydroxyl groups on Bc material, a green and environmentally benign approach for the production of silver nanoparticles may be proposed by using bacterial cellulose as both the reducing and stabilizing agent, without any chemical reagents introduced.

The discovery of antibiotics has been a revolutionary milestone in the history of humans. Unfortunately, the utilization of the novel prodigy medication was followed by a quick increase in tolerant pathogen strain [97]. Frequent and improper use of antibiotics may be blamed for this. In order to find out an alternative for the same, nanotechnology can be applied to beat the drug resistance of many infectious bacteria. In fact, the silver nanoparticle is one of the most suitable ones to hit against pathogenic strains. Moreover in India, the main contaminants of polluted water are Enterobacteriaceae namely *Salmonella typhi*, *Escherichia coli*, *Shigella sonnei*, etc. Enterobacteriaceae contributes to water borne related disorders like

diarrhoea, cholera, typhoid, and other infections. Since ancient times, silver has been the best choice among people for its robust antimicrobial effectiveness. Moreover, silver shows extensive span of efficiency towards various Gram-positive and Gram-negative bacteria, also chance of development of bacteria resistance is remarkably low too.[137].

The usefulness of AgNPs to the medical field is not only restricted to their antimicrobial effect but also gained much attention due to their cytotoxic effect. In some of the previous studies, opposed to cell line of human cervical cancer, it has been showing that the efficiency of AgNPs towards apoptosis, pointing its role as anti cancer drug therapy [34]. It has been estimated that AgNPs synthesised through biological method are safe to human cell upto 50 ug/ml of concentration. Therefore, the cytotoxic effect is an another important factor that needs attention. [1] becomes less toxic when conjugated with cellulose. According to the World Health Organization (2010), 1.1 billion people lack access to improved drinking water. As many as 2.2 million people die of diarrheal related disease every year most often caused by waterborne infections, and the majority of these cases are children under the age of 5. More than ever, existing fresh water resources need protection and new water resources must be developed in order to meet the world's growing demand for clean water. This will require better water treatment technology. Nowadays ,there is an increased demand for membranes favored over other technologies for water treatment, such as disinfection, distillation, or media filtration is because, in principle, they require no chemical additives, thermal inputs, or require regeneration of over the past decade, nanotechnology has rapidly changed from an academic pursuit to commercial reality; already nanotechnology concepts have led to new water treatment membranes that exceed state-of-the-art performance including selective permeability ,high absorption rate etc. Each of these innovative materials concepts promises unique performance enhancements and each has unique hurdles to overcome before it is commercially viable.

In this study, *Gluconacetobacter kombucha*, strain RG3<sup>T</sup> has been isolated from

a popular fermented tea, known as kombucha [36]. The GenBank accession numbers for the strain RG3<sup>T</sup> are respectively AY688433 and DQ141200. This potential Gram-negative, rod shaped bacteria belongs to the Acetobacter family. This bacteria is also responsible for nitrogen fixation and cellulose formation as pointed by [36]. Here in this study, we have used this bacteria for the NPs synthesis by bio-green method and simultaneously for the bacterial cellulose (Bc) production. Single-step fabrication has been done to produce the biocomposite, AgNPs-Bc. The bio-membrane has been applied for the antibacterial assays against two Gram-negative and two Gram-positive bacteria. Simultaneously, cytotoxic effects have also been seen considering the cell lines like WI38 and A549. Further in order to predict the stability and reusability of the biocomposite, silver ion-releasing properties has also been accessed. In the entire text *Glucanoacteobacter kombuchae*, has been addressed as RG3, silver nanoparticles has been mentioned as AgNPs, bacterial cellulose as Bc and the bio-membrane silver nanoparticle bacterial cellulose composite are referred to as AgNPs-BC.

## 5.2 Materials and Methods

### 5.2.1 Chemicals & reagents

Chemicals like Yeast Extract (Yeast Extract Powder. RM027), D-(+)- Glucose anhydrous, Peptone Type I, Bacteriological. RM667, Hydrochloric acid (HCl), Agar Powder, Sodium Hydroxide (NaOH), Sodium Borohydride (NaBH<sub>4</sub>), Mannitol, Hestrin and Schramm medium (H.S medium), and other metal salts were purchased from Hi-media (Mumbai, India). Throughout the entire experimental procedure, only de-ionized water was used. All the mentioned chemical reagents were of extra pure grade and thus were used without further purification. All reagents used here were of unadulterated analytical grade and therefore used without further purification.

### 5.2.2 Microbial strain

*Gluconacetobacter kombuchae*, Strain RG3T (deposited at the International repository of Microbial Type Culture Collection, India, MTCC# 6913) isolated from Kombucha tea [16S ribosomal RNA, partial sequence, GenBank accession no. AY688433] was used in this study as the source of bacterial cellulose.

### 5.2.3 Preparation of Bacterial Cellulose (BC) and biocomposite (AgNPs-BC) formation and purification.

Initially, RG3 was maintained on Mannitol media (2.5% Mannitol, 0.5% yeast extract, 0.5% peptone, pH 5.0) at 30°C for 72 hours. Further, Hestrin and Schramm medium (H. S medium) (2% Glucose, 0.5% peptone, 0.5% yeast extract, 0.27% Na<sub>2</sub>HPO<sub>4</sub>, 0.11% citric acid, pH 5.0 adjusted with acetic acid) was used throughout the in this study based on which the production medium was modified. A 20 mL pre inoculum culture was grown in a 150 mL conical flask for 48 hours at 30°C. Aliquots (2.5 mL) from the resulting cell suspension was inoculated into a 50 mL medium contained in a 250 mL conical flask and grown, either under stationary or under shaking condition, for 6 days at 30°C. The fermentation was carried out in triplicates. Cell growth was evaluated by measuring the optical density at 600 nm in a spectro-photometer. Purification of BC pellet was done by heating the pellet with NaOH for 20 minutes. This procedure were repeated thrice until all sodium were removed and pH was checked to be obtained at 7. For future use, the membrane were vaccum dried using Eleya Speed Vac and stored at cool and dry place.

Using the same bacterial strain (RG3<sup>T</sup>), silver nanoparticle (AgNPs) formation were done as described by the previous studies by [78]. Further, the nanoparticle was measured to 10 mG was dissolved in 10 mL of bacterial soup and immersed in dried BC. The experiment were observed for 2 hours under shaking condition at 30 degree incubator. Later, after the visible colour change of the BC from white to brownish it was further washed with distilled water thrice and spinned at 100000 rpm for 10 mins thrice to remove any impurities and tested.

#### 5.2.4 Characterization of the pellicle

The composite was analyzed and validated using various instrumentation techniques. To detect the crystalline structure, XRD study was performed (Rigaku, Miniflex). Surface structure analysis was performed by advanced microscopy instrumentations like SEM and EDAX (Hitachi S-4500) UV-Vis Spectroscopy (HITACHI U 2900 / U 2910 UV VIS DOUBLE BEAM) was carried out in the range of 300 - 700 nm. To obtain information about the functional group that interacted to form the metallic NPs, FTIR (Shimadzu FTIR spectrophotometer (FTIR 8400) study was conducted in the ranges between 4000–400  $\text{cm}^{-1}$ . The precise size and charge distribution within the composite were examined with the help of DLS (Dynamic Light Scattering) and Zeta potential [ZETA Seizers Nano series (Malvern Instruments Nano ZS)]. To measure the concentrations of any elements, Atomic Absorption (AAS) study has been employed (iCE 3500, Thermo Scientific, Germany).

#### 5.2.5 Optimization of the synthesis conditions

To achieve the best synthesis condition of the composite, both the silver nanoparticles and bacterial cellulose has been optimized separately. The parameters like carbon and nitrogen sources, temperature, pH, and incubation period were varied to get the optimized synthesis condition for the bacterial cellulose. For AgNPs, the parameters like metal ion concentrations, temperature, time, and pH were varied to get the best-optimized condition, following the method of [77].

#### 5.2.6 Ag ion release rate measurements

To predict the stability and reusability of the bio-material, the rate of Ag ions release from AgNPs-BC composite was studied following the method of [137] with some modifications. First, 0.5 g of AgNPs-BC composite was dispersed in 100 mL of deionized water. The experimental setup was kept in sealed containers at 25 °C with gentle agitation conditions. At regular time intervals (2, 8, 12, 24, 48, and 72 h), the suspensions were centrifuged for 5 min at 5000 rpm. Soon after that, 0.2

mL of the supernatant from each sample was taken and analyzed for the amount of Ag<sup>+</sup> ion released, using atomic absorption spectrophotometry (Shimadzu, AA-7000; Japan). All measurements were performed in three replicates.

In both methods, the reusability of the AgNPs-BC composite were investigated by carefully collecting nanocomposite membranes, washing them with deionized water, autoclaving, and employing them for the next cycle with the same previously mentioned methods.

The release characteristic of Ag ions from the AgNPs-Bc composites was evaluated. The obtained composites were cut into circular shapes with a diameter of 15 mm. The samples were dispersed in a phosphate buffer solution, pH=7.4, while shaking on a rotary at 37 °C. Aliquots of the sample (0.5 mL) were pipetted at time intervals over 72 hours, and an equivalent volume of a fresh phosphate buffer was replenished into the system. Finally, the concentrations of Ag ions (solubility 5.933 g/100 mL in phosphate buffer solution) at all of the specified time intervals were evaluated using a UV–Vis spectrophotometer at a wavelength of 735 nm with the three experiments performed for each specimen.

### 5.2.7 Antibacterial property

Antibacterial properties of the AgNPS-BC biocomposite and BC membrane were monitored against using two bacterial strains of Gram-positive origin namely, *Staphylococcus aureus* (ATCC 25923), and *Bacillus cereus* (MTCC 430), and two bacterial strains of Gram-negative origin namely, *Escherichia coli* (ATCC 25922), *Salmonella typhi* (MTCC 531). The strains were maintained on Luria Bertani containing approximately 10<sup>8</sup> CFU/mL were prepared and cultured at 37 °C in a shaking incubator for 24 hours.

Disc diffusion and the colony-forming count method were used to analyze the antimicrobial activity. In the disc diffusion method, the specimens were sterilized by autoclave and prepared into circular discs of 1 cm in diameter and placed on a Luria Bertani agar plate for 24 hours in an incubator at 37 °C. The diameter of inhibition

zone was measured in terms of mm. The results were evaluated in triplicate and are reported as the mean  $\pm$  SD.

For the colony-forming count test, the bacteria suspension having the final density of 10<sup>5</sup> CFU/mL were considered. The samples were poured in the bacterial suspension (2.5 mL) in a flask and shaken at 37 °C for 0, 1, 3, 12 and 24 h. At each of the intervals, the solution (0.1 mL) was withdrawn and diluted with a phosphate buffer solution to prepare a serial dilution. The bacterial suspensions were carefully dropped onto agar plates and counted for the number of colony-forming units. The experiment was performed in triplicate.

### 5.2.8 Cell Culture

The following cell lines of A549 (Lung cancer cells) and WI38 (Normal lung fibroblasts) acquired from National Center for Cell Science (NCCS) Pune, India A549 and WI38 were cultured and maintained in specialized DMEM and MEM respectively with 10% FBS (Fetal Bovine Serum), penicillin, streptomycin (100 units/ml); amphotericin-B (anti-fungal) at 37°C and 5% CO<sub>2</sub> respectively. The entire treatment was performed at 37°C and a minimum cell thickness is maintained to allow optimal growth.

### 5.2.9 Cell Survivability Assay

To access the cell survivability, A549, and WI38 cells were seeded in 48 well cell culture plates. The next day cells were treated with BC, AgNPs-Bc. After 24 hrs, cells were further treated with 3-(4,5 dimethylthiazol-2-yl)-2,5- diphenyl tetrazolium bromide (MTT) (0.5 mg/ml) for 4hrs. The resulting formazan crystals were dissolved in MTT solubilization buffer and the absorbance was taken with a UV–visible spectrophotometer at a wavelength of 570 nM.



## 5.3 Result and discussion

### 5.3.1 One step synthesis of the AgNPs-Bc bio-composite

Bacterial, namely *Glucanoacetobacter kombuchae*, strain RG3<sup>T</sup> has been utilized for both the biogenic synthesis of AgNPs and Bc. Production of the AgNPs was previously reported by [78], here the biogenic synthesis of AgNPs was done by the addition of AgNO<sub>3</sub> to the cell exudate of RG3 together in the concentration of 17 mG/mL of AgNO<sub>3</sub> and 10 mG/mL of dextrose and then observed for 2 hours at room temperature. Simultaneously with the same mixture 2 mm x 2 mm sized purified BC was cut and immersed for 2 hours under shaking conditions in a 30°C.

### 5.3.2 Optimization of the Synthesis Conditions

In order to optimize the biogenic AgNPs-BC composite, at first, the temperatures were varied ranging from 20°C to 45°C. At 45°C and 37°C, a prominent peak was noted at around 430 nM. AgNPs formation at 20°C was indistinct. It has been observed that the NPs tend to aggregate and agglomerate at that temperature, whereas the NPs were found to be more stable at 37°C. Simultaneously, another intense peak was noted at 30°C, but the peak at 37°C was found to be more stable. Therefore, the synthesis can be inferred to be green as it occurs at a room temperature of 37°C.

Secondly, the various reaction times and their effects on the AgNPs-Bc composite formation in the time span between 5 minutes to 2.5 hours were conducted, considering the other parameters fixed. At 5 minutes, the synthesis was not successful, with the increasing reaction time, the rate of production of AgNPs-Bc also increased. Beyond 2 hours, there seems to be a rapid aggregation of NPs, making it more unstable. Therefore, the reaction time of 2 hours has been considered for AgNPs-BC formation.

For the successful formation of nanoparticles, metal ions, and their concentrations are important. The experiments were conducted by a different variety of concentrations of AgNO<sub>3</sub> ranging from 1 mM to 2.5 mM, keeping the other parameters constant. It was found that with increasing concentration, the rate of reaction

was rapid. However, at a concentration after 2 mM, aggregation of nanoparticles occurs. The stability seems to be low by increasing the concentrations beyond 2 mM, thereby suggesting 2 mM as the ideal Ag<sup>+</sup> concentration for the biocomposite formation.

After varying with temperature, reaction time, and concentration of Ag<sup>+</sup>, finally, glucose concentrations were also varied to optimize. It has been observed that without glucose, only AgNO<sub>3</sub> alone fails to contribute to nanoparticle production. However, when glucose was added along with AgNO<sub>3</sub> keeping the other parameters like the temperature set at 37°C, the concentration of AgNO<sub>3</sub> of 2 mM with a pH of 7, distinct nanoparticle formation occurred. Although with the rise in glucose concentrations between 0.05 mM to 0.2 mM, reactions were rapid, it seems to be stable at 0.1 mM of glucose. Therefore, after the experiments it was concluded that the AgNPs-Bc formation best occurred at a temperature of 37°C, with a pH of 7 following 2 mM of AgNO<sub>3</sub> along with 0.1 mM of glucose.

### 5.3.3 FESEM

Field emission scanning electron microscopy (FE-SEM) The morphology of the composite was characterized by a field emission scanning electron microscope (FE-SEM) (Hitachi, Japan) at room temperature. The acceleration voltage and working distance for each image were 30 kV and 1–5 mm, respectively. The samples were coated with a thin conductive gold layer, before observation. Size measurements of AgNPs-Bc and diameter of nanofibers on SEM images were carried out by ImageJ 1.48 software.

### 5.3.4 SEM and EDAX analysis

To investigate and analyse surface topography and also to determine average size of the AgNPs, SEM study were done which specifies different shape of the formed particles. The obtained green-combined AgNPs displayed the presence of polymorphism with respect to shapes like: flake type, spherical, and ellipsoidal. Also the

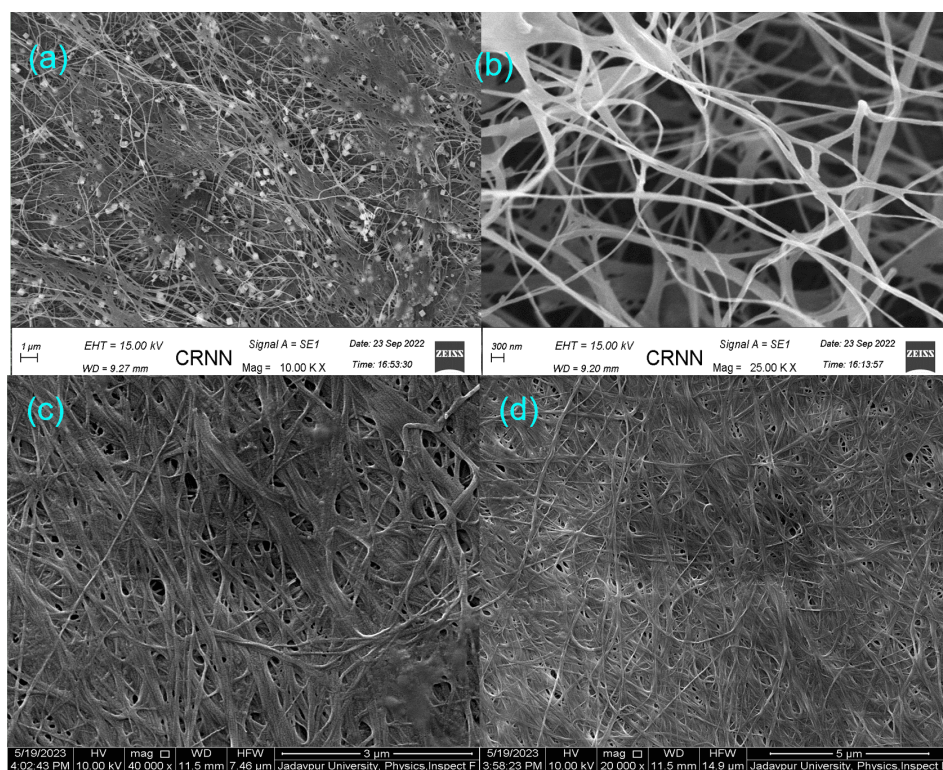


**Figure 5.1:** (a) XRD study of the synthesized biocomposite with the bacterial cellulose, and (b) FTIR analysis of the biocomposite along with bacterial cellulose.

images reveal few large particles that may be due to overlapping of one particle with another.

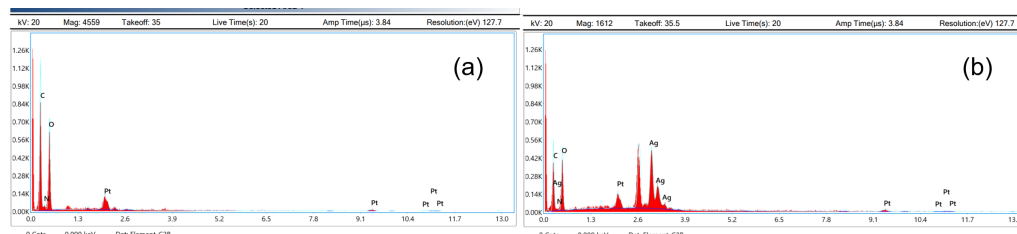


**Figure 5.2:** Edax study of (a) bacterial cellulose, and (b) AgNPs-Bc.

### 5.3.5 FTIR Analysis

To investigate the possible mode of interaction of AgNPs-Bc with various functional groups, FTIR spectroscopy studies were conducted. FTIR spectrum analysis indicates the existence of different functional classes at positional places, as shown in Figure 5.3b. A stretch at  $1377\text{ cm}^{-1}$  pointed towards the symmetry stretched of a well-known nitro compound which corresponds to the C-H bending of aldehyde groups, acquired from skeleton of glucose in aqueous medium [61]. The indication

of the carbonyl group obtained at  $1635\text{ cm}^{-1}$  may be correlated to C–N and C–C stretching indicating protein existence and therefore directly indicates NPs formation [17]. Another well built symmetrical peak at  $2015\text{ cm}^{-1}$  were consonant to the O\C stretching mode [92]. Another powerful, fierce banding at  $2578\text{ cm}^{-1}$  can be allocated to both \NH2 in primary aromatic amines and \OH groups in alcohol [90]. The bands at  $3403\text{--}3799\text{ cm}^{-1}$  in the spectra are consistent with O–H stretching vibrations exhibiting alcohol and phenol.

From the above FTIR analysis, it can be well stated that the OH and C=O group present in glucose can be considered for the bioreduction of Ag<sup>+</sup> ions foremost to Ag<sub>0</sub> NPs formation. FTIR analysis further concludes the carbonyl group of amino acid remnants and peptides of the proteins shows greater affinity towards the metal ions. It thereby avoids agglomeration by establishing a safeguarding coat membrane and stabilizes them too. All peak changes here symbolize the contribution of functional groups to synthesize AgNPs-Bc.

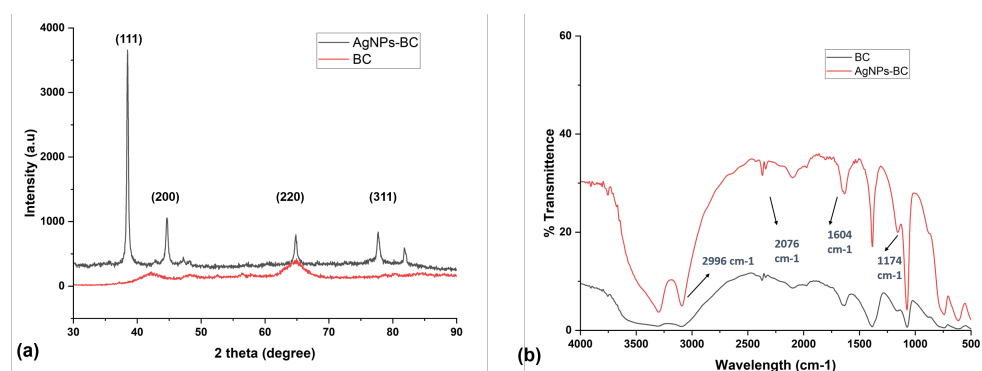


**Figure 5.3:** (a) XRD study of the synthesized biocomposite with the bacterial cellulose, and (b) FTIR analysis of the biocomposite along with bacterial cellulose.

### 5.3.6 XRD

XRD is a direct approach to noting the crystalline structure of the produced AgNPs. The result obtained, depicted in Figure 5.3a, clearly shows the significant peaks at  $(2\theta)$  values of  $38.39^\circ$  and  $44.87^\circ$  which can be correlated to the (111) and (200) planes respectively [112, 99], where  $\theta$  is the half diffraction angle. By collation with JCPDS (file no: 89- 3722), the quintessential design of green-synthesized AgNPs can be

established to have a leading structure [4]. The mean crystallite dimensions of the AgNPs evaluated using the diffractogram by calculating the Scherrer formula given by,  $D = K\lambda/(\beta\cos\theta)$ , where  $\lambda$  is the wavelength of the X-rays used for diffraction,  $K$  is a constant which is dependent on the crystal motif, and  $\beta$  is the full width at half maximum (FWHM) of a peak.

XRD is a direct approach to note the crystalline structure of the produced AgNPs. The result obtained, depicted in Figure 5.3a, clearly shows the significant peaks at  $(2\theta)$  values of 38.39 and 44.87 which can be correlated to the (111) and (200) planes respectively [112, 99], where  $\theta$  is the half diffraction angle. By collation with JCPDS (file no: 89- 3722), the quintessential design of green-synthesized AgNPs can be established to have a leading structure [4]. The mean crystallite dimensions of the AgNPs evaluated using the diffractogram by calculating the Scherrer formula given by,  $D = K\lambda/(\beta\cos\theta)$   $D = \frac{k\lambda}{\beta\cos\theta}$ , where  $\lambda$  is the wavelength of the X-rays used for diffraction,  $K$  is a constant which is dependent on the crystal motif, and  $\beta$  is the full width at half maximum (FWHM) of a peak.

### 5.3.7 Antibacterial Activity

The AgNPs-Bc composite were tested for their antibacterial potency against two Gram-positive bacterial strain namely like *Staphylococcus aureus* ATCC 25923 and *Bacillus cereus* MTCC 430 & two Gram-negative bacterial strains such as *Escherichia coli* ATCC 25922, *Salmonella typhi* MTCC 98, using the disk diffusion assay and colony count method. The photographs of antibacterial activities of AgNPs-BC composite against *E. coli* and *S. aureus* with disk diffusion method was shown in Fig. 5.4. It was seen that in the case of AgNPs-BC membranes developed an inhibition zone against the mentioned bacteria, but no inhibition zone was seen for the pure BC membrane as control. For AgNPs-BC composite, the widths of the inhibition zone were about 3 mm for *Staphylococcus aureus* and 4 mm for *Bacillus cereus*. For the Gram-negative bacteria like *Escherichia coli*, *Salmonella typhi* the zone inhibitions were 4 mm and 3 mm. This clearly indicate that the

observed antimicrobial activity is due to Ag NPs impregnated inside the bacterial cellulose matrix, not due to bacterial cellulose.

The quantitative estimation of antibacterial activity of these nanocomposites were evaluated by plate count method and expressed with three parameters. Commonly, the antimicrobial agents causing less than 1-log reduction were assumed as low antimicrobial activity agents. Those can cause between 1- and 3-log reduction was considered as moderate antimicrobial agents and the high antimicrobial activity was assumed to be greater than 3-log reduction. Both of the produced composites have high antimicrobial. The exact mechanism of bactericidal activity of Ag nanoparticles is still unclear but several studies reported that smaller Ag nanoparticles have better antimicrobial activity. So the strong activity observed in this study can be due to the small size of produced nanoparticles. This great antimicrobial effect against Gram-negative bacteria can be due to damage of the microbial enzymes or cell membrane and electrostatic interactions between the cell walls of bacteria and nanoparticle. In addition, the bacterial species and characteristics of nanoparticles have significant effects on the antibacterial activity of AgNPs-BC too.

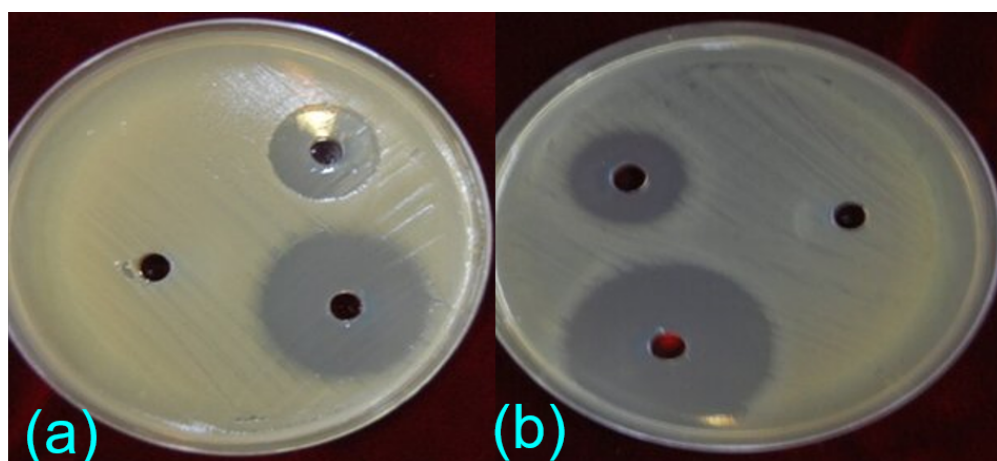


**Figure 5.4:** Antibacterial activity assessment by Disc diffusion assay of the bacteria namely, (a) *E. coli* (Gram-negative bacteria) and (b) *S. aureus* (Gram-positive bacteria).



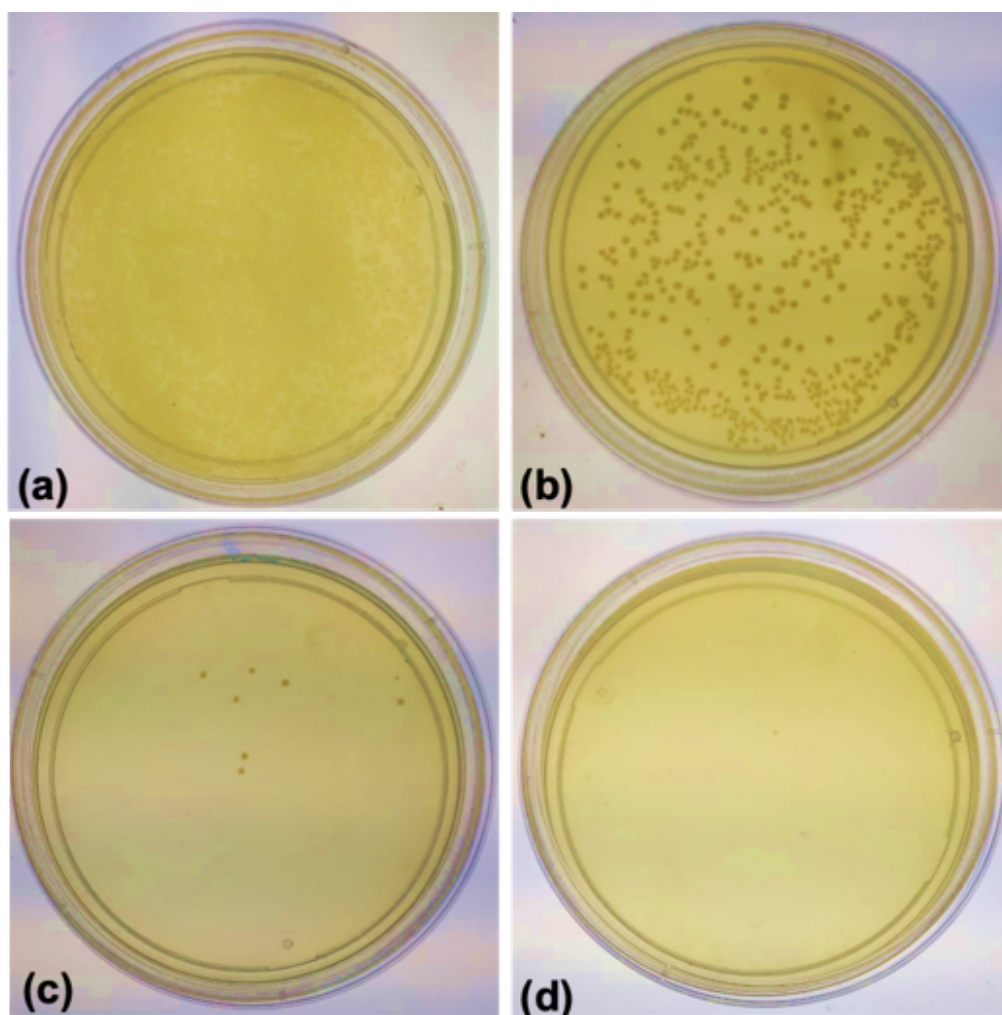


**Figure 5.5:** Colony count method analysis and Bactericidal activities of AgNPs-Bc against sample Gram Positive strain *Bacillus cereus* at (a) 0 µg/ml (Control), (b) 5 µg/ml, and Gram Negative strain *E. coli*, (c) 50 µg/ml, (d) 0 µg/ml (Control).

### 5.3.8 Cytotoxic Activity

The anticancer properties of AgNPs-BC were performed on cancerous cell lines including A549 (Lung cancer cells) and WI38 (Normal lung fibroblasts) using MTT assay. The cancer cells were subjected to different concentrations of these complexes for 24 hours. The cell survivability percentage of WI38 cells treated with AgNPs-BC and BC had been found to be  $93.39 \pm 7.17$ , and  $15.83 \pm 5.15$  respectively. The cell survivability percentage of A549 cells treated with Ag-BC1 and BC had been found to be  $94.61 \pm 4.10$ , and  $24.75 \pm 7.14$  respectively. Therefore it may be concluded that only BC could not show any effective cytotoxic properties but AgNPs-BC showed higher cytotoxic properties.

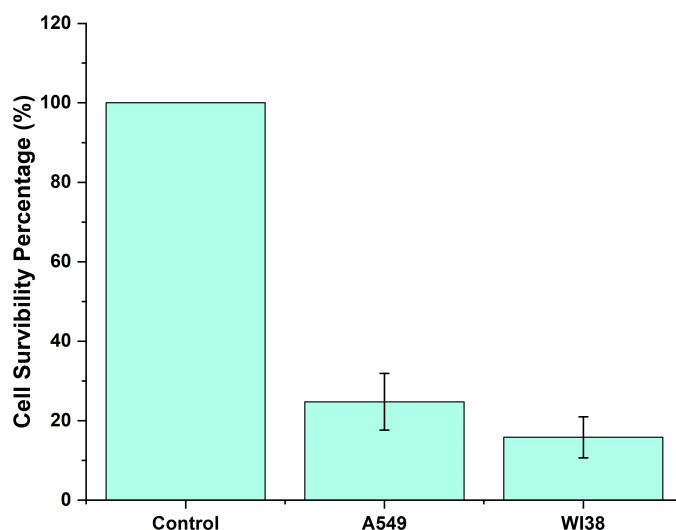


**Figure 5.6:** Cytotoxic activity by Mtt assay by the cell lines A549 and WI38.

### 5.3.9 Silver ion release

For a nanohybrid material with antimicrobial and cytotoxic properties, a stable and prolonged activity is necessary in order to improve its reusability. The initial amounts of  $\text{Ag}^+$  in the dried powder of AgNPS-BC were obtained as  $26723.06 \pm 43.11$ . The releasing percent of loaded Ag molecules and ions from the nanohybrids was shown in Fig. 6. Ag were released gradually from the nanohybrids within four days with about 39.7 % after 72 h.

Interestingly, by considering the porous network of AgNPs-BC, it can be concluded that although the microstructure of organic support is an important factor in the fabrication of nanohybrids, the compatibility of two phases and intensity of NPs entanglement in biopolymer networks are even more important factors in the determination of both loading capacity and release controlling. In a study conducted by [74] investigated the effect of chitosan-alginate system on release controlling of MgO NPs and revealed that these two biopolymers are able to control its release in aqueous solutions.



## 5.4 Conclusions

One-step synthesis biogenic synthesis of silver nanoparticle and bacterial cellulose using the bacteria *Glucanoacteobacter kombuchae* (RG3T) and its fabrication into a biocomposite, AgNP-BC. Synthesis conditions have been optimized and characterized to obtain the membrane morphology and applicability. Biocomposite were applied to test for its cytotoxic effect against the cell lines namely A549 (Lung cancer cells) and WI38 (Normal lung fibroblasts). The biocomposite was further tested for its antibacterial activity using two bacterial strains of Gram-positive origin namely, *Staphylococcus aureus* (ATCC 25923), and *Bacillus cereus* (MTCC 430), and two bacterial strains of Gram-negative origin namely, *Escherichia coli* (ATCC 25922), *Salmonella typhi*. The antibacterial activity of AgNPs-BC against both Gram-positive and Gram-negative bacteria showed good results in both disk-diffusion assay and colony-forming unit assay. After 96 h, Ag+ releasing from AgNP-BC was recorded as 31.7%, respectively. Therefore the study demonstrates the practical applicability of the bio-composite in various fields.

# Chapter 6

## Conclusions

### 6.1 Chapter 2

An innovative green route has been adapted in this study to biosynthesize Silver Nanoparticles (AgNPs) for the first time using the cell exudate of a novel bacteria *Gluconacetobacter kombucha* (RG3<sup>T</sup>). Bio-reduction of silver was carried out by adding AgNO<sub>3</sub> and glucose along with the bacterial cell exudate. The onset of dark brown colour indicated the synthesis of nanoparticles (NPs) and was further validated by absorption spectrum at 430 nm using UV-Vis Spectroscopy. X-ray diffraction (XRD) study clearly illustrated the crystalline phase of the formed NPs. Further, morphological studies was done by Transmission electron microscope (TEM) which showed an approximate size of 20 nm exhibiting the shape of a sphere. Along with this, results obtained from Scanning electron microscope (SEM), Fourier transform infrared spectroscopy (FTIR), and Dynamic light scattering (DLS) particle size analyzer also confirmed the surface morphology and functional group of the NPs. Broad spectrum antibacterial activity with Gram positive and negative bacteria were evaluated along with the antioxidant activity which showed high potency of NPs. RG3<sup>T</sup>-NPs were treated against cell lines like MCF-7, HEPG-2, and notably against Triple negative human breast cancer (TNBC) cell line which showed it's superior efficiency. Therefore, it can be concluded that RG3<sup>T</sup>-NPs points itself to be a significant bio-material with antibacterial, cytotoxic, and antioxidant properties.

## 6.2 Chapter 3

In this study, novel biogenic silver nanoparticles have been developed involving a green method by a yeast strain, *Papiliotrema laurentii* (Y24) cell resuspension exudate. Synthesis conditions have been optimized and the produced nanomaterials have been characterized by DLS, Zeta Potential, FTIR, XRD, SEM, TEM to predict and analyse the particles. High crystallinity, irregular to cubical shape, and an average dimension of 20 nM of AgNPs were obtained from the characterization. Biogenic Y24-NPs were applied to reduce 4-Nitrophenol to 4-Aminophenol by catalytic activity (within 8 minutes). After 5 recycles, high reusability of Y24-NPs was observed ( $\geq 94\%$ ). Y24-NPs were further demonstrated for high selectivity and sensitivity towards  $\text{Fe}^{3+}$  by colorimetric detection with the limit of  $1.8 \mu\text{M}$  in the linear range of  $5\text{--}150 \mu\text{M}$ . Additionally, the developed nanosensor has been tested for  $\text{Fe}^{3+}$  ions in tap water samples. Therefore, Y24-NPs can be used for bioremediation with significant catalytic activity and reusability.

## 6.3 Chapter 4

A novel biogenic silver nanoparticle production has been done using a yeast *Pichia manshurica*, strain CD1 cell resuspension exudates. The characterization of AgNPs by DLS, Zeta Potential, FTIR, XRD, SEM, and TEM was done to obtain spherical particle morphology with 22 nM diameter. Biocatalysis of CD1-NPs was done to obtain the catalytic degradation of azo dyes, Congo red, and Malachite green. Degradation occurred within 30 minutes for Congo red and 40 minutes for Malachite green with degradation efficiency of 98.86 % and 97.54 % respectively. High reusability (approximately 94%) was observed of CD1-NPs up to 5 recycles. CD1-NPs were further tested for selectivity and sensitivity towards  $\text{Hg}^{2+}$  by colorimetric detection with a limit of 21.04 nM in the linear range of 10-80 nM. The nanosensor has been tested for  $\text{Hg}^{2+}$  ions in mercury-treated tap water samples. The efficiency of the biocatalysts was accessed for practical applicability.

## 6.4 Chapter 5

Bio-production of bacterial cellulose (BC) from the strain *Glucanoacteobacter kombuchae* (RG3<sup>T</sup>) has been optimized by varying the different parameters such as media, days of incubation, pH and carbon and nitrogen sources. The optimum time of incubation was 14 d, and the optimum temperature was found to be 30 degrees C. At the optimum pH of 5, the highest production of cellulose was obtained. On the basis of the result obtained On the basis of the above results, the optimum production medium was determined to contain 2% mannitol, 0.5% beef extract, 0.27% disodium hydrogen phosphate, 0.11% citric acid, 0.5 % MgSO<sub>4</sub>, 0.1% lactose and 1.5% (v/v) ethanol with an initial pH of 5.0. RG3 produced 0.728g/l of cellulose in unmodified HS medium whereas in the optimized media it was boosted to 3.0g/L. Cellulose produced by RG3 under these optimized conditions has a thickness of 8 m, a Young's Modulus of 1.92 MPa and a value of 10.6% of extension at breakage. A decrease of 50% cell O.D.600 nM was observed when the membrane was used as a filter for bacterial and yeast cell suspension. Therefore the membrane was further applied to test for antibacterial activity to test as filtrate against one Gram-negative cell *E.coli* and one Gram-positive bacteria *S. aureus*. The filtrates indicated the reduction of 80-90 % decrease cell O.D. 400 nM. The experiment showed that RG3 can synthesize cellulose even in the absence of any nitrogen source in the medium. Hence, the strain RG3 can be maintained in a relatively cheap medium and by using a cheap source like rice straw, it can be directed to synthesize maximum amount of cellulose.

# List of Publications

1. Majumder, J., Pal, K., Chakraborty, W., Karmakar, P., & Gachhui, R. (2022). Glucanoacetobacter kombuchae (RG3T), a novel bacteria for AgNPs biosynthesis: Characterization and comprehensive evaluation of bioactivity. In Materials Today Communications (Vol. 33, p. 104410). Elsevier BV.
2. Majumder, J., Bhunia, T., Gorai, S., De, D., Karmakar, P., & Gachhui, R. (2023). Efficient degradation of 4-nitrophenol and colorimetric detection of Fe (III) by biogenic silver nanoparticles of Papiliotrema laurentii. In Materials Science and Engineering: B (Vol. 296, p. 116647). Elsevier BV.
3. Majumder, J., & Gachhui, R. (2023). Effective degradation of azo dyes and colorimetric detection of Hg<sup>2+</sup> by biogenic silver nanoparticles of Pichia manshurica. In Bioresource Technology Reports (Vol. 23, p. 101498). Elsevier BV.

# References

- [1] Aftab Ahmad et al. “The effects of bacteria-nanoparticles interface on the antibacterial activity of green synthesized silver nanoparticles”. In: *Microbial Pathogenesis* 102 (2017), pp. 133–142. DOI: 10.1016/j.micpath.2016.11.030.
- [2] Jasim Ahmed, Mehrajfatema Zafar Mulla, and Yasir Ali Arfat. “Thermo-mechanical, structural characterization and antibacterial performance of solvent casted polylactide/cinnamon oil composite films”. In: *Food Control* 69 (2016), pp. 196–204. DOI: 10.1016/j.foodcont.2016.05.013.
- [3] Shakeel Ahmed and Saiqa Ikram. “Silver nanoparticles: one pot green synthesis using Terminalia arjuna extract for biological application”. In: *J Nanomed Nanotechnol* 6.4 (2015), p. 309.
- [4] Shakeel Ahmed et al. “A review on plants extract mediated synthesis of silver nanoparticles for antimicrobial applications: A green expertise”. In: *Journal of Advanced Research* 7.1 (2016), pp. 17–28. DOI: 10.1016/j.jare.2015.02.007G.
- [5] Shakeel Ahmed et al. “Green synthesis of silver nanoparticles using Azadirachta indica aqueous leaf extract”. In: *Journal of radiation research and applied sciences* 9.1 (2016), pp. 1–7. DOI: 10.1016/j.jrras.2015.06.006.
- [6] KS Aiswariya and Vimala Jose. “Bioactive molecules coated silver oxide nanoparticle synthesis from Curcuma zanthorrhiza and HR-LCMS monitored validation of its photocatalytic potency towards malachite green degradation”. In: *Journal of Cluster Science* (2022), pp. 1–12. DOI: 10.1007/s10876-021-02099-0.
- [7] B Ajitha, Y Ashok Kumar Reddy, and P Sreedhara Reddy. “Green synthesis and characterization of silver nanoparticles using Lantana camara leaf extract”. In: *Materials Science and Engineering: C* 49 (2015), pp. 373–381. DOI: 10.1016/j.msec.2015.01.035.
- [8] Masahiro Akiyama et al. “Potentiation of methylmercury toxicity by combined metal exposure: In vitro and in vivo models of a restricted metal exposure”. In: *Chemosphere* 299 (2022), p. 134374. DOI: 10.1016/j.chemosphere.2022.134374.
- [9] Shroog Shdied Royji Albeladi, Maqsood Ahmad Malik, and Shaeel Ahmed Al-thabaiti. “Facile biofabrication of silver nanoparticles using Salvia officinalis leaf extract and its catalytic activity towards Congo red dye degradation”. In: *Journal of Materials Research and Technology* 9.5 (2020), pp. 10031–10044. DOI: 10.1016/j.jmrt.2020.06.074.

- [10] Soha M Albukhari et al. "Catalytic reduction of nitrophenols and dyes using silver nanoparticles@ cellulose polymer paper for the resolution of waste water treatment challenges". In: *Colloids and Surfaces A: Physicochemical and Engineering Aspects* 577 (2019), pp. 548–561. DOI: [10.1016/j.colsurfa.2019.05.058](https://doi.org/10.1016/j.colsurfa.2019.05.058).
- [11] Syed Ghazanfar Ali et al. "Antibacterial and antibiofilm potential of green synthesized silver nanoparticles against imipenem resistant clinical isolates of *P. aeruginosa*". In: *BioNanoScience* 8.2 (2018), pp. 544–553. DOI: [10.1007/s12668-018-0505-8](https://doi.org/10.1007/s12668-018-0505-8).
- [12] Hadi Almasi, Laleh Mehryar, and Ali Ghadertaj. "Characterization of CuO-bacterial cellulose nanohybrids fabricated by in-situ and ex-situ impregnation methods". In: *Carbohydrate polymers* 222 (2019), p. 114995. DOI: [10.1016/j.carbpol.2019.114995](https://doi.org/10.1016/j.carbpol.2019.114995).
- [13] Melisew Tadele Alula et al. "Enhanced catalytic activity of silver nanoparticles loaded into Fe<sub>3</sub>O<sub>4</sub> nanoparticles towards reduction of 4-nitrophenol, degradation of organic dyes and oxidation of o-phenylenediamine". In: *Inorganic Chemistry Communications* 127 (2021), p. 108504. DOI: [10.1016/j.inoche.2021.108504](https://doi.org/10.1016/j.inoche.2021.108504).
- [14] Ja-an Annie Ho, Heng-Chia Chang, and Wen-Ta Su. "DOPA-mediated reduction allows the facile synthesis of fluorescent gold nanoclusters for use as sensing probes for ferric ions". In: *Analytical Chemistry* 84.7 (2012), pp. 3246–3253. DOI: [doi.org/10.1021/ac203362g](https://doi.org/10.1021/ac203362g).
- [15] Hassan Anwer et al. "Photocatalysts for degradation of dyes in industrial effluents: Opportunities and challenges". In: *Nano Research* 12.5 (2019), pp. 955–972.
- [16] Mariadhas Valan Arasu et al. "One step green synthesis of larvicidal, and azo dye degrading antibacterial nanoparticles by response surface methodology". In: *Journal of Photochemistry and Photobiology B: Biology* 190 (2019), pp. 154–162. DOI: [10.1016/j.jphotobiol.2018.11.020](https://doi.org/10.1016/j.jphotobiol.2018.11.020).
- [17] C Otero Areán et al. "Quantum chemical and FTIR spectroscopic studies on the linkage isomerism of carbon monoxide in alkali-metal-exchanged zeolites: A review of current research". In: *International Journal of Molecular Sciences* 3.7 (2002), pp. 764–776. DOI: [10.3390/i3070764](https://doi.org/10.3390/i3070764).
- [18] Ameer Azam et al. "One step synthesis and characterization of gold nanoparticles and their antibacterial activities against *E. coli* (ATCC 25922 strain)". In: *International Journal of Theoretical & Applied Sciences* 1.2 (2009), pp. 1–4.
- [19] S Balasurya et al. "Rapid colorimetric detection of mercury using silver nanoparticles in the presence of methionine". In: *Spectrochimica Acta Part A: Molecular and Biomolecular Spectroscopy* 228 (2020), p. 117712.
- [20] Saeedeh Barshan et al. "Optimization and characterization of bacterial cellulose produced by *Komagatacibacter xylinus* PTCC 1734 using vinasse as a cheap cultivation medium". In: *International journal of biological macromolecules* 136 (2019), pp. 1188–1195. DOI: [10.1016/j.ijbiomac.2019.06.192](https://doi.org/10.1016/j.ijbiomac.2019.06.192).

- [21] Sedigheh Basiri, Ali Mehdinia, and Ali Jabbari. “A sensitive triple colorimetric sensor based on plasmonic response quenching of green synthesized silver nanoparticles for determination of  $\text{Fe}^{2+}$ , hydrogen peroxide, and glucose”. In: *Colloids and Surfaces A: Physicochemical and Engineering Aspects* 545 (2018), pp. 138–146.
- [22] Hayelom Dargo Beyene et al. “Synthesis paradigm and applications of silver nanoparticles (AgNPs), a review”. In: *Sustainable materials and technologies* 13 (2017), pp. 18–23. DOI: [10.1016/j.susmat.2017.08.001](https://doi.org/10.1016/j.susmat.2017.08.001).
- [23] Marco Laurence M Budlayan et al. “Functionalized silver nanoparticle-decorated paper sensor for rapid colorimetric detection of copper ions in water”. In: *Functional Composites and Structures* 3.3 (2021), p. 035007. DOI: [10.1088/2631-6331/ac25e9/meta](https://doi.org/10.1088/2631-6331/ac25e9/meta).
- [24] Peter Capek et al. “Coffea arabica instant coffee—chemical view and immunomodulating properties”. In: *Carbohydrate polymers* 103 (2014), pp. 418–426. DOI: [10.1016/j.carbpol.2013.12.068](https://doi.org/10.1016/j.carbpol.2013.12.068).
- [25] Somnath Chakravorty et al. “Kombucha tea fermentation: Microbial and biochemical dynamics”. In: *International journal of food microbiology* 220 (2016), pp. 63–72. DOI: [10.1016/j.ijfoodmicro.2015.12.015](https://doi.org/10.1016/j.ijfoodmicro.2015.12.015).
- [26] Somnath Chakravorty et al. “Kombucha: a promising functional beverage prepared from tea”. In: *Non-alcoholic beverages*. Elsevier, 2019, pp. 285–327. DOI: [10.1016/B978-0-12-815270-6.00010-4](https://doi.org/10.1016/B978-0-12-815270-6.00010-4).
- [27] Nagalakshmi Chinthalapudi et al. “Composites of cellulose nanofibers and silver nanoparticles for malachite green dye removal from water”. In: *Carbohydrate Polymer Technologies and Applications* 2 (2021), p. 100098. DOI: [10.1016/j.carpta.2021.100098](https://doi.org/10.1016/j.carpta.2021.100098).
- [28] Manoj Kumar Choudhary et al. “Green biomimetic silver nanoparticles as invigorated colorimetric probe for  $\text{Hg}^{2+}$  ions: A cleaner approach towards recognition of heavy metal ions in aqueous media”. In: *Materials Chemistry and Physics* 240 (2020), p. 122164. DOI: [10.1016/j.matchemphys.2019.122164](https://doi.org/10.1016/j.matchemphys.2019.122164).
- [29] SS Chougule et al. “Low density polyethylene films incorporated with Biosynthesised silver nanoparticles using Moringa oleifera plant extract for antimicrobial, food packaging, and photocatalytic degradation applications”. In: *Journal of Plant Biochemistry and Biotechnology* 30 (2021), pp. 208–214. DOI: [10.1007/s13562-020-00584-7](https://doi.org/10.1007/s13562-020-00584-7).
- [30] Claire M Copley et al. “Controlled etching as a route to high quality silver nanospheres for optical studies”. In: *The Journal of Physical Chemistry C* 113.39 (2009), pp. 16975–16982. DOI: [10.1021/jp906457f](https://doi.org/10.1021/jp906457f).
- [31] Tikam Chand Dakal et al. “Mechanistic basis of antimicrobial actions of silver nanoparticles”. In: *Frontiers in microbiology* 7 (2016), p. 1831. DOI: [10.3389/fmicb.2016.01831](https://doi.org/10.3389/fmicb.2016.01831).
- [32] Sonika Dawadi et al. “Current research on silver nanoparticles: Synthesis, characterization, and applications”. In: *Journal of nanomaterials* 2021 (2021). DOI: [10.1155/2021/6687290](https://doi.org/10.1155/2021/6687290).



- [33] Jiawei Du et al. “Colorimetric detection of cadmium in water using L-cysteine functionalized gold–silver nanoparticles”. In: *Analytical Letters* 51.18 (2018), pp. 2906–2919. DOI: [10.1080/00032719.2018.1455103](https://doi.org/10.1080/00032719.2018.1455103).
- [34] Renpeng Du et al. “Production, optimization and partial characterization of bacterial cellulose from *Gluconacetobacter xylinus* TJU-D2”. In: *Waste and Biomass Valorization* 11 (2020), pp. 1681–1690. DOI: [10.1007/s12649-018-0440-5](https://doi.org/10.1007/s12649-018-0440-5).
- [35] Junling Duan et al. “Facile colorimetric detection of Hg<sup>2+</sup> based on anti-aggregation of silver nanoparticles”. In: *Biosensors and Bioelectronics* 57 (2014), pp. 139–142. DOI: [10.1016/j.bios.2014.02.007](https://doi.org/10.1016/j.bios.2014.02.007).
- [36] Debasree Dutta and Ratan Gachhui. “Nitrogen-fixing and cellulose-producing *Gluconacetobacter kombuchae* sp. nov., isolated from Kombucha tea”. In: *International Journal of Systematic and Evolutionary Microbiology* 57.2 (2007), pp. 353–357. DOI: [10.1099/ijs.0.64638-0](https://doi.org/10.1099/ijs.0.64638-0).
- [37] Scott D Dyer et al. “Comparison of species sensitivity distributions derived from interspecies correlation models to distributions used to derive water quality criteria”. In: *Environmental science & technology* 42.8 (2008), pp. 3076–3083. DOI: [10.1021/es702302e](https://doi.org/10.1021/es702302e).
- [38] Wael H Eisa et al. “Clean production of powdery silver nanoparticles using *Zingiber officinale*: The structural and catalytic properties”. In: *Journal of Cleaner Production* 241 (2019), p. 118398. DOI: [10.1016/j.jclepro.2019.118398](https://doi.org/10.1016/j.jclepro.2019.118398).
- [39] Ali Serol Ertürk. “Biosynthesis of silver nanoparticles using *Epilobium parviflorum* green tea extract: Analytical applications to colorimetric detection of Hg<sup>2+</sup> ions and reduction of hazardous organic dyes”. In: *Journal of Cluster Science* 30.5 (2019), pp. 1363–1373. DOI: [10.1007/s10876-019-01634-4](https://doi.org/10.1007/s10876-019-01634-4).
- [40] Amanulla Mohammed Fayaz et al. “Biogenic synthesis of silver nanoparticles and their synergistic effect with antibiotics: a study against gram-positive and gram-negative bacteria”. In: *Nanomedicine: Nanotechnology, Biology and Medicine* 6.1 (2010), pp. 103–109. DOI: [10.1016/j.nano.2009.04.006](https://doi.org/10.1016/j.nano.2009.04.006).
- [41] Jie Feng et al. “Polyethyleneimine-templated copper nanoclusters via ascorbic acid reduction approach as ferric ion sensor”. In: *Analytica Chimica Acta* 854 (2015), pp. 153–160. DOI: <https://doi.org/10.1016/j.aca.2014.11.024>.
- [42] Xiaohui Gao et al. “Colorimetric detection of iron ions (III) based on the highly sensitive plasmonic response of the N-acetyl-L-cysteine-stabilized silver nanoparticles”. In: *Analytica chimica acta* 879 (2015), pp. 118–125. DOI: [10.1016/j.aca.2015.04.002](https://doi.org/10.1016/j.aca.2015.04.002).
- [43] Milan Gautam et al. “Plug-in safe-by-design nanoinorganic antibacterials”. In: *ACS nano* 13.11 (2019), pp. 12798–12809. DOI: [10.1021/acsnano.9b04939](https://doi.org/10.1021/acsnano.9b04939).
- [44] S Ghosh et al. “Antimicrobial activity of highly stable silver nanoparticles embedded in agar–agar matrix as a thin film”. In: *Carbohydrate Research* 345.15 (2010), pp. 2220–2227. DOI: [10.1016/j.carres.2010.08.001](https://doi.org/10.1016/j.carres.2010.08.001).

- [45] Sougata Ghosh et al. “Synthesis of silver nanoparticles using *Dioscorea bulbifera* tuber extract and evaluation of its synergistic potential in combination with antimicrobial agents”. In: *International journal of nanomedicine* 7 (2012), p. 483. DOI: **10.2147/IJN.S24793**.
- [46] Samchetshabam Gita, Ajmal Hussan, and TG Choudhury. “Impact of textile dyes waste on aquatic environments and its treatment”. In: *Environ. Ecol* 35.3C (2017), pp. 2349–2353.
- [47] Jian Guan et al. “pH-dependent aggregation of histidine-functionalized Au nanoparticles induced by Fe<sup>3+</sup> ions”. In: *The Journal of Physical Chemistry C* 112.9 (2008), pp. 3267–3271. DOI: **doi.org/10.1021/jp7097763**.
- [48] Xia Guo et al. “Lateral etching of core-shell Au@ metal nanorods to metal-tipped Au nanorods with improved catalytic activity”. In: *ACS nano* 6.2 (2012), pp. 1165–1175. DOI: **10.1021/nn203793k**.
- [49] Nikesh Gupta, Henam Premananda Singh, and Rakesh Kumar Sharma. “Metal nanoparticles with high catalytic activity in degradation of methyl orange: an electron relay effect”. In: *Journal of Molecular Catalysis A: Chemical* 335.1-2 (2011), pp. 248–252. DOI: **10.1016/j.molcata.2010.12.001**.
- [50] Sangiliyandi Gurunathan et al. “Biosynthesis, purification and characterization of silver nanoparticles using *Escherichia coli*”. In: *Colloids and Surfaces B: Biointerfaces* 74.1 (2009), pp. 328–335. DOI: **10.1016/j.colsurfb.2009.07.048**.
- [51] Cathierine Haefeli, CHRISTOPHER Franklin, and KIMBER Hardy. “Plasmid-determined silver resistance in *Pseudomonas stutzeri* isolated from a silver mine”. In: *Journal of bacteriology* 158.1 (1984), pp. 389–392. DOI: **10.1128/jb.158.1.389-392.1984**.
- [52] Mohammad J Hajipour et al. “Antibacterial properties of nanoparticles”. In: *Trends in Biotechnology* 30.10 (2012), pp. 499–511. DOI: **10.1016/j.tibtech.2012.06.004**.
- [53] Chanel Tri Handoko, Adri Huda, and Fakhili Gulo. “Synthesis pathway and powerful antimicrobial properties of silver nanoparticle: a critical review”. In: *Asian J. Sci. Res* 12.1 (2019), pp. 1–17.
- [54] Ana María Herrera-González, Martín Caldera-Villalobos, and Alejandra-Alicia Peláez-Cid. “Adsorption of textile dyes using an activated carbon and crosslinked polyvinyl phosphonic acid composite”. In: *Journal of environmental management* 234 (2019), pp. 237–244. DOI: **10.1016/j.jenvman.2019.01.012**.
- [55] Jessica Huber and Kerstin Leopold. “Nanomaterial-based strategies for enhanced mercury trace analysis in environmental and drinking waters”. In: *TrAC Trends in Analytical Chemistry* 80 (2016), pp. 280–292. DOI: **10.1016/j.trac.2015.09.007**.
- [56] Karuppusamy Indira et al. “Photocatalytic degradation of congo red dye using nickel-titanium dioxide nanoflakes synthesized by *Mukia madrasapatna* leaf extract”. In: *Environmental Research* 202 (2021), p. 111647. DOI: **10.1016/j.envres.2021.111647**.

- [57] Margaret Ip et al. “Antimicrobial activities of silver dressings: an in vitro comparison”. In: *Journal of Medical Microbiology* 55.1 (2006), pp. 59–63. DOI: [10.1099/jmm.0.46124-0](https://doi.org/10.1099/jmm.0.46124-0).
- [58] Gehan A Ismail et al. “The role of silver nanoparticles biosynthesized by *Anabaena variabilis* and *Spirulina platensis* cyanobacteria for malachite green removal from wastewater”. In: *Environmental Technology* 42.28 (2021), pp. 4475–4489. DOI: [10.1080/09593330.2020.1766576](https://doi.org/10.1080/09593330.2020.1766576).
- [59] Muhammad Ismail et al. “Biosynthesis of silver nanoparticles: a colorimetric optical sensor for detection of hexavalent chromium and ammonia in aqueous solution”. In: *Physica E: Low-dimensional Systems and Nanostructures* 103 (2018), pp. 367–376. DOI: [10.1016/j.physe.2018.06.015](https://doi.org/10.1016/j.physe.2018.06.015).
- [60] Mohammed Abdullah Issa et al. “Fluorescent recognition of  $\text{Fe}^{3+}$  in acidic environment by enhanced-quantum yield N-doped carbon dots: Optimization of variables using central composite design”. In: *Scientific reports* 10.1 (2020), pp. 1–18. DOI: [10.1038/s41598-020-68390-8](https://doi.org/10.1038/s41598-020-68390-8).
- [61] Chidambaram Jayaseelan et al. “Green synthesis of gold nanoparticles using seed aqueous extract of *Abelmoschus esculentus* and its antifungal activity”. In: *Industrial Crops and Products* 45 (2013), pp. 423–429. DOI: [10.1016/j.indcrop.2012.12.019](https://doi.org/10.1016/j.indcrop.2012.12.019).
- [62] Anal K Jha, K Prasad, et al. “Yeast mediated synthesis of silver nanoparticles”. In: *International Journal of Nanoscience and Nanotechnology* 4.1 (2008), pp. 17–22. DOI: [article\\_3994\\_812.html](https://doi.org/article_3994_812.html).
- [63] Yu Jiang et al. “Biodegradation of phenol by entrapped cell of *Debaryomyces* sp. with nano- $\text{Fe}_3\text{O}_4$  under hypersaline conditions”. In: *International Biodegradation & Biodegradation* 123 (2017), pp. 37–45.
- [64] Hao Jing et al. “Tunable plasmonic nanoparticles with catalytically active high-index facets”. In: *Nano letters* 14.6 (2014), pp. 3674–3682. DOI: [10.1021/nl5015734](https://doi.org/10.1021/nl5015734).
- [65] Suresh Kumar Kailasa et al. “Influence of ligand chemistry on silver nanoparticles for colorimetric detection of  $\text{Cr}^{3+}$  and  $\text{Hg}^{2+}$  ions”. In: *Spectrochimica Acta Part A: Molecular and Biomolecular Spectroscopy* 195 (2018), pp. 120–127. DOI: [10.1016/j.saa.2018.01.038](https://doi.org/10.1016/j.saa.2018.01.038).
- [66] S Kandakumar, V Sathya, and V Manju. “Synthesis and characterization of silver nanoparticles using *Hydnocarpus alpina*, its application as A potent antimicrobial and antioxidant agent—a novel study”. In: *International Journal of Chemtech Research* 6 (2014), pp. 4770–4776.
- [67] Hassan Karimi-Maleh et al. “Recent advances in using of chitosan-based adsorbents for removal of pharmaceutical contaminants: A review”. In: *Journal of Cleaner Production* 291 (2021), p. 125880. DOI: [10.1016/j.jclepro.2021.125880](https://doi.org/10.1016/j.jclepro.2021.125880).
- [68] Nitasha Khatri, Sanjiv Tyagi, and Deepak Rawtani. “Recent strategies for the removal of iron from water: A review”. In: *Journal of Water Process Engineering* 19 (2017), pp. 291–304. DOI: [10.1016/j.jwpe.2017.08.015](https://doi.org/10.1016/j.jwpe.2017.08.015).

- [69] S Pakya Lakshmi, S Dhanya, and D Sheeba. “Photocatalytic degradation of malachite green using silver nanoparticles synthesised from gooseberry extract”. In: *J Chem Mater Res* 5 (2016), pp. 68–73.
- [70] M Latha et al. “N-doped oxidized carbon dots for methanol sensing in alcoholic beverages”. In: *RSC advances* 10.38 (2020), pp. 22522–22532. DOI: [10.1039/D0RA02694H](https://doi.org/10.1039/D0RA02694H).
- [71] Van Thuan Le et al. “Highly effective degradation of nitrophenols by biometal nanoparticles synthesized using *Caulis spatholobi* extract”. In: *Journal of Nanomaterials* 2021 (2021). DOI: [10.1155/2021/6696995](https://doi.org/10.1155/2021/6696995).
- [72] Seung Jun Lee, Jayaraman Theerthagiri, and Myong Yong Choi. “Time-resolved dynamics of laser-induced cavitation bubbles during production of Ni nanoparticles via pulsed laser ablation in different solvents and their electrocatalytic activity for determination of toxic nitroaromatics”. In: *Chemical Engineering Journal* 427 (2022), p. 130970. DOI: [10.1016/j.cej.2021.130970](https://doi.org/10.1016/j.cej.2021.130970).
- [73] Seung Jun Lee et al. “Nanogap-tailored Au nanoparticles fabricated by pulsed laser ablation for surface-enhanced Raman scattering”. In: *Biosensors and Bioelectronics* 197 (2022), p. 113766. DOI: [10.1016/j.bios.2021.113766](https://doi.org/10.1016/j.bios.2021.113766).
- [74] Xiaoli Li et al. “Preparation and characterization of new foam adsorbents of poly (vinyl alcohol)/chitosan composites and their removal for dye and heavy metal from aqueous solution”. In: *Chemical Engineering Journal* 183 (2012), pp. 88–97.
- [75] Yun Liu et al. “Adsorption of cations onto the surfaces of silver nanoparticles”. In: *Journal of colloid and interface science* 257.2 (2003), pp. 188–194. DOI: [https://doi.org/10.1016/S0021-9797\(02\)00027-9](https://doi.org/10.1016/S0021-9797(02)00027-9).
- [76] Jhila Majumder and Ratan Gachhui. “Effective degradation of azo dyes and colorimetric detection of Hg<sup>2+</sup> by biogenic silver nanoparticles of *Pichia manshurica*”. In: *Bioresource Technology Reports* (2023), p. 101498.
- [77] Jhila Majumder et al. “Efficient degradation of 4-nitrophenol and colorimetric detection of Fe (III) by biogenic silver nanoparticles of *Papiliotrema laurentii*”. In: *Materials Science and Engineering: B* 296 (2023), p. 116647.
- [78] Jhila Majumder et al. “Glucanoacetobacter kombuchae (RG3T), a novel bacteria for AgNPs biosynthesis: Characterization and comprehensive evaluation of bioactivity”. In: *Materials Today Communications* 33 (2022), p. 104410.
- [79] Sivasankari Marimuthu et al. “Silver nanoparticles in dye effluent treatment: A review on synthesis, treatment methods, mechanisms, photocatalytic degradation, toxic effects and mitigation of toxicity”. In: *Journal of Photochemistry and Photobiology B: Biology* 205 (2020), p. 111823. DOI: [10.1016/j.jphotobiol.2020.111823](https://doi.org/10.1016/j.jphotobiol.2020.111823).
- [80] Moorthy Maruthapandi et al. “Facile ultrasonic preparation of a polypyrrole membrane as an absorbent for efficient oil-water separation and as an antimicrobial agent”. In: *Ultrasonics Sonochemistry* 78 (2021), p. 105746. DOI: [10.1016/j.ultsonch.2021.105746](https://doi.org/10.1016/j.ultsonch.2021.105746).
- [81] Sukanya Mehra, Mandeep Singh, and Pooja Chadha. “Adverse impact of textile dyes on the aquatic environment as well as on human beings”. In: *Toxicology International* 28.2 (2021), pp. 165–176.

- [82] Amit Kumar Mittal, Yusuf Chisti, and Uttam Chand Banerjee. "Synthesis of metallic nanoparticles using plant extracts". In: *Biotechnology Advances* 31.2 (2013), pp. 346–356. DOI: 10.1016/j.biotechadv.2013.01.003.
- [83] Vicky V Mody et al. "Introduction to metallic nanoparticles". In: *Journal of Pharmacy and Bioallied Sciences* 2.4 (2010), p. 282. DOI: 10.4103/0975-7406.72127.
- [84] D MubarakAli et al. "Plant extract mediated synthesis of silver and gold nanoparticles and its antibacterial activity against clinically isolated pathogens". In: *Colloids and Surfaces B: Biointerfaces* 85.2 (2011), pp. 360–365. DOI: 10.1016/j.colsurfb.2011.03.009.
- [85] Maxwell Murphy et al. "Current development of silver nanoparticle preparation, investigation, and application in the field of medicine". In: *Journal of Nanomaterials* 2015 (2015). DOI: 10.1155/2015/696918.
- [86] Shreyanka Shankar Naik et al. "Rapid and highly selective electrochemical sensor based on ZnS/Au-decorated f-multi-walled carbon nanotube nanocomposites produced via pulsed laser technique for detection of toxic nitro compounds". In: *Journal of Hazardous Materials* 418 (2021), p. 126269. DOI: /10.1016/j.jhazmat.2021.126269.
- [87] Nguyen Thi Anh Nga et al. "Green fabrication of silver nanoparticles using Chloroxylon swietenia leaves and their application towards dye degradation and food borne pathogens". In: *Food and Chemical Toxicology* (2022), p. 113192. DOI: 10.1016/j.fct.2022.113192.
- [88] Thi Hong Anh Nguyen et al. "Novel biogenic silver and gold nanoparticles for multifunctional applications: Green synthesis, catalytic and antibacterial activity, and colorimetric detection of Fe (III) ions". In: *Chemosphere* 287 (2022), p. 132271. DOI: 10.1155/2021/6696995.
- [89] F Orts et al. "Electrochemical treatment of real textile wastewater: Trichromy Procion HEXL®". In: *Journal of Electroanalytical Chemistry* 808 (2018), pp. 387–394. DOI: 10.1016/j.jelechem.2017.06.051.
- [90] Donald L Pavia et al. *Introduction to spectroscopy*. Cengage Learning, 2014.
- [91] S Ponarulselvam et al. "Synthesis of silver nanoparticles using leaves of Catharanthus roseus Linn. G. Don and their antiplasmodial activities". In: *Asian Pacific journal of tropical biomedicine* 2.7 (2012), pp. 574–580. DOI: 10.1016/S2221-1691(12)60100-2.
- [92] P Prakash et al. "Green synthesis of silver nanoparticles from leaf extract of Mimosa elengi, Linn. for enhanced antibacterial activity against multi drug resistant clinical isolates". In: *Colloids and Surfaces B: Biointerfaces* 108 (2013), pp. 255–259. DOI: 10.1016/j.colsurfb.2013.03.017.
- [93] P Prema et al. "Statistical optimization of silver nanoparticle synthesis by green tea extract and its efficacy on colorimetric detection of mercury from industrial waste water". In: *Environmental Research* 204 (2022), p. 111915. DOI: 10.1016/j.envres.2021.111915.
- [94] Paolo Proposito, Luca Burratti, and Iole Venditti. "Silver nanoparticles as colorimetric sensors for water pollutants". In: *Chemosensors* 8.2 (2020), p. 26. DOI: 10.3390/chemosensors8020026.

- [95] M Raffi et al. “Antibacterial characterization of silver nanoparticles against E. coli ATCC-15224”. In: *Journal of materials science and technology* 24.2 (2008), pp. 192–196.
- [96] P Iyyappa Rajan et al. “Green-fuel-mediated synthesis of self-assembled NiO nano-sticks for dual applications—photocatalytic activity on Rose Bengal dye and antimicrobial action on bacterial strains”. In: *Materials Research Express* 4.8 (2017), p. 085030. DOI: [10.1088/2053-1591/aa7e3c](https://doi.org/10.1088/2053-1591/aa7e3c).
- [97] S Rajeshkumar, LV Bharath, and R Geetha. “Broad spectrum antibacterial silver nanoparticle green synthesis: Characterization, and mechanism of action”. In: *Green Synthesis, Characterization and Applications of Nanoparticles*. Elsevier, 2019, pp. 429–444. DOI: [10.1016/B978-0-08-102579-6.00018-6](https://doi.org/10.1016/B978-0-08-102579-6.00018-6).
- [98] W Raut Rajesh et al. “Phytosynthesis of silver nanoparticle using Gliricidia sepium (Jacq.)” In: *Current Nanoscience* 5.1 (2009), pp. 117–122. DOI: [10.5185/amlett.2012.11470](https://doi.org/10.5185/amlett.2012.11470).
- [99] Poovathinhodiyil Raveendran, Jie Fu, and Scott L Wallen. “Completely “green” synthesis and stabilization of metal nanoparticles”. In: *Journal of the American Chemical Society* 125.46 (2003), pp. 13940–13941. DOI: [10.1021/ja029267j](https://doi.org/10.1021/ja029267j).
- [100] Roberta Re et al. “Antioxidant activity applying an improved ABTS radical cation decolorization assay”. In: *Free Radical Biology and Medicine* 26.9-10 (1999), pp. 1231–1237. DOI: [10.1016/S0891-5849\(98\)00315-3](https://doi.org/10.1016/S0891-5849(98)00315-3).
- [101] Andrea Rossi et al. “Silver Nanoparticle-Based Sensor for the Selective Detection of Nickel Ions”. In: *Nanomaterials* 11.7 (2021), p. 1733. DOI: <https://doi.org/10.3390/nano11071733>.
- [102] Priyadarshani S Sadalage et al. “Almond skin extract mediated optimally biosynthesized antibacterial silver nanoparticles enable selective and sensitive colorimetric detection of Fe<sup>2+</sup> ions”. In: *Colloids and Surfaces B: Biointerfaces* 193 (2020), p. 111084. DOI: [10.1016/j.colsurfb.2020.111084](https://doi.org/10.1016/j.colsurfb.2020.111084).
- [103] Apichart Saenchoopa et al. “Colorimetric detection of Hg (II) by  $\gamma$ -aminobutyric acid-silver nanoparticles in water and the assessment of antibacterial activities”. In: *Spectrochimica Acta Part A: Molecular and Biomolecular Spectroscopy* 251 (2021), p. 119433. DOI: [10.1016/j.saa.2021.119433](https://doi.org/10.1016/j.saa.2021.119433).
- [104] Tapendu Samanta et al. “Unusual red-orange emission from rhodamine-derived polynorbornene for selective binding to Fe<sup>3+</sup> ions in an aqueous environment”. In: *Analytical Methods* 12.33 (2020), pp. 4159–4165. DOI: [10.1039/D0AY00505C](https://doi.org/10.1039/D0AY00505C).
- [105] Mitali Sarkar et al. “Statistical optimization of bio-mediated silver nanoparticles synthesis for use in catalytic degradation of some azo dyes”. In: *Chemical Physics Impact* 3 (2021), p. 100053. DOI: [10.1016/j.chphi.2021.100053](https://doi.org/10.1016/j.chphi.2021.100053).
- [106] Soumyadev Sarkar et al. “Homology modeling, molecular docking and molecular dynamics studies of the catalytic domain of chitin deacetylase from *Cryptococcus laurentii* strain RY1”. In: *International journal of biological macromolecules* 104 (2017), pp. 1682–1691. DOI: [10.1007/s40011-017-0898-0](https://doi.org/10.1007/s40011-017-0898-0).

- [107] Juliana Barden Schallemberger et al. “Textile azo dyes discolouration using spent mushroom substrate: enzymatic degradation and adsorption mechanisms”. In: *Environmental Technology* (2021), pp. 1–22.
- [108] Felix Scholkmann et al. “A review on continuous wave functional near-infrared spectroscopy and imaging instrumentation and methodology”. In: *Neuroimage* 85 (2014), pp. 6–27. DOI: [10.1016/j.neuroimage.2013.05.004](https://doi.org/10.1016/j.neuroimage.2013.05.004).
- [109] Shiv Shankar and Jong-Whan Rhim. “Preparation and characterization of agar/lignin/silver nanoparticles composite films with ultraviolet light barrier and antibacterial properties”. In: *Food Hydrocolloids* 71 (2017), pp. 76–84. DOI: [10.1016/j.foodhyd.2017.05.002](https://doi.org/10.1016/j.foodhyd.2017.05.002).
- [110] Thangaraj Shankar et al. “Green synthesis of silver nanoparticles using *Cap-sicum frutescence* and its intensified activity against *E. coli*”. In: *Resource-Efficient Technologies* 3.3 (2017), pp. 303–308. DOI: [10.1016/j.reffit.2017.01.004](https://doi.org/10.1016/j.reffit.2017.01.004).
- [111] Rekha Sharma, Ankita Dhillon, and Dinesh Kumar. “Mentha-stabilized silver nanoparticles for high-performance colorimetric detection of Al (III) in aqueous systems”. In: *Scientific reports* 8.1 (2018), pp. 1–13. DOI: [10.1038/s41598-018-23469-1](https://doi.org/10.1038/s41598-018-23469-1).
- [112] Virender K Sharma, Ria A Yngard, and Yekaterina Lin. “Silver nanoparticles: green synthesis and their antimicrobial activities”. In: *Advances in Colloid and Interface science* 145.1-2 (2009), pp. 83–96. DOI: [10.1016/j.cis.2008.09.002](https://doi.org/10.1016/j.cis.2008.09.002).
- [113] Kazuko. Shimada et al. “Antioxidative properties of xanthan on the autoxidation of soybean oil in cyclodextrin emulsion”. In: *Journal of Agricultural and Food Chemistry* 40.6 (June 1992), pp. 945–948. DOI: [10.1021/jf00018a005](https://doi.org/10.1021/jf00018a005).
- [114] Ganesh Shimoga, Eun-Jae Shin, and Sang-Youn Kim. “Silver nanoparticles incorporated PVC films: evaluation of structural, thermal, dielectric and catalytic properties”. In: *Polímeros* 29 (2019). DOI: [10.1590/0104-1428.08218](https://doi.org/10.1590/0104-1428.08218).
- [115] Kamlesh Shrivastava et al. “Colorimetric and paper-based detection of lead using PVA capped silver nanoparticles: Experimental and theoretical approach”. In: *Microchemical Journal* 150 (2019), p. 104156. DOI: [10.1016/j.microc.2019.104156](https://doi.org/10.1016/j.microc.2019.104156).
- [116] Harpreet Singh et al. “Recent advances in the application of noble metal nanoparticles in colorimetric sensors for lead ions”. In: *Environmental Science: Nano* 8.4 (2021), pp. 863–889.
- [117] Rajat Singh et al. “Colorimetric sensing approaches based on silver nanoparticles aggregation for determination of toxic metal ions in water sample: A review”. In: *International Journal of Environmental Analytical Chemistry* (2021), pp. 1–16. DOI: [10.1080/03067319.2021.1873315](https://doi.org/10.1080/03067319.2021.1873315).
- [118] Karthikey Devadatta Sirdeshpande et al. “Structural characterization of mesoporous magnetite nanoparticles synthesized using the leaf extract of *Callian-dra haematocephala* and their photocatalytic degradation of malachite green dye”. In: *Applied Nanoscience* 8 (2018), pp. 675–683. DOI: [10.1007/s13204-018-0698-8](https://doi.org/10.1007/s13204-018-0698-8).

- [119] Sylvie Skalickova, Mojmir Baron, and Jiri Sochor. “Nanoparticles biosynthesized by yeast: a review of their application”. In: *Kvasny Prumysl* 63.6 (2017), pp. 290–292. DOI: [10.18832/kp201727](https://doi.org/10.18832/kp201727).
- [120] Ivan Sondi and Branka Salopek-Sondi. “Silver nanoparticles as antimicrobial agent: a case study on *E. coli* as a model for Gram-negative bacteria”. In: *Journal of colloid and interface science* 275.1 (2004), pp. 177–182. DOI: [10.1016/j.jcis.2004.02.012](https://doi.org/10.1016/j.jcis.2004.02.012).
- [121] T Sowmyya. “Lagenaria siceraria peel waste aqueous extract mediated silver nanoparticles for degradation of Congo red dye”. In: *Journal of Physics: Conference Series*. Vol. 2267. 1. IOP Publishing. 2022, p. 012101. DOI: [10.1088/1742-6596/2267/1/012101](https://doi.org/10.1088/1742-6596/2267/1/012101).
- [122] Mahmoud Tavakoli et al. “EGaIn-Assisted Room-Temperature Sintering of Silver Nanoparticles for Stretchable, Inkjet-Printed, Thin-Film Electronics”. In: *Advanced Materials* 30.29 (2018), p. 1801852. DOI: [10.1002/adma.201801852](https://doi.org/10.1002/adma.201801852).
- [123] Sheenam Thatai et al. “A new way in nanosensors: gold nanorods for sensing of Fe (III) ions in aqueous media”. In: *Microchemical Journal* 113 (2014), pp. 77–82. DOI: <https://doi.org/10.1016/j.microc.2013.11.004>.
- [124] Jayaraman Theerthagiri et al. “Fabrication strategies and surface tuning of hierarchical gold nanostructures for electrochemical detection and removal of toxic pollutants”. In: *Journal of Hazardous Materials* 420 (2021), p. 126648. DOI: [10.1016/j.jhazmat.2021.126648](https://doi.org/10.1016/j.jhazmat.2021.126648).
- [125] Madhavi Thomas and Joseph Jankovic. “Neurodegenerative disease and iron storage in the brain”. In: *Current opinion in neurology* 17.4 (2004), pp. 437–442.
- [126] Hailong Tian et al. “Biodegradation of phenolic compounds in high saline wastewater by biofilms adhering on aerated membranes”. In: *Journal of hazardous materials* 392 (2020), p. 122463. DOI: [10.1016/j.jhazmat.2020.122463](https://doi.org/10.1016/j.jhazmat.2020.122463).
- [127] Adeline Su Yien Ting, Chloe Kai Wai Cheng, and Krystle Angelique Aguda Santiago. “Decolourization of malachite green dye by endolichenic fungi from the lichen *Usnea* sp.: A novel study on their dye removal potential”. In: *Journal of King Saud University-Science* 33.7 (2021), p. 101579. DOI: [10.1016/j.jksus.2021.101579](https://doi.org/10.1016/j.jksus.2021.101579).
- [128] G Vanitha et al. “Physiochemical charge stabilization of silver nanoparticles and its antibacterial applications”. In: *Chemical Physics Letters* 669 (2017), pp. 71–79. DOI: <https://doi.org/10.1016/j.cplett.2016.11.037>.
- [129] Thivaharan Varadavenkatesan, Raja Selvaraj, and Ramesh Vinayagam. “Green synthesis of silver nanoparticles using *Thunbergia grandiflora* flower extract and its catalytic action in reduction of Congo red dye”. In: *Materials Today: Proceedings* 23 (2020), pp. 39–42. DOI: [10.1016/j.matpr.2019.05.441](https://doi.org/10.1016/j.matpr.2019.05.441).
- [130] Kanokorn Wechakorn et al. “A rhodamine–bistriazole based fluorescent and colorimetric sensor containing a phenyl linker for Fe (III) detection”. In: *Chemical Papers* 75.3 (2021), pp. 883–892. DOI: [10.1007/s11696-020-01349-1](https://doi.org/10.1007/s11696-020-01349-1).



- [131] Benjamin J. Wiley et al. “Maneuvering the Surface Plasmon Resonance of Silver Nanostructures through Shape-Controlled Synthesis”. In: *The Journal of Physical Chemistry B* 110.32 (2006). PMID: 16898709, pp. 15666–15675. DOI: **10.1021/jp0608628**.
- [132] Yu Yang et al. “A patterned aluminum/reduced graphene oxide/silver sheet for detection and degradation of malachite green in water”. In: *Separation and Purification Technology* 272 (2021), p. 118892. DOI: **10.1016/j.seppur.2021.118892**.
- [133] Dilek Demirezen Yilmaz, Derya Aksu Demirezen, and Hamdi Mihçioğur. “Colorimetric detection of mercury ion using chlorophyll functionalized green silver nanoparticles in aqueous medium”. In: *Surfaces and Interfaces* 22 (2021), p. 100840. DOI: **10.1016/j.surfin.2020.100840**.
- [134] Yiseul Yu et al. “Reconciling of experimental and theoretical insights on the electroactive behavior of C/Ni nanoparticles with AuPt alloys for hydrogen evolution efficiency and Non-enzymatic sensor”. In: *Chemical Engineering Journal* 435 (2022), p. 134790. DOI: **10.1016/j.cej.2022.134790**.
- [135] Huiping Zeng et al. “As (V) adsorption by a novel core-shell magnetic nanoparticles prepared with Iron-containing water treatment residuals”. In: *Science of the Total Environment* 753 (2021), p. 142002. DOI: **10.1016/j.scitotenv.2020.142002**.
- [136] Kaiqiang Zhang et al. “Recent advances in the nanocatalyst-assisted NaBH<sub>4</sub> reduction of nitroaromatics in water”. In: *ACS omega* 4.1 (2019), pp. 483–495. DOI: **10.1021/acsomega.8b03051**.
- [137] Keqiang Zhang et al. “Preparation of controlled nano-MgO and investigation of its bactericidal properties”. In: *Chemosphere* 89.11 (2012), pp. 1414–1418. DOI: **10.1016/j.chemosphere.2012.06.007**.



# Glucanoacetobacter kombuchae (RG3<sup>T</sup>), a novel bacteria for AgNPs biosynthesis: Characterization and comprehensive evaluation of bioactivity

Jhilam Majumder<sup>a</sup>, Kunal Pal<sup>b</sup>, Writachit Chakraborty<sup>a</sup>, Parimal Karmakar<sup>a</sup>, Ratan Gachhui<sup>a,\*</sup>

<sup>a</sup> Department of Life Science and Biotechnology, Jadavpur University, Jadavpur, Kolkata, 700032, West Bengal, India

<sup>b</sup> Techno India University, Department of Biotechnology, Bidhannagar, Kolkata, 700091, West Bengal, India

## ARTICLE INFO

### Keywords:

Bio-green synthesis  
Novel bacteria  
Antibacterial  
Antioxidant  
Cytotoxic

## ABSTRACT

An innovative green route has been adapted in this study to biosynthesize Silver Nanoparticles (AgNPs) for the first time using the cell exudate of a novel bacteria *Glucanoacetobacter kombuchae* (RG3<sup>T</sup>). Bio-reduction of silver was carried out by adding AgNO<sub>3</sub> and glucose along with the bacterial cell exudate. The onset of dark brown colour indicated the synthesis of nanoparticles (NPs) and was further validated by absorption spectrum at 430 nm using UV-Vis Spectroscopy. X-ray diffraction (XRD) study clearly illustrated the crystalline phase of the formed NPs. Further, morphological studies was done by Transmission electron microscope (TEM) which showed an approximate size of 20 nm exhibiting the shape of a sphere. Along with this, results obtained from Scanning electron microscope (SEM), Fourier transform infrared spectroscopy (FTIR), and Dynamic light scattering (DLS) particle size analyser also confirmed the surface morphology and functional group of the NPs. Broad spectrum antibacterial activity with Gram positive and negative bacteria were evaluated along with the antioxidant activity which showed high potency of NPs. RG3<sup>T</sup>-NPs were treated against cell lines like MCF-7, HEPG-2, and notably against Triple negative human breast cancer (TNBC) cell line which showed its superior efficiency. Therefore, it can be concluded that RG3<sup>T</sup>-NPs points itself to be a significant bio-material with antibacterial, cytotoxic, and antioxidant properties.

## 1. Introduction

Over the past years, nanotechnology has been emerging as the cutting-edge interdisciplinary technology along with the other branches of science and technology. These have gained significant importance because of its broad scope applications and promising outcomes that can be correlated to the unique properties of nano-materials compared to other standard materials. Commonly, a particle is only considered nano-sized if it has reached the dimensions close to 100 nm or less [1].

Preferably, cost effectiveness and non toxicity should be of primary focus for synthesizing nanoparticles (NPs). When these two criteria are fulfilled, only then the focus needs to be shifted in obtaining the NPs with superior quality and utility. Innovations in the way of production and modifications of the NPs with different utilitarian groups of chemicals and also their conglomeration unlock a broad range of utmost utilization in the field of biotechnology. Metallic NPs are always in trends of nanotechnology owing to the fact of huge potentiality in the field of the areas of physical, chemical, medicine, pharmaceutical, and biotechnology [2,3].

Although there are a variety of metallic nanoparticles, among them silver NPs have gained significant importance due to their virtuous

properties and their utility in the areas of photo-catalysts, photonics, micro-electronics, and lithography [4]. But the sole property of massive antimicrobial activity makes silver stands out alone in gratitude [5].

Silver nanoparticles (AgNPs) can be synthesized in various ways such as bottom up like pyrolysis, sol gel method, chemical method, physical method, physio-chemical method, etc. [6]. These methods often result in generation of secondary pollutants that may further lead to toxicity towards the environment and also they require working under high temperature and pressure [7,8]. In order to overcome these drawbacks, an economic, eco-friendly, feasible, and greener approach is the need of the hour. Therefore we propose a solution of eliminating the odds of all the physical and chemical approaches by introducing the bio-inspired method of NPs synthesis [5]. The greener method of synthesis is not only environmental cordial, but also can be waged to manufacture enormous volumes of NPs with nullifying contamination [9].

Over the past decades, there has been few studies pointing on the green synthesis method of NPs synthesis, including plant extracts, biodegradable polymers, and microbes. Particularly, microorganism based synthesis is the new trend because they are secured, sustainable,

\* Corresponding author.

E-mail address: [ratangachhui@yahoo.com](mailto:ratangachhui@yahoo.com) (R. Gachhui).

<https://doi.org/10.1016/j.mtcomm.2022.104410>

Received 12 March 2022; Received in revised form 29 August 2022; Accepted 6 September 2022

Available online 17 September 2022

2352-4928/© 2022 Elsevier Ltd. All rights reserved.

low cost and therefore environmental friendly too. In the last few years, bacteria have been widely explored to synthesize inorganic nano-materials particularly gold and silver. It can be directly contributed to the property of versatility and survivability of the bacteria at higher concentrations of metallic ions [10].

Discovery of antibiotics has been a revolutionary milestone in the history of humans. Unfortunately, the utilization of the novel prodigy medication were followed by a quick increase in tolerant pathogen strain [11]. Frequent and improper use of antibiotics may be blamed for this. In order to find out an alternative for the same, nanotechnology can be applied to beat the drug resistance of many infectious bacteria. In fact, silver nanoparticle is one of the most suitable one to fight against the pathogenic strains. Moreover in India, main contaminants of polluted water are Enterobacteriaceae namely *Salmonella typhi*, *Escherichia coli*, *Shigella sonnei*, etc. Enterobacteriaceae contributes to water borne related disorders like diarrhoea, cholera, typhoid, and other infections. Since ancient times, silver has been the best choice among people for its robust antimicrobial effectiveness. Moreover, silver shows extensive span of efficiency towards various Gram-positive and Gram-negative bacteria, also chance of development of bacteria resistance is remarkably low too [12].

Usefulness of AgNPs to the medical field is not only restricted to its antimicrobial effect but also gained much attention due to its cytotoxic effect. In some of the previous studies, opposed to cell line of human cervical cancer, it has been showed that the efficiency of AgNPs towards apoptosis, pointing its role as anti cancer drug therapy [13, 14]. It has been estimated that AgNPs synthesized through biological method are safe to human cell up to 50  $\mu\text{g/ml}$  of concentration. Therefore, the cytotoxic effect is an another important factor that needs attention [15].

*Glucanoacetobacter kombucha*, strain RG3<sup>T</sup> has been isolated from a popular fermented tea, known as kombucha [16]. The GenBank accession numbers for the strain RG3<sup>T</sup> are respectively AY688433 and DQ141200. This potential Gram negative, rod shaped bacteria belongs to the Acetobacter family. This bacteria is also responsible for nitrogen fixation and cellulose formation as pointed by Dutta and Gachhui [16]. Here in this study, we have used this bacteria for the NPs synthesis by bio-green method. The present study aims to develop a feasible green alternative towards the synthesis of AgNPs and to enlighten its broad spectrum antimicrobial effect in some of the common Gram positive/negative bacteria including *Salmonella typhi*, *Shigella sonnei*, *Vibrio cholera*, *Bacillus cereus*, *E. coli*, and *Staphylococcus aureus*. Once its antibacterial property is successfully fulfilled, our attention is then shifted to explore its cytotoxic activity. The cytotoxicity has been measured against HEPG-2 hepatocellular carcinoma cell lines, MCF-7 breast carcinoma cell lines, and MDA-MB-468 corresponding to the Triple Negative Breast Cancer (TNBC) cell lines. HEPG-2 is a human hepatoma origin, non-tumorigenic with elevated proliferating rate and most frequently applied in drug catabolism and hepato-toxicity studies. MCF-7 is characterized with presence of estrogen, progesterone, and glucocorticoid receptors. Further, MDA-MB-48 holds for about 10–15 percentage of the breast cancer lines. This triple-negative breast cancer cited to the non availability of estrogen or progesterone receptors and is also responsible to produce insufficient protein commonly known as HER2. Studies have been conducted on RG3<sup>T</sup> NPs to check the cytotoxic activities of these cell lines.

Oxidants are produced as a result of normal metabolism in the body and also in the environment. These molecules are very reactive and can rapidly react with other cellular activities of the body leading to noxious effects in body including cancer and other diseases. In order to get rid of these oxidants and its stresses, scavenging activity is helpful. Thus, DPPH (2,2-diphenyl-2-picrylhydrazyl hydrate) and ABTS (2, 2'-azino-bis 3-ethylbenzthiazoline-6-sulfonic acid) free radical scavenging activity has been performed to check the effectiveness of the produced AgNPs against oxidants. Therefore, it may be concluded that the produced NPs has a long way to go and establish itself as an

antioxidant, antibacteria and anticytotoxic bio-material. Also, a deep interest has been generated towards further exploring and analysing this NPs for more potential benefits that are applicable towards the society. In the remaining text, RG3<sup>T</sup>AgNPs and RG3<sup>T</sup>NPs is referred to as RG3-NPs. Simultaneously, pellet resuspension of RG3<sup>T</sup> in de-ionized water for the entire experiment has been termed as cell exudate of bacteria or bacterial cell exudate or simply cell exudate.

## 2. Materials and methods

### 2.1. Chemicals & reagents

Silver nitrate ( $\text{AgNO}_3$ ), Agar agar Powder, D-(+)-Glucose anhydrous, D-Mannitol, 2,2-diphenyl-2-picrylhydrazyl hydrate (DPPH), 2,2'-Azino-bis-(3-ethylbenzothiazoline-6-sulfonic acid) diammonium salt (ABTS) were purchased from Hi-media (Mumbai, India) and de-ionized water was used throughout the entire experiment. Every reagents used here were of unadulterated analytical grade and therefore used without any further purification.

### 2.2. Preparation of bacterial cell exudate

*Glucanoacetobacter kombucha*, strain RG3<sup>T</sup> (= LMG 23726T = MTCC 6913T), was isolated from Kombucha tea (Kombucha is a sweet, slightly alkaline fermented beverage, consumed world widely specially by the South Asian Countries. Mannitol broth (Yeast extract 0.75%, Peptone 0.45%, Manitol 2.5%, pH 5) of 100 ml was prepared to grow 50  $\mu\text{l}$  of previous culture of the strain RG3<sup>T</sup>, and kept overnight at 30 °C under shaking condition at 120 rpm. Next, the culture was centrifuged at 5000 rpm for 5 min and the pellet was collected, washed with deionized water twice. Washed pellet was re-suspended with 100 ml de-ionized water and again kept overnight at 30 °C under shaking condition at 120 rpm. It was then centrifuged at 5000 rpm for 5 min, then the pellet was discarded and the supernatant was collected. The later was stored at 4 °C for further use.

### 2.3. Bio-green synthesis of silver nanoparticle using bacterial cell exudate and it's optimization

For the formation of AgNPs, different parameters such as concentration of  $\text{AgNO}_3$  and glucose, pH, and reaction time were varied. Each parameter was varied keeping the other parameters constant to optimize the synthesis. These parameters were varied in the order of  $\text{AgNO}_3$  concentration, followed by pH, glucose concentration, and finally reaction time. Based on the Zeta Potential and UV-Vis spectroscopy values obtained by varying these parameters, it was noted that RG3-NPs formation were optimized at ambient temperature with a pH of 7–7.5,  $\text{AgNO}_3$  concentration of 17 mg/ml of and 10 mg/ml of glucose. Details of these experiment and variation of different parameters has been also shown in Supplementary Data.

Simultaneously, a control setup was established with only bacterial cell exudate and  $\text{AgNO}_3$  without glucose. The result obtained indicated that the bacterial cell exudate plus  $\text{AgNO}_3$  and glucose together lead to the formation of a brownish yellow coloured solution, while the controlled set up without glucose and only with the cell exudate content remained colourless (Fig. 1). This indicates the importance of both bacterial exudate and glucose in AgNPs formation.

### 2.4. Characterization of RG3-NPs

Various instrumentation analysis were done to check the existence of the produced bio-green NPs and to determine it's characteristics. The confirmation of genesis and escalation of NPs were surveilled through UV-vis Spectrophotometer (HITACHI U 2900/U 2910 UV VIS DOUBLE BEAM) settled to range including 200 to 800 nm. Crystalline nature attributed to metallic silver was examined through XRD (Rigaku,



# Efficient degradation of 4-nitrophenol and colorimetric detection of Fe (III) by biogenic silver nanoparticles of *Papiliotrema laurentii*

Jhila Majumder, Tinku Bhunia, Satabdi Gorai, Debojyoti De, Parimal Karmakar, Ratan Gachhui\*

Department of Life Science and Biotechnology, Jadavpur University, Jadavpur, Kolkata, 700032, West Bengal, India

## ARTICLE INFO

### Keywords:

Biogenic AgNPs  
Environmental management  
4-Nitrophenol  
Fe (III)  
Bio-catalysis  
Colorimetric detections

## ABSTRACT

In this study, novel biogenic silver nanoparticles have been developed involving a green method by a yeast strain, *Papiliotrema laurentii* (Y24) cell resuspension exudate. Synthesis conditions have been optimized and the produced nanomaterials have been characterized by DLS, Zeta Potential, FTIR, XRD, SEM, TEM to predict and analyse the particles. High crystallinity, irregular to cubical shape, and an average dimension of 20 nm of AgNPs were obtained from the characterization. Biogenic Y24-NPs were applied to reduce 4-Nitrophenol to 4-Aminophenol by catalytic activity (within 8 min). After 5 recycles, high reusability of Y24-NPs was observed ( $\geq 94\%$ ). Y24-NPs were further demonstrated for high selectivity and sensitivity towards  $\text{Fe}^{3+}$  by colorimetric detection with the limit of 1.8  $\mu\text{M}$  in the linear range of 5–150  $\mu\text{M}$ . Additionally, the developed nanosensor has been tested for  $\text{Fe}^{3+}$  ions in tap water samples. Therefore, Y24-NPs can be used for bioremediation with significant catalytic activity and reusability.

## 1. Introduction

Environmentally benign processes like biocatalysis in nanotechnology studies are gaining importance to meet the growing population demand. Compared to the traditional chemical and physical mode of synthesis, bio-green synthesis of nanoparticles has received significant importance due to their non-toxic and non-hazardous nature. Although several nanoparticles serve well in nanotechnology and related fields, among them, silver nanoparticles (AgNPs) have been used largely due to their specific physical, chemical, and biological properties and application in areas such as catalysis [1,2], antimicrobial activity [3], anticancerous activity [4], etc. In recent years, nanoparticles are being widely applied in the field of bioremediation, particularly for industrial effluents such as textile dyes, which normally constitutes 80% of the total emissions produced by this industry [5].

Among the notable textile dyes, 4-Nitrophenol (4-NP) is one of most usable dyes, particularly in the tannery for dark colouration, fabrication of fertilizers, explosives, rubber, pesticides, fungicides, etc. There are high level of biochemical oxygen demand (BOD) and chemical oxygen demand (COD) in the residual waters of these dye contaminated textile industries. The colour associated with the dyes causes aesthetic damage to the water bodies and also prevents penetration of light through water. This leads to a reduction in the rate of photosynthesis [6] and dissolved oxygen levels, affecting the entire aquatic biota [7].

Therefore, this study attempts to degrade toxic 4-NP into non-toxic 4-Aminophenol (4-AP).

Traditional methods of conversion of 4-NP to 4-AP can be done using adsorption involving carbon activation, flocculation, electrocoagulation [7]. Additional methods like ion exchange, flotation of froth, ozonation, membrane filtration, and reverse osmosis have also been used for this purpose [8]. Although these methods have been successful in dye degradation, however, they can generate secondary waste products. To come up with a eco-friendly solution, we propose biogenically synthesized AgNPs as a catalyst to degrade 4-NP to 4-AP. Also, high surface area and potential electrical conductivity makes AgNPs an effective catalyst for dye reduction process by bio-catalysis [9].

Apart from dye degradation, AgNPs also play a vital role in colorimetric detection of several harmful metals in both aquatic and biological environments [10], due to their strong Surface plasmon resonance (SPR) and optical properties depending on the size and shape. Various toxic metals ions like  $\text{Fe}^{2+}$ ,  $\text{Fe}^{3+}$  [11],  $\text{Hg}^{2+}$  [12],  $\text{Ni}^{2+}$  [13],  $\text{Cu}^{2+}$  [14],  $\text{Cr}^{2+}$  [15],  $\text{Pb}^{2+}$  [16],  $\text{Al}^{3+}$  [17],  $\text{Cd}^{2+}$  [18], etc. have been successfully detected by AgNPs. Among these metal ions, water contamination by iron is one of the major concern. Higher levels of iron in food and water may directly lead to haemoglobinopathy and can cause mild to severe damage in vital organs such as liver, pancreas, and heart, and may also lead to Alzheimer's and Parkinson's diseases [19].

\* Corresponding author.

E-mail address: [ratangachhui@yahoo.com](mailto:ratangachhui@yahoo.com) (R. Gachhui).

<https://doi.org/10.1016/j.mseb.2023.116647>

Received 13 January 2023; Received in revised form 31 May 2023; Accepted 7 June 2023

Available online 26 June 2023

0921-5107/© 2023 Elsevier B.V. All rights reserved.

AgNPs can be applied to address this problem by detecting and quantifying these metal ions, even at low concentrations. For colorimetric detection, the principal involved mainly is the change of colour or shift of the SPR band when the analyte binds to the catalysts [20]. The colorimetric sensing method by AgNPs provides a significant advantage over various other analytical sensitive instrumentation, such as Atomic absorption spectroscopy (AAS), Inductively coupled plasma mass spectrometry (ICP-MS), X-ray fluorescence (XRF), etc., thereby making AgNPs more valuable and applicable in practical fields. Use of biogenic AgNPs makes the colorimetric detection process ecofriendly since there would be no generation of secondary waste products.

This study has been designed and applied to produce AgNPs using yeast cell resuspension exudate from *Papiliotrema laurentii* strain Y24. To the best of our knowledge, this is the first attempt to synthesize AgNPs using this yeast cell. *Papiliotrema laurentii* (formerly *Cryptococcus laurentii*) strain Y24 was isolated from Kombucha tea [21] in our laboratory [22] and deposited to Microbial Type Culture Collection of Chandigarh, India (MTCC 6930). Y24<sup>T</sup> belongs to the family of Rhynchogastremaceae. The objective of this research is to utilize and justify the green synthesized nanoparticles towards sensitivity and selectivity for iron (III) detection and catalytic degradation of 4-NP. The nanoparticle synthesis process has been optimized and characterized with different instrumentation to obtain specific sizes, shapes, and characteristic features. Further, the performance of AgNPs with respect to their kinetic rate constants, stability, and reusability for the reduction of 4-NP have also been investigated. Finally, the applicability of AgNPs as a colorimetric sensor for Fe (III) has been demonstrated to obtain sensitivity and selectivity and real water testing has been done successfully. In the remaining text, *Papiliotrema laurentii* has been mentioned as Y24<sup>T</sup> and Y24-AgNPs is referred to as Y24-NPs.

## 2. Materials and methods

### 2.1. Chemicals & reagents

Chemicals namely, Silver Nitrate (AgNO<sub>3</sub>, A.R. 99.9%), Yeast Extract (Yeast Extract Powder. RM027), D-(+)-Glucose anhydrous, Peptone Type I, Bacteriological. RM667, Hydrochloric acid (HCl), Sodium Hydroxide (NaOH), p-Nitrophenol (C<sub>6</sub>H<sub>5</sub>NO<sub>3</sub>), Sodium Borohydride (NaBH<sub>4</sub>), other metal salts like Magnesium sulfate heptahydrate (MgSO<sub>4</sub> · 7H<sub>2</sub>O), Calcium sulfate (CaSO<sub>4</sub>), Copper (II) acetate monohydrate (C<sub>4</sub>H<sub>10</sub>CuO<sub>5</sub>), Nickel (II) chloride hexahydrate (NiCl<sub>2</sub> · 6H<sub>2</sub>O), Zinc Sulfate (ZnSO<sub>4</sub>), Iron (III) chloride anhydrous (FeCl<sub>3</sub>) were purchased from Hi-media (Mumbai, India). Whatman filter paper No. 1 was purchased from Thomas Baker (Thomas Baker Chemicals, Pvt. Ltd. Mumbai, India). Deionized water was used throughout the entire experimentation procedure. All the above-mentioned reagents were of extra pure grade and therefore were used without any further purification.

### 2.2. Preparation of Y24 cell resuspension exudate

*Papiliotrema laurentii* (formerly *Cryptococcus laurentii*) strain Y24, deposited to Microbial Type Culture Collection of Chandigarh [22], India (MTCC 6930), was isolated from Kombucha tea [23]. Y24<sup>T</sup> was grown and maintained in modified YPD (Yeast, Peptone, Dextrose) media (Yeast extract 0.75%, Peptone 0.45%, Dextrose 2.5%, pH 5). 100 mL of YPD was made to grow with 50 µL of the previous culture of Y24<sup>T</sup>, at 30 °C under shaking condition at 120 rpm observed overnight. On the next day, the culture was centrifuged at 5000 rpm for 5 min and the pellet was collected and washed with deionized water twice to remove further impurities. This process was repeated twice. Then the washed cell pellet was resuspended with 100 mL deionized water and again kept overnight at 30 °C under shaking conditions at 120 rpm. It was then centrifuged at 5000 rpm for 5 min and the pellet was discarded. The yeast cell resuspension exudate was collected in the form of a supernatant. The yeast cell resuspension exudate was stored at 4 °C for further use [4].

### 2.3. Bio-green synthesis of silver nanoparticles from yeast cell resuspension exudate

The biogenic synthesis of AgNPs was done by adding AgNO<sub>3</sub> and the cell exudate of Y24 together in the concentration of 2.0 mM of AgNO<sub>3</sub> and 0.1 mM of dextrose and then observed for 45 min at room temperature. The glucose here in the bio-synthesis acts as a co-factor to enhance AgNPs formation along with Y24 cell exudate. The effects of temperature, reaction time, conc. of AgNO<sub>3</sub>, and conc. of glucose was further studied to optimize the formation of the nanoparticles. The formation of silver nanoparticles was noted by a change in the colour spectrum from colourless to brownish yellow as recognized by the naked eye. Further investigation was done by UV-Vis Spectroscopy, scanned in the range of 300–700 nm which showed a significant peak at around 430 nm, thereby confirming the nanoparticle formation. For further applications, nanoparticles were centrifuged at 10,000 rpm for 10 min and washed twice with deionized water to remove unwanted impurities. The entire process of purification was repeated twice and vacuum dried (ELEYA speed Vac) and stored in the dark for further use. The aqueous solution of Y24-NPs was used to carry out the catalytic reduction of 4-NP and colorimetric detection of Fe (III).

### 2.4. Characterization of Y24-NPs

The characteristics of the bio-synthesized nanoparticles were specified and validated using various instrumentation analyses. To detect the formation of the nanoparticle, UV-Vis Spectroscopy (HITACHI U 2900/U 2910 UV VIS DOUBLE BEAM) was carried out in the range of 300–700 nm. Crystalline features of the green synthesized NPs were determined by XRD study (Rigaku, Miniflex). Surface structure analysis was performed by advanced microscopy instrumentations like SEM (Hitachi S-4500), TEM (JEM-2100 Electron Microscopy). To obtain information about the functional group that interacted to form the metallic NPs, FTIR (Shimadzu FTIR spectrophotometer (FTIR 8400)) study was conducted in the ranges between 4000–400 cm<sup>-1</sup>. The precise size and charge distribution within the nanoparticles were examined with the help of DLS (Dynamic Light Scattering) and Zeta potential [ZETA Seizers Nanoseries (Malvern Instruments Nano ZS)]. To measure the concentrations of any elements, Atomic Absorption (AAS) study has been employed. (iCE 3500, Thermo Scientific, Germany)

### 2.5. Catalytic activity

The catalysts (Y24-NPs) have been assessed against 4-NP degradation activity by optimizing different parameters. Firstly, to check the effect of different concentrations of NaBH<sub>4</sub>, various concentrations of NaBH<sub>4</sub> like 0.05 mM, 0.1 mM, 0.2 mM has been used along with 2.0 mM of AgNPs. Secondly, to assess the effect of 4-NP concentration on its reduction, different concentrations of 4-NP like 0.1 mM, 0.5 mM, 1.0 mM, 1.5 mM, and 2.0 mM was used along with AgNPs and NaBH<sub>4</sub>. Thirdly, the effect on the catalyst's concentration has been studied using 1.0 mM, 1.5 mM, 2.0 mM, and 2.5 mM of AgNPs. Finally, the effect of reaction time is also observed from 0 to 8 min, keeping the concentration of NaBH<sub>4</sub> and AgNPs the same.

### 2.6. Colorimetric detection of Fe(III)

Initially, selectivity towards six different metal ions namely, Fe<sup>3+</sup>, Zn<sup>2+</sup>, Ni<sup>2+</sup>, Mg<sup>2+</sup>, Ca<sup>2+</sup>, and Cu<sup>2+</sup> with Y24-NPs was performed. UV-Vis Spectroscopy was done in the range of 300–600 nm to note the change if any. Further, to predict the sensitivity of the developed AgNPs-sensor, different concentrations of Fe<sup>3+</sup> from the ranges between 5–3000 µM were made to react with Y24-NPs solution and the SPR potency was determined. Quantitative determination of Fe<sup>3+</sup> was done by increasing the concentration of Fe<sup>3+</sup> from 0 to 3000 µM. The resultants were scanned by UV-Vis Spectroscopy. To authenticate the feasibility of





Contents lists available at ScienceDirect

# Bioresource Technology Reports

journal homepage: [www.sciencedirect.com/journal/bioresource-technology-reports](http://www.sciencedirect.com/journal/bioresource-technology-reports)



## Effective degradation of azo dyes and colorimetric detection of $\text{Hg}^{2+}$ by biogenic silver nanoparticles of *Pichia manshurica*

Jhilam Majumder, Ratan Gachhui\*

Department of Life Science and Biotechnology, Jadavpur University, Jadavpur, Kolkata 700032, West Bengal, India

### ARTICLE INFO

#### Keywords:

Biogenic AgNPs  
In-situ characterization  
*Pichia manshurica*  
Azo dyes  
Catalytic reduction  
Colorimetric detection of  $\text{Hg}^{2+}$

### ABSTRACT

A novel biogenic silver nanoparticle production has been done using a yeast *Pichia manshurica*, strain CD1 cell resuspension exudates. The characterization of AgNPs by DLS, Zeta Potential, FTIR, XRD, SEM, and TEM was done to obtain spherical particle morphology with 22 nm diameter. Biocatalysis of CD1-NPs was done to obtain the catalytic degradation of azo dyes, Congo red, and Malachite green. Degradation occurred within 30 min for Congo red and 40 min for Malachite green with degradation efficiency of 98.86 % and 97.54 % respectively. High reusability (approximately 94 %) was observed of CD1-NPs up to 5 recycles. CD1-NPs were further tested for selectivity and sensitivity towards  $\text{Hg}^{2+}$  by colorimetric detection with a limit of 21.04 nM in the linear range of 10–80 nM. The nanosensor has been tested for  $\text{Hg}^{2+}$  ions in mercury-treated tap water samples. The efficiency of the biocatalysts was accessed for practical applicability.

### 1. Introduction

Environmentally cordial technologies are in great need in the field of material synthesis, and the biosynthesis of nanoparticles has received great attention too. The biogenic methods of synthesis that involve a variety of microorganisms like bacteria, fungi and actinomycetes, algae, and plant extracts are gaining importance as simple replacements to the chemical and physical methods. Studies showing synthesis from microbes such as yeasts are particularly important for the synthesis of inorganic nanoparticles (NPs) like Au and Ag. This can be directly attributed to the factor of versatility and survivability of the yeast species at higher concentrations of metallic ions (Skalickova et al., 2017). Among the other nanoparticles, silver nanoparticles (AgNPs) are used largely due to specified physical, chemical, and biological properties and application in the areas such as catalyst (Eisa et al., 2019), photonics (Marimuthu et al., 2020), micro-electronics (Tavakoli et al., 2018), and other activities like antimicrobial, antioxidant, anticancerous activities (Majumder et al., 2022).

Due to rapid industrialization and to meet the growing population demands, industrial effluents have become a serious threat to the environment. The industries like textile, leather, paper, etc., release organic dyes in the form of their effluents (Ting et al., 2021). Those dyes notably compromise the aesthetic quality of water bodies, thereby increasing the biological and chemical oxygen demand (BOD and COD),

reducing the photosynthesis rate, and preventing plant growth and development (Varadavenkatesan et al., 2020). Eventually, they enter the food chain, causing bioaccumulation that directly promotes toxicity, mutagenicity, and carcinogenicity. Among the notable organic dyes, commonly used in various fields are Congo red (CR) and Malachite green (MG) (Dawadi et al., 2021). All these organic water-soluble dyes belong to the azo group. Azo dyes are the largest group of commercial dyes, including 70 % of the organic dyes generated in the world (Eisa et al., 2019). Congo red (CR) belongs to the benzidine-based anionic diazo dye and is responsible for causing allergic reactions by the metabolism of benzidine, which is a carcinogenic product (Nga et al., 2022). Malachite green (MG) is a cationic water-soluble azo dye belonging to the triphenylmethane category. The toxicity of this dye depends on exposure time, temperature, and concentration. MG has been reported to cause carcinogenesis, mutagenesis, chromosomal fractures, teratogenicity, and respiratory toxicity (Ting et al., 2021). They are also reported to cause serious harm to the central nervous system and other vital parts of the human body (Chinthalapudi et al., 2021). Both CR and MG have been selected as the subject model for the degradation study because of their wide utility among other azo dyes in different fields such as dying agent (particularly in textile, paper, and tannery industry), fabrication of fertilizers, rubber, pesticides, fungicides, staining of histological tissues, endospores, etc. (Albeladi et al., 2020). Therefore, the reduction of these dyes is important to address high environmental toxicities.

\* Corresponding author.

E-mail address: [ratangachhui@yahoo.com](mailto:ratangachhui@yahoo.com) (R. Gachhui).

<https://doi.org/10.1016/j.biteb.2023.101498>

Received 20 March 2023; Received in revised form 4 June 2023; Accepted 5 June 2023

Available online 14 June 2023

2589-014X/© 2023 Elsevier Ltd. All rights reserved.

Azo dyes, being commercially important dyes, alone can contribute to almost 60 % of water pollution. Degradation of these dyes is therefore much needed to restore the water quality and also to make it suitable for aquatic life. Bio-inspired green synthesized AgNPs provide one of the best solutions to the above-mentioned problem. AgNPs, by their property, as potent absorbent (Maruthapandi et al., 2021), can be used as a catalyst (Dawadi et al., 2021) to degrade both CR and MG from the wastewater sources. In recent times, silver nanoparticles have been employed as catalysts in catalytic degradation of the harmful azo dyes (Albeladi et al., 2020). Azo dyes successfully bind to the surface of the silver nanoparticles and due to reduction, they are reduced to produce the degraded product. The degraded products are chemically non-toxic and less harmful to the environment. Thereby AgNPs as nanocatalysts are more significant and applicable as biocatalysts in practical fields.

Heavy metals, mainly like  $Pb^{2+}$ ,  $Cr^{2+}$ ,  $Ni^{2+}$ ,  $Cd^{2+}$ ,  $Mn^{2+}$ ,  $Hg^{2+}$  are being released from the industry to the environment, which causes the hazardous effects to both humans and environment (Dawadi et al., 2021). Among the other heavy metals, mercury is a persistent, bio-accumulative, toxic pollutant. Mercury may exist in three forms depending on the environmental condition, such as mercury salt, organic mercury, and inorganic mercury. Methyl mercury is the most toxic form of mercury and is responsible to cause tumors in the human body. Thereby, it enters the food chain by consumption of the methyl mercury accumulated fishes (Akiyama et al., 2022).

Several studies in recent times showed AgNPs to be a successful catalyst in the colorimetric detection of several harmful metals in both aquatic and biological environments (Dawadi et al., 2021; Saenchoopa et al., 2021; Singh et al., 2021). A study conducted by (Singh et al., 2021), offers a solution to address  $Hg^{2+}$  contamination in an aqueous solution with the help of nanoparticle acting as a catalyst to colorimetrically detect, and quantify the metal ions at low concentrations. The principle of colorimetric detection governs mainly the colour change or shift of the SPR band when the analyte binds to the catalysts (Prema et al., 2022). Moreover, colorimetric sensing deployed by AgNPs provides a significant advantage over various other analytically sensitive instrumentations such as AAS, ICP-MS, XRF, etc., (Huber and Leopold, 2016; Skalickova et al., 2017) thereby making silver nanoparticles more significant and applicable in practical fields.

The present study has been designed to biosynthesize AgNPs using yeast cell resuspension or cell exudate from *Pichia manshurica* strain CD1. CD1 belonging to the phylum Ascomycota and subphylum Saccharomycotina. The GenBank accession number of the strain CD1 is KY799109. To the best of our knowledge, this is the first attempt to synthesize AgNPs using this yeast cell *Pichia manshurica*, strain CD1 has been extracted from Kombucha tea (Chakravorty et al., 2016; Dutta and Gachhui, 2007). The biogenic nanoparticle was applied as bio-catalysts to assess the catalytic property in azo dyes (Congo red and Malachite green) degradation and also to detect the presence of  $Hg^{2+}$  ion by colorimetric sensing. The azo dye degradation was done in a much more efficient time and the colorimetric detection was done at the nano-molar level. Further quantification and real water sample testing were successfully performed. The nano-catalysts showed efficient reusability up to 5 cycles. The study, therefore, attempts to apply silver nanoparticles of *Pichia manshurica*, strain CD1 as a catalyst for bioremediation with practical utility. In the remaining text, *Pichia manshurica* has been mentioned as CD1<sup>T</sup> and CD1-AgNPs are referred to as CD1-NPs.

## 2. Materials and methods

### 2.1. Chemicals & reagents

Chemicals required for the experimentation were as follows; Silver Nitrate ( $AgNO_3$ , A.R. 99.9 %), Yeast Extract (Yeast Extract Powder. RM027), D-(+)-Glucose anhydrous, Peptone Type I, Bacteriological. RM667, Hydrochloric acid (HCl), Sodium Hydroxide (NaOH), Sodium Borohydride ( $NaBH_4$ ), other metal salts like Magnesium sulfate

heptahydrate ( $MgSO_4 \cdot 7 H_2O$ ), Calcium sulfate ( $CaSO_4$ ), Copper (II) acetate monohydrate ( $C_4H_{10}CuO_5$ ), Mercuric chloride ( $HgCl_2$ ), Manganese dioxide ( $MnO_2$ ), Zinc Sulphate ( $ZnSO_4$ ), were purchased from Himedia (Mumbai, India). Whatman filter paper No. 1 was purchased from Thomas Baker (Thomas Baker Chemicals, Pvt. Ltd. Mumbai, India). De-ionized water has been used throughout the experimentation procedure. All the above-mentioned reagents were of extra pure grade and therefore were used without any further purification.

### 2.2. Preparation of CD1 cell resuspension exudate

*Pichia manshurica* strain CD1 was isolated from Kombucha tea (Chakravorty et al., 2016). CD1 was grown and maintained in modified YPD (Yeast, Peptone, Dextrose) media (Yeast extract 0.75 %, Peptone 0.45 %, Dextrose 2.5 %, pH 5). 100 mL of YPD broth were made to grow 50  $\mu$ L of the previous culture of CD1, at 30 °C under shaking condition at 120 rpm observed overnight. On the next day, the culture was centrifuged at 5000 rpm for 5 min and the pellet was collected and washed with de-ionized water twice to remove further impurities. This process was repeated twice. Then the washed cell pellet was resuspended with 100 mL de-ionized water and again kept overnight at 30 °C under shaking conditions at 120 rpm. It was then centrifuged at 5000 rpm for 5 min and the pellet was discarded. The yeast cell resuspension exudate was collected in the form of a supernatant. The yeast cell resuspension exudate was stored at 4 °C for further use.

### 2.3. Bio-green synthesis of silver nanoparticles from yeast cell resuspension exudate

The biogenic synthesis of AgNPs was done by the addition of  $AgNO_3$  to the cell exudate of CD1 together in the concentration of 2 mM of  $AgNO_3$  and 0.1 mM of dextrose and then observed for 45 min at room temperature. The dextrose here in this study acts as a co-factor to enhance AgNPs formation along with CD1 cell exudate. The effects of temperature, reaction time, the concentration of  $AgNO_3$ , and the concentration of glucose were further studied to optimize the formation of the nanoparticles. The formation of silver nanoparticles was noted by a change in the colour spectrums from colorless to brownish yellow as recognized by the naked eye. Further absorption measurements were done by UV–Vis Spectroscopy, by scanning in the range of 300–700 nm. For future applications, nanoparticles were centrifuged at 10,000 rpm for 10 min and washed twice with deionized water to remove any unwanted impurities. The entire process of purification was repeated twice and vacuum dried (ELEVA speed Vac) and stored in the dark for further use. The aqueous solution of CD1-NPs was used to carry out the catalytic degradation and colorimetric detections.

### 2.4. Characterization of CD1-NPs

The characteristics of the bio-synthesized nanoparticles were specified and validated using various instrumentation analyses. To detect the formation of the nanoparticles, UV–Vis Spectroscopy (HITACHI U 2900/ U 2910 UV VIS DOUBLE BEAM) was carried out in the range of 300–700 nm. Crystalline features of the green synthesized NPs were determined by XRD study (Rigaku, Miniflex). Surface structure analysis was performed by advanced microscopy instrumentations like SEM (Hitachi S-4500), TEM (JEM-2100 Electron Microscopy). To obtain information about the functional group that interacted to form the metallic NPs, FTIR (Shimadzu FTIR spectrophotometer (FTIR 8400)) study was conducted in the ranges between 4000–400  $cm^{-1}$ . The precise size and charge distribution within the nanoparticles were examined with the help of DLS (Dynamic Light Scattering) and Zeta potential [ZETA Seizers Nano series (Malvern Instruments Nano ZS)]. To measure the concentrations of any elements, Atomic Absorption (AAS) study has been employed (iCE 3500, Thermo Scientific, Germany).